Spring March 2015

Design, Syntheses and Study of BODIPY-based Materials for Use as Electron Transporters in Organic Electronics

Ambata Poe
University of Massachusetts - Amherst

DESIGN, SYNTHESES AND STUDY OF BODIPY-BASED MATERIALS FOR USE AS ELECTRON TRANSPORTERS IN ORGANIC ELECTRONICS

A Dissertation Presented

by

Ambata M. Poe

Submitted to the Graduate School of the
University of Massachusetts Amherst in partial fulfillment
of the requirements for the degree of

DOCTOR OF PHILOSOPHY

February 2015

Department of Chemistry

DESIGN, SYNTHESES AND STUDY OF BODIPY-BASED MATERIALS FOR USE AS ELECTRON TRANSPORTERS IN ORGANIC ELECTRONICS

A Dissertation Presented

by

AMBATA M. POE

Approved as to style and content by:

_____
Sankaran Thayumanavan, Chair

_____
Paul M. Lahti, Member

_____
Ricardo Metz, Member

_____
Kenneth Carter, Member

_____
Craig T. Martain, Department Head
Chemistry

DEDICATION

For ASP, AKP and BBP.
We love you

ACKNOWLEDGMENTS

The PhD process was very intense and difficult and I would not have made it through without the help and support of many people.

First, I would like to thank Prof. S. Thayumanavan for everything that he has done for me. For allowing me to work in his lab during the summer of 2008, looking past my quiet, calm and laid back demeanor and knowing that I have more to offer. I am forever grateful for his guidance and insight.

Next, I would like to thank my committee members, Prof. Paul Lahti, Prof. Ricardo Metz and Prof. Kenneth Carter. Because of them, each of the milestones in this process has been nothing less than exciting. The feedback that I received from them during my time here absolutely changed my approach to research. I would also like to thank Prof. Elizabeth Young, for agreeing to look deeper into our BODIPY molecules, and Prof. Guillaume Wantz, for not only collaborating with me, but allowing me to conduct research in his lab (and giving me an excuse to visit the beautiful city of Bordeaux, France).

I would also like to thank my past collaborators: Dr. Andrea Della Pelle, Dr. Yangbin Chen, Dr. Nagamani Chikkannagari, Dr. Scott Christensen, Dr. Craig Versek, Dr. Bhooshan Popere and Dr. Sompit Wanwong. I appreciate all of the time and energy they each took to discuss various topics and their individual roles in the development of my knowledge about proton and electron transport. I would also like to thank the members of our Energy Subgroup over the years: Dr. Sreedhar Reddy Jaggavarapu, Dr. A. Chandrasekaran, Dr. G. Balaji, Youngju Bae, Piyachai

Khomein, William White, Laura Stirchak, Sean Byrnes, and Samuel Hendel. Working with each of them was more than a pleasure.

I would like to thank the entire Thai Research Group for their support and encouragement over the years, especially Jing Guo, Krishna Raghupathi, Judy Ventura and Jiaming Zhuang. I also thank the Chemistry department and the excellent staff that were always there when they whenever we needed: JMS, Robert Sabola, Ryan Feyrer, Dennis Glick, Elizabeth (Betsy) Louise Blunt. Special thanks to Karen Hakala for her help every snack that I ate, meeting that I scheduled, or invoice I submitted, as well as her time outside of the office (thanks again for the baby blanket!).

I also need to thank the Northeast Alliance for Graduate Education and the Professoriate and all of the members of this program for their support during my graduate career. And I would be remiss if I did not mention my undergraduate mentor Dr. Derrick Swinton for pushing me to do more than I thought I was capable of in 2004 by sparking my interest in the sciences.

Next, I would like to thank the entire Davis/Poe/Roberts family for all of their emotional support and prayers through this entire process. Thanks to Jumatatu, Mjumbe, Tayarisha and Watufani for always taking an interest in what I am doing and loving me in my absence. Thank you to my mother Evelyn, and my father Zizwe for giving me the tools to succeed (in spite of myself, at times) and never being satisfied with mediocrity.

Lastly, I would like to thank my wife Sharnell Davis, my son Ayinde Silas Poe, and my daughter Amina Kaye Poe for their unconditional love and patience. When I

would come home frustrated, they would listen to my gripes. When I would resist leaving for the lab, they would kick me out of bed. They are the reason that I was able to get this far and are the reason why I continue to push forward. I share this thesis with them.

Thank You

ABSTRACT

DESIGN, SYNTHESES AND STUDY OF BODIPY-BASED MATERIALS FOR USE AS ELECTRON TRANSPORTERS IN ORGANIC ELECTRONICS

FEBRUARY 2015

AMBATA M. POE, B.S., LINCOLN UNIVERSITY

Ph.D., UNIVERSITY OF MASSACHUSETTS AMHERST

Directed by: Professor Sankaran Thayumanavan

Organic photovoltaics (OPVs) are desirable for the harvesting of solar energy. They provide distinct advantages over their inorganic counterparts, especially the high absorption coefficients of organic materials and their ability to be processed using inexpensive solution methods. This allows for potential development of lightweight and flexible devices for portable electronics. One of the drawbacks of organic photovoltaics is the low power conversion efficiency of the devices. Efforts to improve the efficiency often take place through molecular design of the electron rich donor material to improve light absorption of the active layer. However, significantly less effort has been put into modifying the acceptor.

BODIPY-dye based materials are well known for their photostability, strong visible absorption and tunable optical and electrochemical properties. Incorporation of these materials into an A-D-A architecture, in which the *meso* coupled BODIPY moiety acts as the acceptor cap is particularly advantageous. This instills predictable absorption properties, low lying LUMO level and consistent n-type characteristics, making these materials suitable for use as light harvesting electron acceptors in OPV devices. Using these materials in bulk heterojunction OPV devices with poly(3-hexylthiophene) (P3HT) as the donor material yielded efficiencies up to 1.5%. This

efficiency was reached after mild optimization using solvent additives and thermal annealing, methods similar to those used with the most commonly employed acceptor, PCBM.

Analysis of the fabricated devices showed the BODIPY molecules contribute to the photogenerated current in the Vis-NIR region. In an effort to improve BODIPY absorption associated with the donor-acceptor intramolecular charge transfer (ICT) interaction, the linker between the donor core and BODIPY cap was systemically modified to increase the delocalization of the frontier molecular orbitals (*m*-phenylene < *p*-phenylene < fluoro-*p*-phenylene < 3-hexylthiophene < directly linked < ethynyl). This variation not only improved the red edge absorption as the delocalization increased, it also provided a method to tune the LUMO energy level, a valuable tool in the design of electron acceptors. The ethynyl linked, BDP-CC-DTP, yielded the best electron mobility ($\sim 10^{-3}$ cm^2 V^{-1} s^{-1}), likely due to the low lying LUMO (-4.06 eV) and its ability to form nanoscale aggregates to promote long range electron transport. Given the improved red edge absorption and higher electron mobility of BDP-CC-DTP compared to BDP-Th-DTP, which showed respectable efficiencies when used as an acceptor in BHJ OPV devices, we plan to investigate the use of this semiconductor in organic solar cells.

TABLE OF CONTENTS

Page

LIST OF TABLES

Table Page

LIST OF FIGURES

Figure Page

LIST OF SCHEMES

Scheme Page

CHAPTER 1

INTRODUCTION

1.1 Clean Energy

A proper investment in the survival of the global community requires advances and improvements in clean energy. Although various renewable energy sources, such as biomass, geothermal, hydropower and wind, are contributing to energy consumption, over 80% of our energy comes from the use of fossil fuels.[1] The need for low-cost, efficient, clean alternatives is immediate due to the detrimental impact on the environment and exhaustible nature of fossil fuels.[2, 3] Two promising devices that are capable of generating electrical energy from sustainable, renewable sources are fuel cells, which convert chemical energy directly into electric energy, and solar cells, which convert sunlight into electrical energy.[4] Improvements made in the development of these devices could be the first step in increasing the contribution of less often used alternative energy sources and minimization of the enormous carbon footprint that accompanies the use of fossil fuels.[5]

Organic materials are attractive for use in electronic applications such as field effect transistors (FET), light emitting diodes (LED) and photovoltaics (PV) for several reasons: the active materials are fashioned from synthetic material, making them relatively inexhaustible compared to inorganic materials; the active materials are capable of being dissolved in organic solvents and coated using various low-cost methods including, spin coating, slot-die coating, roll-to-roll and inkjet printing.[6-9]

These combined benefits give organic materials the potential to be used in the development of both large area and flexible devices at a very low cost, which is very attractive for commercial applications including, wearable devices, portable electronics, and many others. In this chapter, I will briefly describe the properties and characteristics of FET and PV devices.

1.2 Photovoltaics

Solar energy use is generally divided into two categories: *(a)* solar thermal, typically used to heat water in households; *(b)* solar electricity, which is the conversion of solar irradiation into electrical current due to the photovoltaic effect. Since the development of the first silicon-based solar cell by Bell Laboratories in 1954, the efficiency of inorganic devices has steadily improved. The highly ordered atomic network and the built-in electric field in inorganic semiconductors allow for facile charge separation and transport through valence and conduction bands.[10]

Figure 1.1 shows research-cell efficiencies since 1975. The most efficient devices are commonly multijunction inorganic cells, which include one or more p-n junctions.[11, 12] Combining single inorganic cells, with their own respective absorption band gaps, allows for maximized light absorption and power output. Power conversion efficiencies are very high for these devices, often exceeding 40%. They also benefit from being lightweight, making them desirable for use in spacecraft. However, these devices are composed of group III-V compound semiconductors, such as indium-gallium-arsenide (InGaAs), aluminum-arsenide

(AlAs), etc., which are very difficult and expensive to process, as well as environmentally harmful.

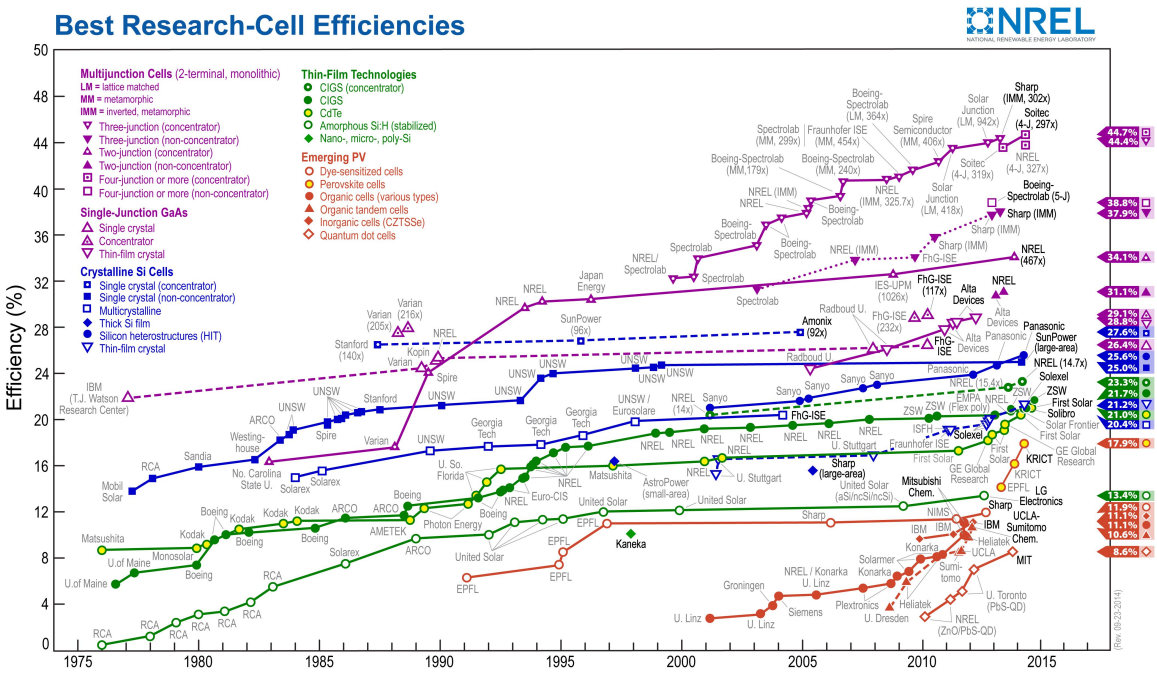

Figure 1.1: National renewable energy laboratory (NREL) chart of best performing research solar cell efficiencies, organized by the reporting lab and device type.[13]

Silicon (Si) based cells are widely used in applications from solar powered calculators to rooftop solar paneling. This is primarily due to a combination of their high power conversion efficiency (PCE ~ 20%) and the decreasing cost of silicon leading to a decrease in the overall energy cost.[14] However, to achieve high efficiencies, very pure and crystalline Si must be used to process thick enough (150-200 um) wafers. This process expends significant amounts of CO_2 and can have issues with durability, which can affect their long term use under harsh environmental conditions.[15]

Kallmann and Pope first observed the photovoltaic effect with organic materials in 1959.[16, 17] Upon exciting a single crystal of anthracene (Figure 1.2) between two transparent electrical contacts, they observed a significant reduction

in resistance compared to the dark resistance, indicative of the formation of a photodiode. These results sparked the investigation of a variety of other vapor deposited single crystals, however, the response from these materials was very low.

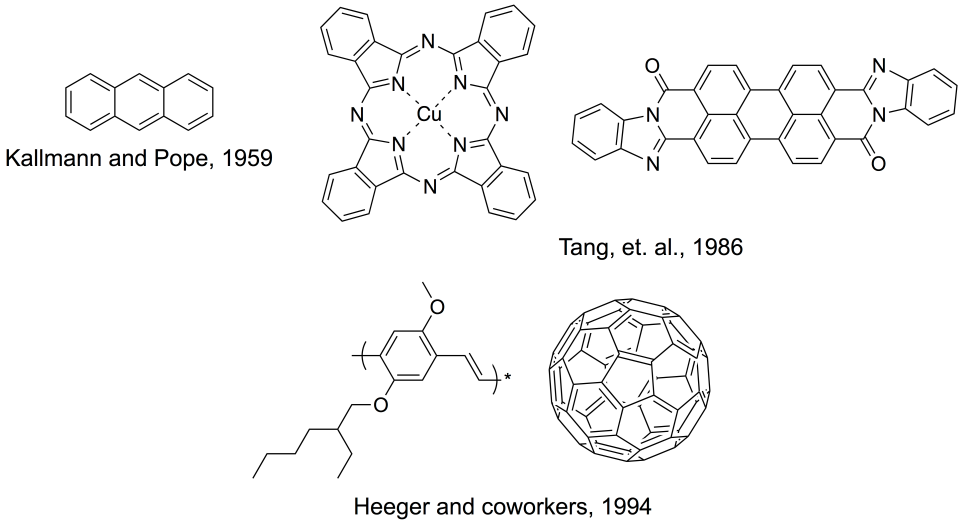

Figure 1.2: Materials used in early organic photovoltaic devices.

In 1986, Tang reported the formation of a bilayer device that reached a power conversion efficiency (PCE) of 1%.[18, 19] This was achieved through the deposition of perylene derivative onto copper phthalocyanine (Figure 1.2). The interface between the electron rich (phthalocyanine) and electron deficient (perylene) molecules, both of which acted as light harvesters, facilitated the generation of free charged through exciton dissociation. In 1994, Heeger and coworkers reported a device composed of a phenylene vinylene based conjugated polymer (MEH-PPV) blended with the electron deficient C_{60} molecule prior to active layer deposition (Figure 1.2). They observed a significant improvement in the photoresponsive behavior of the active materials due to the formation of a bulk heterojunction (BHJ).[20] Since then, the conjugated polymer: fullerene BHJ combination has become the premier method for fabrication of OPV devices.

1.2.1 Organic Photovoltaic Device Operation

Compared to inorganic photovoltaic materials, conjugated polymer and small molecule based photovoltaics are in their nascent stage. However, several intrinsic properties have allowed their efficiencies to exceed 10%. Such properties include the advancement in the design of semiconductors, processing techniques, BHJ morphology and increased absorption coefficients of organic materials. Organic photovoltaic devices undergo a four-step process to convert solar energy to electrical current: photoexcitation and exciton diffusion, exciton dissociation, free charge transport and charge collection.

1.2.1.1 Photoexcitation

Irradiation of the chromophore promotes an electron from the highest occupied molecular orbital (HOMO) to the lowest unoccupied molecular orbital (LUMO) generating a couloumbically bound electron-hole pair, or exciton. The ability to do so depends on two factors, the energy of the photon exciting the chromophore and the energy difference between the HOMO and LUMO of the chromophore, or the band gap. Figure 1.3 shows the solar irradiance spectrum, which describes the energy and intensity of solar light according to the AM 1.5G classification.[21] The spectrum is most intense in the Vis-NIR region of the electromagnetic spectrum (400-1000 nm). To harness as many photons as possible, the absorption of the chromophore should overlap the solar irradiance as much as possible. Because of this, significant effort has gone into the development of low band gap (LBG) materials.

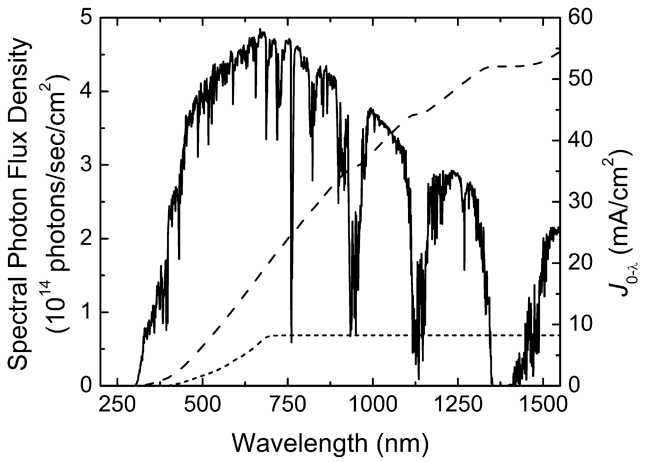

Figure 1.3: Solar irradiance flux density of the AM1.5 G spectrum (solid line), and cumulative photon current density for the photons in the spectrum (dashed line).

Once the exciton is formed, it can follow several pathways including relaxation to the ground state through recombination of the electron and hole, intersystem transfer to generate the triplet excited state or diffusion and exciton dissociation. The distance that an exciton can diffuse before relaxation is called the exciton diffusion length, L_D, and is often in the sub-50 nm length scale.[22, 23] If an exciton is generated a distance greater than L_D from a D-A interface, it will be unable to contribute to the photogenerated current due to its relaxation. Because of this, bulk heterojunction devices, where the donor and acceptor materials are intimately mixed in such a way that the active layer consists of interpenetrating nano-sized donor and acceptor domains, are favorable for effective harvesting of excitons.

1.2.1.2 Charge Transfer

At the D-A interface, the electron residing in the LUMO of the donor can be transferred to the acceptor through an energetically favorable charge transfer process. The efficiency of this process is dependent on the energy difference

between the LUMO of the donor and the LUMO of the acceptor. This optimum energy difference for effective charge transfer between the two LUMOs should be ≥ 0.3 eV; differences lower than this value can result in reversible charge transfer (Figure 1.4). Since the LUMO level of one of the most commonly used acceptor, [6,6]-phenyl C_{61}-butyric acid methyl ester ($PC_{61}BM$), is between -3.7 and -4.2 eV, the ideal donor polymer is believed to have a LUMO of -3.9 eV. The tunability of organic semiconductors lends itself well to the need for this energy difference, as conjugated polymers can be intelligently designed with this need in mind.

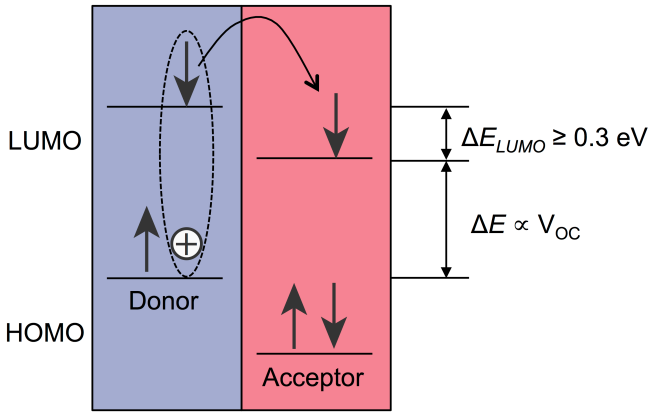

Figure 1.4: : Schematic energy level diagram of the donor-acceptor interface in an organic photovoltaic, illustrating the energetically favorable charge transfer process.

You, et. al., reported the use of a "weak donor-strong acceptor" concept to tune the energy levels of donor polymers.[24, 25] While LBG materials are generated through orbital mixing between the donor and acceptor units, it has been shown that independent tuning of the HOMO and LUMO is possible through conjugation of a "weak donor" with a "strong acceptor". This ensures proper orbital overlap for charge transfer, as well as optimization of the open circuit voltage (V_{OC}), which is directly related to the energy difference between the LUMO of the acceptor and HOMO of the donor.

1.2.1.3 Charge Transport

Once in the charge separated state, the free electron and hole can be transported away from the D-A interface through the hole transporting (p-type) and electron transporting (n-type) materials, respectively. Hole and electron transport in organic semiconductors is facilitated through intra- and intermolecular mechanisms through the HOMOs and LUMOs, respectively. Delocalization of these orbitals throughout the bulk through planarization of the conjugated semiconductors encourages intrachain charge transport and interchain charge hopping. However, these charges are still susceptible to relaxation pathways that would render them unable to be collected at their respective electrodes. Ensuring balanced transport of each charge is helpful to limit charge annihilation. With that, tuning the morphology towards a well-organized bulk heterojunction is ideal.

Bulk heterojunction devices are achieved by deposition of a blended solution of donor and acceptor materials. This yields a somewhat random distribution of donor and acceptor throughout the film but cannot guarantee nanoscale phase segregation. Continuous D-A domains are required for uninhibited transport of free charges. Various techniques including thermal annealing, solvent annealing, co-solvent addition and molecular engineering can be very useful to limit the formation of large domains. These methods can also improve crystallinity within the domains, increasing intermolecular orbital overlap and improving the charge transport properties.

1.2.1.4 Charge Extraction

Once these charges reach their respective electrodes, they can be extracted, generating the electrical current. Device architecture and interfacial layers play a large role in optimizing the correct charge at each electrode. Several device architectures have been explored, including direct, inverted and tandem cells (Figure 1.5).[26-30] The most commonly used are the direct cells. These devices incorporate a hole transporting layer between the transparent indium-tin-oxide (ITO) electrode and the active layer to facilitate hole extraction by this electrode, while blocking any electrons that may reach this interface. While a variety of materials have been developed for this application, poly(ethylenedioxy)thiophene:polystyrene sulfonate (PEDOT:PSS) is the most commonly used hole-transporting layer. Also, through modification of its work function, the properties of the back metal electrode can also be tuned to improve electron extraction from the active layer. Generally, LiF/Al or Ca/Al electrodes are used, with Ca/Al often yielding improved interfacial contact. Inverted devices reverse the flow of charges, extracting electrons at ITO and holes at the back electrode. This is achieved using a film of metal oxide (TiO_2, ZnO) semiconducting nanostructures at the ITO-active layer interface and a hole-transporting layer at the back electrode interface.

Tandem cells combine a high band gap front cell capable of harvesting high-energy photons, an interconnecting interfacial layer and a LBG back cell to harvest low energy photons.[31] Placing these devices in series yield very high V_{OC} due to the minimization of photonic energy loss. Yang and coworkers demonstrated this to

yield efficiencies above 10%.[32] However, due to the complex device architecture, this method is less often explored, compared to direct and inverted cells.

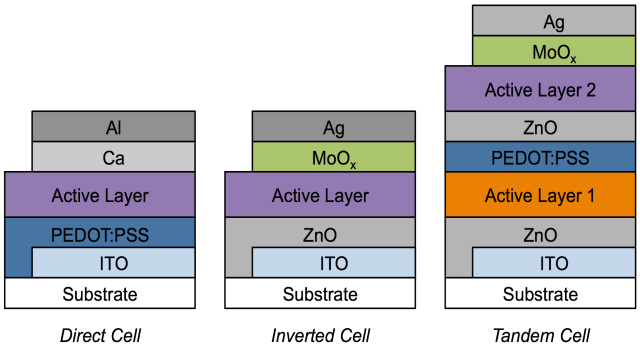

Figure 1.5: Examples of the architectural components in various organic photovoltaic devices.

1.2.2 OPV Device Evaluation

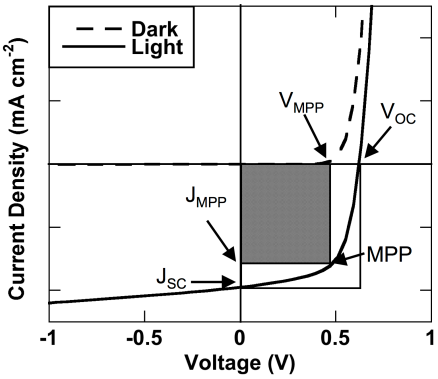

Figure 1.6: Example of *J-V* curve obtained under dark (dashed) and illuminated (solid) conditions.

Fabricated OPV devices are evaluated based on several figures of merit extracted from the current density-voltage (*J-V*) curve obtained when a voltage is applied to the device either in the dark or under illumination. Figure 1.6 shows representative *J-V* curves under each state. Devices showing proper operation exhibit diode-like behavior, with saturated current at reverse bias and exponential current growth at forward bias. The power conversion efficiency (PCE) is determined under illumination using the following equation:

$$PCE = \frac{P_{out}}{P_{in}}$$

where P_{in} is the power input of the irradiant light, generally 100 mW/cm^2. P_{out} is defined by the following equation:

$$P_{out} = J_{SC} \times V_{OC} \times FF$$

where J_{SC} is the short circuit current density, or the maximum current across the cell when no voltage is applied, V_{OC} is the open circuit voltage, or the maximum potential across the cell when no current is flowing, FF is the fill factor, which is the ratio of theoretical power output, given by the product of the short circuit current density and the open circuit voltage, to the maximum power output, given by the maximum power point (MPP), as shown below.

$$FF = \frac{(J_{MPP} \times V_{MPP})}{(J_{SC} \times V_{OC})}$$

1.2.3 Conjugated Semiconductors for OPVs

Conjugated polymer and small molecule semiconductors are prime candidates for chromophores in PV devices since their delocalized π electron systems allow for the absorption of light. The absorption spectra for these compounds often fall in the visible range of the electromagnetic spectrum. Moreover, through molecular engineering, the optical and electronic properties can be effectively tuned to broaden the absorption spectrum and maximize light absorption.[23, 33, 34] The design of conjugated polymer or small molecule

chromophores often begins with the selection of an electron rich "donor" unit and electron deficient "acceptor" unit. Placing these moieties in conjugation allows for mixing of their respective frontier molecular orbitals, generating a "push-pull" system and an intramolecular charge transfer (ICT) band in the absorption band.[30] The extent of orbital mixing is changed by effective conjugation, planarity of conjugated backbone and relative donor or acceptor strength of the electron rich or electron poor moiety, respectively.

Conjugated polymer semiconductors benefit from several properties for use in organic electronics including high molecular weight and solubility in a variety of organic solvents. These allow for good processability and film forming characteristics. Also, the extended conjugated backbone can allow for good interchain overlap, facilitating effective charge hopping. One of the most extensively studied conjugated polymer semiconductors in the field of organic photovoltaics is poly(3-hexylthiophene) (P3HT). [35, 36] P3HT is used in BHJ devices consisting of P3HT:PCBM active layers showed a range of efficiencies, with the device properties affected by a variety of properties including molecular weight, dispersity, regioregularity, processing solvent, etc. This is true in other conjugated polymers as well.[37, 38]

1.2.4 BODIPY for OPVs

Although polymers have extended conjugation and good film forming properties, they often suffer from variations in molecular weight and batch-to-batch inconsistencies due to their difficult purification. This can greatly affect the

crystallinity of the polymer in thin films. Alternatively, small molecules possess a well-defined molecular structure with high purity from batch-to-batch. However, their short conjugation lengths can potentially limit their absorption properties. One approach to improve the absorption properties includes the introduction of dye molecules for light harvesting.[39]

Since the inception of photovoltaics, dye materials have been used as light harvesters, drawing inspiration from the process of photosynthesis, where solar energy is converted into sustenance for plant life. Small molecule dyes, such as isoindigo, diketopyrrolopyrrole, squaraine, porphyrin derivatives, etc., are widely used in both natural and industrial applications due to their light harvesting and emission properties and they have gained much attention as building blocks for both small molecule and polymeric organic semiconductors.[40-46] These dyes are generally composed of fused aromatic systems, which give large, multicyclic planar moieties capable of intense visible absorption. Depending on the heteroatoms incorporated into the dye structure, either an electron rich "donor" moiety or an electron deficient "acceptor" moiety can be generated.

4,4-difluoro-4-bora-3a,4a-diaza-s-indacene, or BODIPY, is a unique dye molecule that has been extensively studied for use in a variety of applications including molecular imaging, stimuli responsive indication and photodynamic

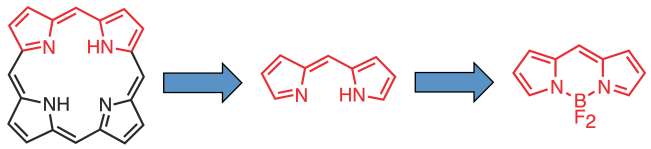

Figure 1.7: Molecular structure of 4,4-difluoro-4-bora-3a,4a-diaza-s-indacene (BODIPY), derived from the building block of chlorophyll (porphyrin).

therapy due to its robust absorption and emission properties. The structure of the BODIPY dye is shown in Figure 1.7. The BODIPY structure is essentially one half of porphyrin, the aromatic building block of chlorophyll, chelated with a boron difluoride unit. While the large, aromatic, heterocyclic structure is capable of acting as an efficient light harvester, its rigid molecular structure makes solution processing difficult without significant structural modification.[46] Also, structural modification of porphyrin is not at all trivial. BODIPY retains the intense visible absorption and excellent photochemical stability of porphyrin with the benefit of being smaller and easier to synthesize.[47] In addition, several positions on the BODIPY structure are available for substitution. This provides the potential for introducing BODIPY into "push-pull" systems to tune their optical and electrochemical properties.[48, 49]

We have recently incorporated the BODIPY dye in a series of conjugated alternating copolymers in which the BODIPY was determined to act as either a donor or acceptor, depending on the ionization potential and electron affinity of the comonomer unit.[50, 51] As a result we were able to demonstrate control of both the oxidation and reduction potential of the resulting polymer through careful selection of the comonomer unit. The tunable electrochemical properties lend themselves well to the use of BODIPY based materials as organic semiconductors.

The crystallinity of polymer thin films often suffers due to the molecular variations and purification difficulties. Alternatively, small molecules possess a well-defined molecular structure with high purity from batch-to-batch, which often leads to great crystallinity.[39] There have been many examples of BODIPY based materials

being used in field effect transistors, as well as organic and dye sensitized solar cells.[52-57]

1.3 Organic Field Effect Transistors

Field effect transistors (FETs) have many applications in our day-to-day life including portable, label free sensors, RFIDs, and logic based devices, which can impact in biomedical and electronics fields.[58, 59] While inorganic devices are widely used, organic field effect transistors are especially attractive, as organic materials soluble in organic solvents, facilitating the fabrication of flexible and lightweight devices.

1.3.1 Device Architecture

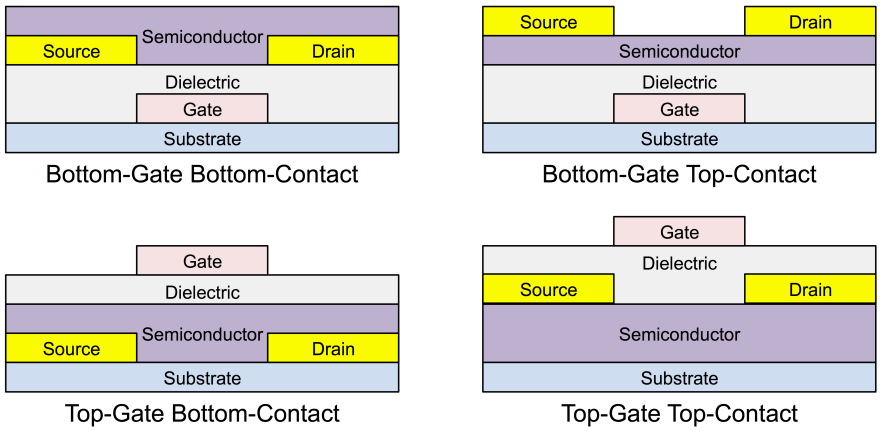

Figure 1.8: Various field effect transistor device architectures.

The typical FET device architecture is classified according to the structure of the gate and source and drain electrodes with respect to the semiconductor. Figure 1.8 shows the various available device architectures. In bottom-gate devices, the gate/dielectric is coated with the semiconductor through solution (polymer, small

molecules) or vapor (volatile small molecules and oligomers) deposition techniques.[60-63] The source and drain electrodes are then deposited on top of the semiconductor in top contact devices; whereas in bottom-contact devices, the source and drain electrodes are deposited onto the substrate, followed by deposition of the semiconductor. Alternatively, in top-gated devices, the gate electrode is deposited on top of the semiconductor, with the source and drain electrodes being on either the top or the bottom, depending of the type of contact.

1.3.2 Device Operation

Operation of the FET device requires the induction of charge carriers in the semiconductor through the application of a bias at the gate electrode. The electric field generated by applying a negative V_G destabilizes the frontier molecular orbitals in the semiconductor, bringing the HOMO level closer to the Fermi level of the source and drain electrodes and inducing positive charges in the semiconductor. Application of a negative voltage at the drain electrode drives the transport of the mobile charges through the semiconductor. Alternatively, application of a positive voltage at the gate electrode stabilizes the HOMO and LUMO, bringing the LUMO to the Fermi level of the source and drain electrodes and inducing negative charges, which can be transported upon applying a positive drain voltage. The mobility of the transported charge is specifically of interest when evaluating the effectiveness of the semiconducting material.

The charge carrier type of the semiconductor is believed to be directly related to HOMO/LUMO energy levels as they relate to the Fermi level of source and

drain electrodes.[64] Molecular orientation at the insulator/semiconductor interface, intermolecular interactions and the overall order can greatly affect the available pathways for charge transport along the length of the channel.[65]

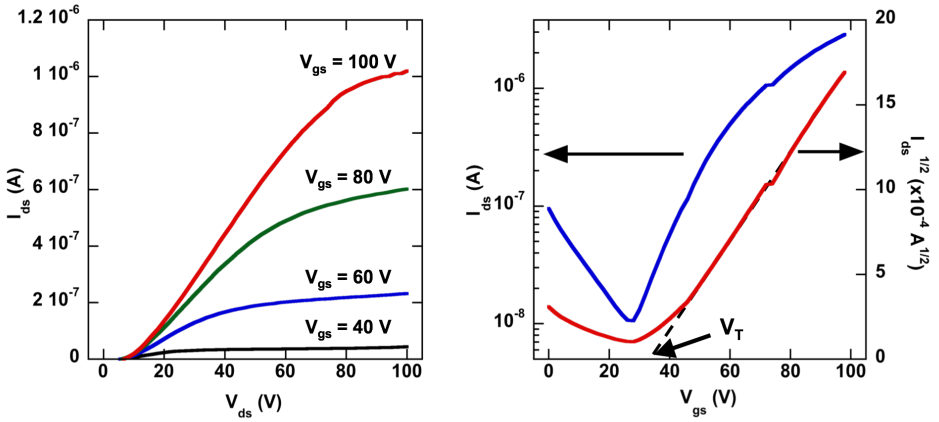

Figure 1.9: Output (left) and transfer (right) characteristics of a solution processed n-type small molecule organic semiconductor fabricated using the bottom-gate bottom-contact device architecture.[66]

Figure 1.9 shows the output and transfer FET characteristics of an organic semiconducting small molecule measured in a bottom-gate bottom-contact device. The output characteristics were obtained by plotting the source-drain current (I_{ds}) against the applied drain voltage (V_{ds}) at various gate voltages (V_{gs}). From here, we can qualitatively determine if the semiconductor is p-type, n-type or ambipolar according to which quadrant shows gate-dependent improvements in I_{ds} during the sweeping of V_{ds}. Given that the I_{ds}-V_{ds} plots in Figure 1.9 show gate dependent characteristics in quadrant II, the semiconductor can be considered n-type. If a similar response were observed in quadrant IV, the semiconductor would be considered p-type.

Analysis of the saturated regime of the transfer characteristics, which are generated by sweeping V_{gs} at a constant V_{ds}, can quantify the charge carrier mobility using the following equation:

$$I_{ds}^{sat} = \frac{\mu^{sat} C_i W}{2L} \left(V_{gs} - V_T\right)^2$$

where I_{ds}^{sat} is the drain current in the saturated regime of the transfer characteristics, C_i is the dielectric capacitance, W is the width of the transport channel, L is distance between the source and drain electrodes and V_T is the threshold voltage.

1.4 Summary

The need for clean, renewable energy sources is imperative. While there are a variety of available options, they all combine for a very small fraction of global energy consumption. Organic electronics, specifically organic photovoltaics, hold great potential as renewable energy sources. Organic photovoltaics benefit from high absorption coefficients, tunable electronic properties, facile processing methods and overall low device cost. However, they also suffer from low efficiencies compared to their inorganic counterparts.

Significant efforts in intelligent design have been put forth to generate the "ideal" semiconductor for use as a donor material in the active layer of OPV devices. Alternating copolymers often use the "weak donor-strong acceptor" approach to predict the positions of the frontier molecular orbitals and lower the band gap for maximum absorption and favorable charge dissociation. Dye materials have also

been incorporated in conjugated polymers and small molecules for improved light absorption.

In this dissertation, a small molecule BODIPY dye based acceptor-donor-acceptor system will be investigated for organic photovoltaic applications. In Chapter 2, the initial design of the system will be discussed, highlighting the versatility of the synthetic method and the predictable optical and electrochemical properties. Results obtained from fabricated organic electronic devices will also be discussed. In Chapter 3, the implications of modification to the optical and electrochemical properties of the "acceptor-donor-acceptor" (A-D-A) system will be described. In Chapter 4, previously mentioned results and conclusions will be summarized, along with the future directions for this work.

1.5 References

1. *Annual Energy Review (2012)*; U.S. Energy Information Administration.

2. Kamat, P. V., Meeting the Clean Energy Demand: Nanostructure Architectures for Solar Energy Conversion. *J. Phys. Chem. C* **2007**, 111, 2834-2860.

3. Swanson, R. M., Applied physics. Photovoltaics power up. *Science* **2009**, 324, 891-892.

4. Dresselhaus, M. S.; Thomas, I. L., Alternative energy technologies. *Nature* **2001**, 414, 332-337.

5. Dickinson, R. E.; Cicerone, R. J., Future Global Warming from Atmospheric Trace Gases. *Nature* **1986**, 319, 109-115.

6. Newman, C. R.; Frisbie, C. D.; da Silva Filho, D. A.; Brédas, J.-L.; Ewbank, P. C.; Mann, K. R., Introduction to Organic Thin Film Transistors and Design of n-Channel Organic Semiconductors. *Chem. Mater.* **2004**, 16, 4436-4451.

7. Yan, H.; Chen, Z.; Zheng, Y.; Newman, C.; Quinn, J. R.; Dotz, F.; Kastler, M.; Facchetti, A., A high-mobility electron-transporting polymer for printed transistors. *Nature* **2009**, 457, 679-686.

8. Smith, J.; Hamilton, R.; McCulloch, I.; Stingelin-Stutzmann, N.; Heeney, M.; Bradley, D. D. C.; Anthopoulos, T. D., Solution-processed organic transistors based on semiconducting blends. *J. Mater. Chem.* **2010**, 20, 2562-2574.

9. Zhao, Y.; Di, C. A.; Gao, X.; Hu, Y.; Guo, Y.; Zhang, L.; Liu, Y.; Wang, J.; Hu, W.; Zhu, D., All-solution-processed, high-performance n-channel organic transistors and circuits: toward low-cost ambient electronics. *Adv. Mater.* **2011**, 23, 2448-2453.

10. Gregg, B. A.; Hanna, M. C., Comparing Organic to Inorganic Photovoltaic Cells: Theory, Experiment, and Simulation. *J. Appl. Phys.* **2003**, 93, 3605-3614.

11. del Alamo, J. A., Nanometre-scale electronics with III-V compound semiconductors. *Nature* **2011**, 479, 317-323.

12. Yan, X.; Poxson, D. J.; Cho, J.; Welser, R. E.; Sood, A. K.; Kim, J. K.; Schubert, E. F., Enhanced Omnidirectional Photovoltaic Performance of Solar Cells Using Multiple-Discrete-Layer Tailored- and Low-Refractive Index Anti-Reflection Coatings. *Adv. Funct. Mater.* **2013**, 23, 583-590.

13. Best Research-Cell Efficiencies http://www.nrel.gov/ncpv/images/efficiency_chart.jpg.

14. Chu, S.; Majumdar, A., Opportunities and challenges for a sustainable energy future. *Nature* **2012**, 488, 294-303.

15. Fthenakis, V.; Alsema, E., Photovoltaics Energy Payback Times, Greenhouse Gas Emissions and External Costs: 2004–early 2005 Status. *Prog. Photovolt. Res. Appl.* **2006**, 14, 275-280.

16. Kallmann, H.; Pope, M., Photovoltaic Effect in Organic Crystals. *J. Chem. Phys.* **1959**, 30, 585-586.

17. Benanti, T. L.; Venkataraman, D., Organic solar cells: an overview focusing on active layer morphology. *Photosyn. Res.* **2006**, 87, 73-81.

18. Tang, C. W., Two-layer organic photovoltaic cell. *Appl. Phys. Lett.* **1986**, 48, 183-185.

19. Spanggaard, H.; Krebs, F. C., A brief history of the development of organic and polymeric photovoltaics. *Sol. Energ. Mat. Sol. Cells* **2004**, 83, 125-146.

20. Yu, G.; Pakbaz, K.; Heeger, A. J., Semiconducting polymer diodes: Large size, low cost photodetectors with excellent visibleultraviolet sensitivity. *Appl. Phys. Lett.* **1994**, 64, 3422-3424.

21. Potscavage, W. J.; Sharma, A.; Kippelen, B., Critical interfaces in organic solar cells and their influence on the open-circuit voltage. *Acc. Chem. Res.* **2009**, 42, 1758-1767.

22. Mikhnenko, O. V.; Azimi, H.; Scharber, M.; Morana, M.; Blom, P. W. M.; Loi, M. A., Exciton diffusion length in narrow bandgap polymers. *Energy Environ. Sci.* **2012**, 5, 6960-6965.

23. Günes, S.; Neugebauer, H.; Sariciftci, N. S., Conjugated polymer-based organic solar cells. *Chem. Rev.* **2007**, 107, 1324-1338.

24. Zhou, H.; Yang, L.; Liu, S.; You, W., A Tale of Current and Voltage: Interplay of Band Gap and Energy Levels of Conjugated Polymers in Bulk Heterojunction Solar Cells. *Macromolecules* **2010**, 43, 10390-10396.

25. Zhou, H.; Yang, L.; You, W., Rational Design of High Performance Conjugated Polymers for Organic Solar Cells. *Macromolecules* **2012**, 45, 607-632.

26. Carsten, B.; Szarko, J. M.; Son, H. J.; Wang, W.; Lu, L.; He, F.; Rolczynski, B. S.; Lou, S. J.; Chen, L. X.; Yu, L., Examining the effect of the dipole moment on charge separation in donor-acceptor polymers for organic photovoltaic applications. *J. Am. Chem. Soc.* **2011**, 133, 20468-20475.

27. Thambidurai, M.; Kim, J. Y.; Ko, Y.; Song, H. J.; Shin, H.; Song, J.; Lee, Y.; Muthukumarasamy, N.; Velauthapillai, D.; Lee, C., High-efficiency inverted organic solar cells with polyethylene oxide-modified Zn-doped TiO2 as an interfacial electron transport layer. *Nanoscale* **2014**, 6, 8585-8589.

28. Yao, K.; Intemann, J. J.; Yip, H. L.; Liang, P. W.; Chang, C. Y.; Zang, Y.; Li, Z. A.; Chen, Y. W.; Jen, A. K. Y., Efficient all polymer solar cells from layer-evolved processing of a bilayer inverted structure. *J. Mater. Chem. C* **2014**, 2, 416-420.

29. Takacs, C. J.; Sun, Y.; Welch, G. C.; Perez, L. A.; Liu, X.; Wen, W.; Bazan, G. C.; Heeger, A. J., Solar cell efficiency, self-assembly, and dipole-dipole interactions of isomorphic narrow-band-gap molecules. *J. Am. Chem. Soc.* **2012**, 134, 16597-16606.

30. Beaujuge, P. M.; Frechet, J. M., Molecular design and ordering effects in pi-functional materials for transistor and solar cell applications. *J. Am. Chem. Soc.* **2011**, 133, 20009-20029.

31. Jo, J.; Pouliot, J. R.; Wynands, D.; Collins, S. D.; Kim, J. Y.; Nguyen, T. L.; Woo, H. Y.; Sun, Y.; Leclerc, M.; Heeger, A. J., Enhanced efficiency of single and tandem organic solar cells incorporating a diketopyrrolopyrrole-based low-bandgap polymer by utilizing combined ZnO/polyelectrolyte electron-transport layers. *Adv. Mater.* **2013**, 25, 4783-4788.

32. You, J.; Dou, L.; Yoshimura, K.; Kato, T.; Ohya, K.; Moriarty, T.; Emery, K.; Chen, C. C.; Gao, J.; Li, G.; Yang, Y., A polymer tandem solar cell with 10.6% power conversion efficiency. *Nat. Commun.* **2013**, 4, 1446.

33. Scharber, M. C.; Mühlbacher, D.; Koppe, M.; Denk, P.; Waldauf, C.; Heeger, a. J.; Brabec, C. J., Design Rules for Donors in Bulk-Heterojunction Solar Cells—Towards 10 % Energy-Conversion Efficiency. *Adv. Mater.* **2006**, 18, 789-794.

34. Lin, Y.; Li, Y.; Zhan, X., Small molecule semiconductors for high-efficiency organic photovoltaics. *Chem. Soc. Rev.* **2012**, 41, 4245-4272.

35. Dang, M. T.; Hirsch, L.; Wantz, G., P3HT:PCBM, Best Seller in Polymer Photovoltaic Research. *Adv. Mater.* **2011**, 23, 3597-3602.

36. Wu, P.-T.; Xin, H.; Kim, F. S.; Ren, G.; Jenekhe, S. A., Regioregular Poly(3-pentylthiophene): Synthesis, Self-Assembly of Nanowires, High-Mobility Field-Effect Transistors, and Efficient Photovoltaic Cells. *Macromolecules* **2009**, 42, 8817-8826.

37. Chen, C.-P.; Chan, S.-H.; Chao, T.-C.; Ting, C.; Ko, B.-T., Low-Bandgap Poly(Thiophene-Phenylene-Thiophene) Derivatives with Broaden Absorption Spectra for Use in High-Performance Bulk-Heterojunction Polymer Solar Cells. *J. Am. Chem. Soc.* **2008**, 130, 12828-12833.

38. Li, C.; Liu, M.; Pschirer, N. G.; Baumgarten, M.; Mullen, K., Polyphenylene-Based Materials for Organic Photovoltaics. *Chem. Rev.* **2010**, 110, 6817-6855.

39. He, G.; Li, Z.; Wan, X.; Liu, Y.; Zhou, J.; Long, G.; Zhang, M.; Chen, Y., Impact of dye end groups on acceptor–donor–acceptor type molecules for solution-processed photovoltaic cells. *J. Mater. Chem.* **2012**, 22, 9173-9180.

40. Deng, P.; Zhang, Q., Recent developments on isoindigo-based conjugated polymers. *Polym. Chem.* **2014**, 5, 3298-3305.

41. Liu, J. H.; Walker, B.; Tamayo, A.; Zhang, Y.; Nguyen, T. Q., Effects of Heteroatom Substitutions on the Crystal Structure, Film Formation, and Optoelectronic Properties of Diketopyrrolopyrrole-Based Materials. *Adv. Funct. Mater.* **2013**, 23, 47-56.

42. Yuan, J.; Huang, X.; Zhang, F.; Lu, J.; Zhai, Z.; Di, C.; Jiang, Z.; Ma, W., Design of benzodithiophene-diketopyrrolopyrrole based donor–acceptor copolymers for efficient organic field effect transistors and polymer solar cells. *J. Mater. Chem.* **2012**, 22, 22734-22742.

43. Sonar, P.; Ng, G.-M.; Lin, T. T.; Dodabalapur, A.; Chen, Z.-K., Solution processable low bandgap diketopyrrolopyrrole (DPP) based derivatives: novel acceptors for organic solar cells. *J. Mater. Chem.* **2010**, 20, 3626-3636.

44. Della Pelle, A. M.; Homnick, P. J.; Bae, Y.; Lahti, P. M.; Thayumanavan, S., Effect of Substituents on Optical Properties and Charge-Carrier Polarity of Squaraine Dyes. *J. Phys. Chem. C* **2014**, 118, 1793-1799.

45. Wei, G.; Xiao, X.; Wang, S.; Sun, K.; Bergemann, K. J.; Thompson, M. E.; Forrest, S. R., Functionalized squaraine donors for nanocrystalline organic photovoltaics. *ACS Nano* **2012**, 6, 972-8.

46. Huang, X.; Zhu, C.; Zhang, S.; Li, W.; Guo, Y.; Zhan, X.; Liu, Y.; Bo, Z., Porphyrin-Dithienothiophene π-Conjugated Copolymers: Synthesis and Their Applications in Field-Effect Transistors and Solar Cells. *Macromolecules* **2008**, 41, 6895-6902.

47. Benniston, A. C.; Copley, G., Lighting the way ahead with boron dipyrromethene (Bodipy) dyes. *Phys. Chem. Chem. Phys.* **2009**, 11, 4124-4131.

48. Yoshii, R.; Yamane, H.; Nagai, A.; Tanaka, K.; Taka, H.; Kita, H.; Chujo, Y., π-Conjugated Polymers Composed of BODIPY or Aza-BODIPY Derivatives Exhibiting High Electron Mobility and Low Threshold Voltage in Electron-Only Devices. *Macromolecules* **2014**, 47, 2316-2323.

49. Singh, S.; Venugopalan, V.; Krishnamoorthy, K., Organic soluble and uniform film forming oligoethylene glycol substituted BODIPY small molecules with improved hole mobility. *Phys. Chem. Chem. Phys.* **2014**, 16, 13376-82.

50. Popere, B. C.; Della Pelle, A. M.; Poe, A.; Balaji, G.; Thayumanavan, S., Predictably tuning the frontier molecular orbital energy levels of panchromatic low band gap BODIPY-based conjugated polymers. *Chem. Sci.* **2012**, 3, 3093-3102.

51. Popere, B. C.; Della Pelle, A. M.; Thayumanavan, S., BODIPY-Based Donor–Acceptor π-Conjugated Alternating Copolymers. *Macromolecules* **2011**, 44, 4767-4776.

52. Usta, H.; Yilmaz, M. D.; Avestro, A. J.; Boudinet, D.; Denti, M.; Zhao, W.; Stoddart, J. F.; Facchetti, A., BODIPY-thiophene copolymers as p-channel semiconductors for organic thin-film transistors. *Adv. Mater.* **2013**, 25, 4327-4334.

53. Lin, H. Y.; Huang, W. C.; Chen, Y. C.; Chou, H. H.; Hsu, C. Y.; Lin, J. T.; Lin, H. W., BODIPY dyes with beta-conjugation and their applications for high-efficiency inverted small molecule solar cells. *Chem. Commun.* **2012**, 48, 8913-8915.

54. Hayashi, Y.; Obata, N.; Tamaru, M.; Yamaguchi, S.; Matsuo, Y.; Saeki, A.; Seki, S.; Kureishi, Y.; Saito, S.; Yamaguchi, S.; Shinokubo, H., Facile synthesis of biphenyl-fused BODIPY and its property. *Org. Lett.* **2012**, 14, 866-869.

55. Bura, T.; Leclerc, N.; Fall, S.; Leveque, P.; Heiser, T.; Retailleau, P.; Rihn, S.; Mirloup, A.; Ziessel, R., High-performance solution-processed solar cells and ambipolar behavior in organic field-effect transistors with thienyl-BODIPY scaffoldings. *J. Am. Chem. Soc.* **2012**, 134, 17404-17407.

56. Kim, B.; Ma, B.; Donuru, V. R.; Liu, H.; Frechet, J. M., Bodipy-backboned polymers as electron donor in bulk heterojunction solar cells. *Chem. Commun.* **2010**, 46, 4148-4150.

57. Kumaresan, D.; Thummel, R. P.; Bura, T.; Ulrich, G.; Ziessel, R., Color tuning in new metal-free organic sensitizers (Bodipys) for dye-sensitized solar cells. *Chem. Eur. J.* **2009**, 15, 6335-6339.

58. Reese, C.; Roberts, M.; Ling, M.-m.; Bao, Z., Organic thin film transistors. *Mater. Today* **2004**, 7, 20-27.

59. Sokolov, A. N.; Roberts, M. E.; Bao, Z., Fabrication of low-cost electronic biosensors. *Mater. Today* **2009**, 12, 12-20.

60. Li, C.-Z.; Chueh, C.-C.; Yip, H.-L.; Zou, J.; Chen, W.-C.; Jen, A. K. Y., Evaluation of structure–property relationships of solution-processible fullerene acceptors and their n-channel field-effect transistor performance. *J. Mater. Chem.* **2012**, 22, 14976-14981.

61. Durban, M. M.; Kazarinoff, P. D.; Luscombe, C. K., Synthesis and Characterization of Thiophene-Containing Naphthalene Diimide n-Type Copolymers for OFET Applications. *Macromolecules* **2010**, 43, 6348-6352.

62. Horowitz, G.; Kouki, F.; Spearman, P.; Fichou, D.; Nogues, C.; Pan, X.; Garnier, F., Evidence for n-type conduction in a perylene tetracarboxylic diimide derivative. *Adv. Mater.* **1996**, 8, 242-245.

63. Ie, Y.; Nitani, M.; Uemura, T.; Tominari, Y.; Takeya, J.; Honsho, Y.; Saeki, A.; Seki, S.; Aso, Y., Comprehensive Evaluation of Electron Mobility for a Trifluoroacetyl-Terminated Electronegative Conjugated Oligomer. *J. Phys. Chem. C* **2009**, 113, 17189-17193.

64. Glowatzki, H.; Sonar, P.; Singh, S. P.; Mak, A. M.; Sullivan, M. B.; Chen, W.; Wee, A. T. S.; Dodabalapur, A., Band Gap Tunable N-Type Molecules for Organic Field Effect Transistors. *J. Phys. Chem. C* **2013**, 117, 11530-11539.

65. Dong, H.; Fu, X.; Liu, J.; Wang, Z.; Hu, W., 25th anniversary article: key points for high-mobility organic field-effect transistors. *Adv. Mater.* **2013**, 25, 6158-6183.

66. Poe, A. M.; Della Pelle, A. M.; Subrahmanyam, A. V.; White, W.; Wantz, G.; Thayumanavan, S., Small molecule BODIPY dyes as non-fullerene acceptors in bulk heterojunction organic photovoltaics. *Chem. Commun.* **2014**, 50, 2913-2915.

CHAPTER 2

BODIPY-BASED SMALL MOLECULES AS ELECTRON ACCEPTORS IN BULK HETEROJUNCTION ORGANIC PHOTOVOLTAICS

2.1 Introduction

The field of organic photovoltaics (OPV) has advanced in recent years through extensive investigation into various conjugated polymer and small molecule structures; examination of the properties of these materials and their potential for use as donors in bulk heterojunction (BHJ) organic solar cells has led to a better understanding of the structural criteria required to yield optimal device performance.[1-6] While significant advances have been made in the design and synthesis of donor materials, yielding high efficiency photovoltaic devices, the oft-chosen acceptor, the fullerene based [6,6]-phenyl C_{61}-butyric acid methyl ester (PCBM), remains the first, and often only choice for use in active layer blends.

Fullerene derivatives are very attractive as acceptors in BHJ OPV devices for several reasons, including high electron affinity, high electron mobility, and the ability to form favorable nanoscale morphologies when blended with many small molecule and polymeric donors.[7, 8] However, these molecules show weak absorption in the visible range of the electromagnetic spectrum, limiting their contribution to photogenerated current and requiring the donor to act as the sole light harvester. Synthesis and purification of fullerene-based acceptors is also non-trivial, making structural modifications that would lead to perturbations in the electronic structure of the material very difficult. Development of new non-fullerene based acceptors

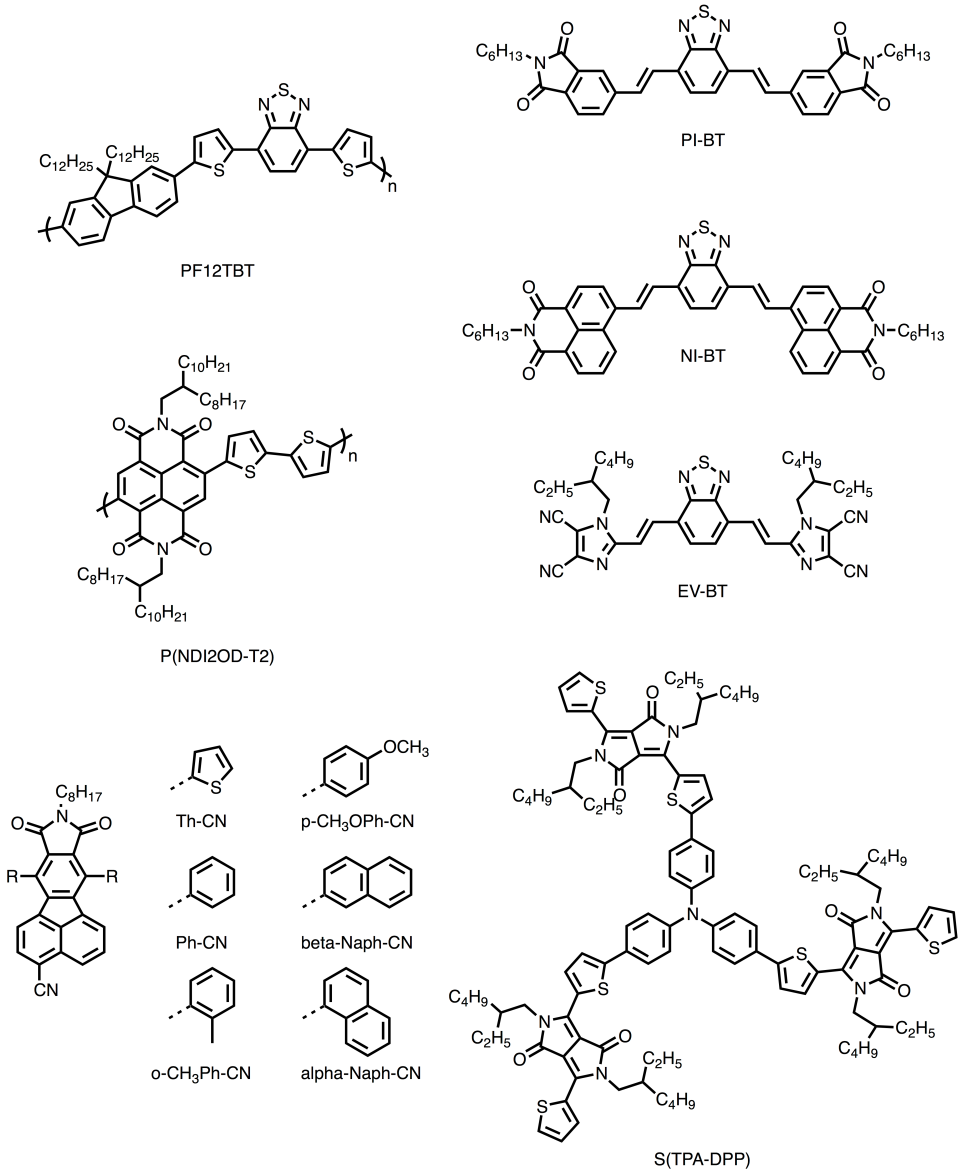

Figure 2.1: Molecular structures of several non-fullerene acceptors successfully used in P3HT based organic photovoltaic devices. Polymeric and small molecule designs often employ D-A architectures, as well as dye moieties.

will lead to the generation of a library of acceptors which may be better matched with new donor materials than current fullerene based acceptors, potentially leading to more efficient devices.[9-11]

While there has been significant effort to improve OPV device performance through the optimization of the structure and electronic properties of the donor

materials, non-fullerene electron acceptors are rarely used in bulk BHJ OPV devices. The use of non-fullerene acceptors in BHJ OPVs has gained attention in recent years.[12-15] The structures of several successful small molecule and conjugated polymer non-fullerene acceptors (NFAs) are shown in Figure 2.1. Recent examples of small molecule non-fullerene acceptors for poly(3-hexylthiophene) (P3HT) based BHJ OPV have shown promising results due to (a) improved light harvesting through the inclusion of dyes for enhanced absorption in the visible region of the solar spectrum and (b) raising of the LUMO energy level, compared to PCBM, to improve open-circuit voltages (V_{OC}) of the resultant OPV devices.[2, 10, 14, 16]

Concurrently, there has also been a surge in developing specifically small molecules as active materials for OPVs. While conjugated polymers are often regarded as low band gap materials with good film forming properties, small molecules offer several advantages over polymeric materials: they have a well defined molecular structure; their molecular weight is definite; highly pure compounds are achieved through relatively facile purification methods; small molecule synthesis provides much greater consistency from batch to batch.[2, 5] The combination of these interests has triggered our search for small molecule non-fullerene acceptors for BHJ OPV.[2, 10, 13-16] Our approach to the development of materials as NFAs for BHJ OPVs began with the investigation into methods to improve the light harvesting capabilities of the acceptor. For these purposes, we conceived the use of the 4,4-difluoro-4-bora-3a,4a-diaza-s-indacene (BODIPY) dye.

Employing BODIPY in materials for OPVs is particularly advantageous for several reasons: it possesses excellent photochemical stability; it shows strong

absorbance in the visible region, with maximum absorption falling at ca. 500 nm; its partial benzenoid and quinoid character provides the potential for stable oxidation and reduction; the optoelectronic properties of the dye are capable of being tuned through facile structural modification at several positions on the BODIPY core.[17, 18]

BODIPY based materials have had great success as small molecule donors in BHJ OPV devices,[19-21] and used as a molecular antennae in P3HT:PCBM devices.[22] Also, there are several examples of electron transporting materials based on the BODIPY dye.[23, 24] To the best of our knowledge, this is the first report of BODIPY based materials used as the sole electron acceptor in BHJ OPVs.

2.2 Molecular Design

For our design, we chose to use an acceptor-donor-acceptor (A-D-A) type architecture where BODIPY acts as the acceptor moiety, as shown in Figure 2.2. The donor moiety was decided to be variable in order to evaluate the affect of its structure on the optoelectronic properties of the final molecules. We decided to incorporate an alkylthiophene unit between the donor and the BODIPY to insure solubility of the resulting molecule in common organic solvents. This property is crucial for the solution processability of the material.

We decided to use thieno(3,2-b)thiophene (TTh), 2,2'-bithiophene (biTh), 4,8-bis(5-(2-ethylhexyl) thiophen-2-yl)benzo[1,2-b:4,5-b']dithiophene (BDT), 4,4-bis(2-ethylhexyl)-4H-cyclopenta-[2,1-b:3,4-b]dithiophene (CPDT) or N-(2-ethylhexyl)-dithieno [3,2-b:2′,3′-d]pyrrole (DTP), several well know donor moieties in the field of organic electronics. These moieties can be characterized as either

"weak donors" (TTh, biTh, BDT) or "strong donors" (CPDT, DTP) according to their ionization potential.[25] We hypothesized that this design would provide convenient access to low band-gap small molecules that could be used as acceptors in BHJ OPVs.

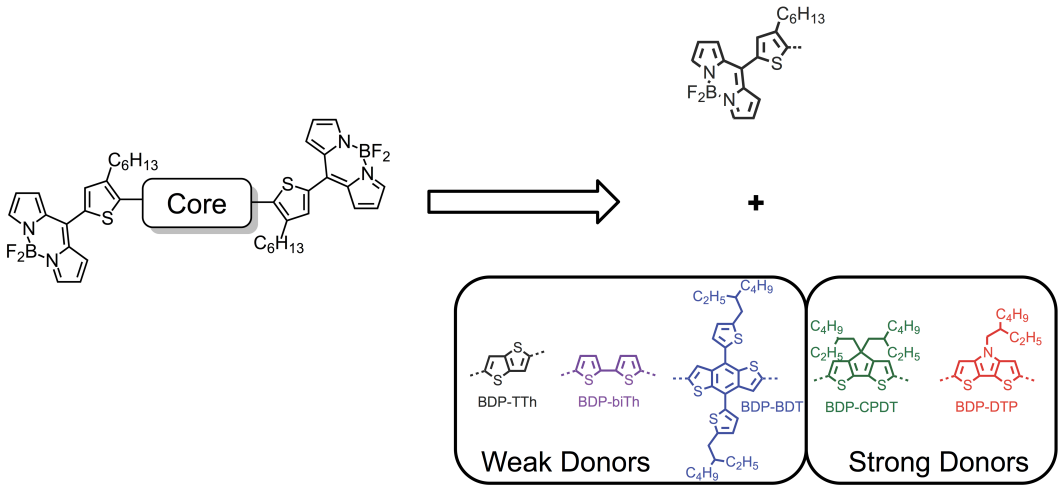

Figure 2.2: : Molecular design of small molecule BODIPY-based acceptor molecules incorporating "weak" (TTh, biTh, BDT) and "strong" (CPDT, DTP) donor core structures.

In this chapter, we report five such molecules, in which BODIPY is conjugated through its *meso* position using a 3-hexylthiophene linker to donor molecules to afford BDP-TTh, BDP-biTh, BDP-BDT, BDP-CPDT, and BDP-DTP respectively (Figure 2.2). These molecules show strong visible absorption with low lying LUMO levels, making them electronically suitable as acceptors for many donor materials. To examine their potential as acceptors in BHJ OPVs, devices were fabricated using P3HT as the donor.

2.3 Results and Discussion

2.3.1 Synthesis

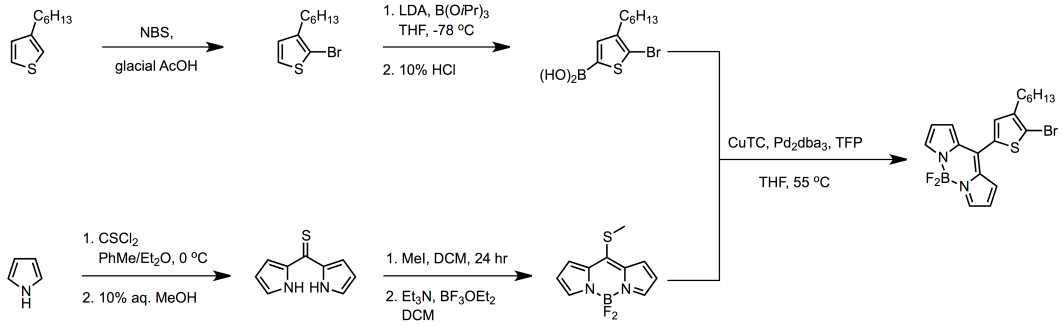

Scheme 2.1: Synthetic scheme detailing the synthesis of the BODIPY cap (8-(2-bromo-3-hexylthien-5-yl)-4,4-difluoro-4-bora-3a,4a-diaza-s-indacene).

Retrosynthetic analysis of the final BODIPY molecules allowed us to determine the synthetic approach. BODIPY based materials are often synthesized through trifluoroacetic acid catalyzed condensation of a pyrrole derivative with an aromatic aldehyde, followed by oxidation and installation of the difluoroborane unit in the presence of triethylamine (TEA). While this method is direct, the three-step process often yields the BODIPY in very poor yields.

Rather than using this approach to install the BODIPY moieties onto a dialdehyde-terminated core, we chose to take a modular approach. We synthesized the donor core and the BODIPY cap separately, allowing for a "plug-and-play" approach to generating the final molecules described here. This also greatly increases the potential of this design, since any compatible unit can be easily incorporated to yield a BODIPY capped molecule in relatively high yields.

The BODIPY cap can be further dissected into the BODIPY unit and the brominated hexylthiophene unit. The lack of β-substituents on the BODIPY moiety was expected to greatly benefit the overall planarity of the molecule due to the

limited steric interactions that often force a twist between the meso substituent and BODIPY core.[22, 26]

The detailed synthetic steps for generation of the BODIPY cap are shown in Scheme 2.1. Synthesis of the thiophene unit began with the bromination of 3-hexylthiophene using N-bromosuccinimide (NBS) in glacial acetic acid to yield 2-bromo-3-hexylthiophene. Next, the boronic acid moiety was installed at the 5-position. Lithium diisopropylamine (LDA) was used to deprotonate the second alpha position of the thiophene, which reacted with triisopropylborate, followed by acidification using dilute hydrochloric acid. The bulky base was used to ensure that the bromine survived the reaction.

Synthesis of the BODIPY unit began with a condensation reaction between pyrrole and thiophosgene to give the thione, which was then methylated using iodomethane. Finally, the difluoroboron unit was installed in the presence of TEA to give 8-(thiomethyl)-BODIPY.[27] These two units were combined through Liebeskind-Srogl coupling between 8-(thiomethyl)-BODIPY and 2-bromo-3-hexylthiophene-5-boronic acid.[28, 29]

The bis(stannylated) donors were synthesized using several well established methods, described as follows. TTh was lithiated using n-butyllithium and reacted with trimethyltin chloride to give 2,5-bis(trimethylstannyl)-thieno[3,2-b]thiophene. 5,5′-Bis(tributylstannyl)-2,2′-bithiophene was purchased and used as received. BDT was synthesized starting from thiophene-3-carboxylic acid, which was converted to

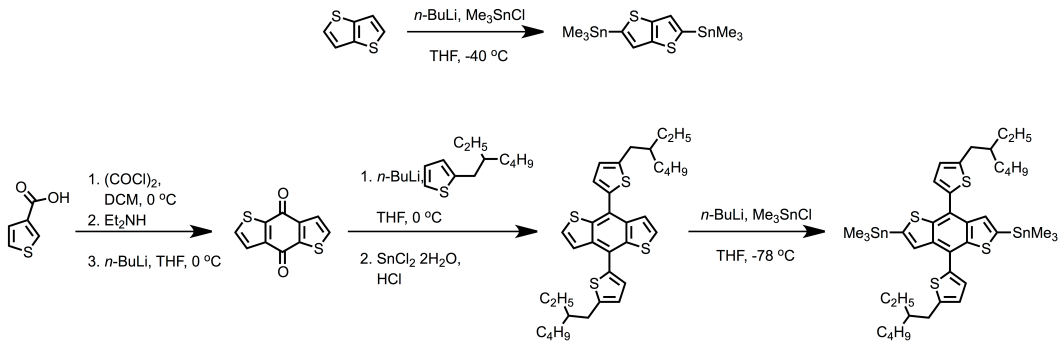

Scheme 2.2: Synthetic scheme detailing the synthesis of weak donors TTh and BDT.

thiophene-3-carbonyl chloride, followed by conversion to thiophene-3-carboxylicacid amide. The 2-position of the amide was lithiated, which prompted an intermolecular condensation to benzo[1,2-b:4,5-b']dithiophene-4,8-dione. The dione was substituted with 2-(2-ethylhexyl)thiophene, followed by aromatization/reduction to BDT, which was then stannylated under similar conditions described for TTh (Scheme 2.2).[4, 30]

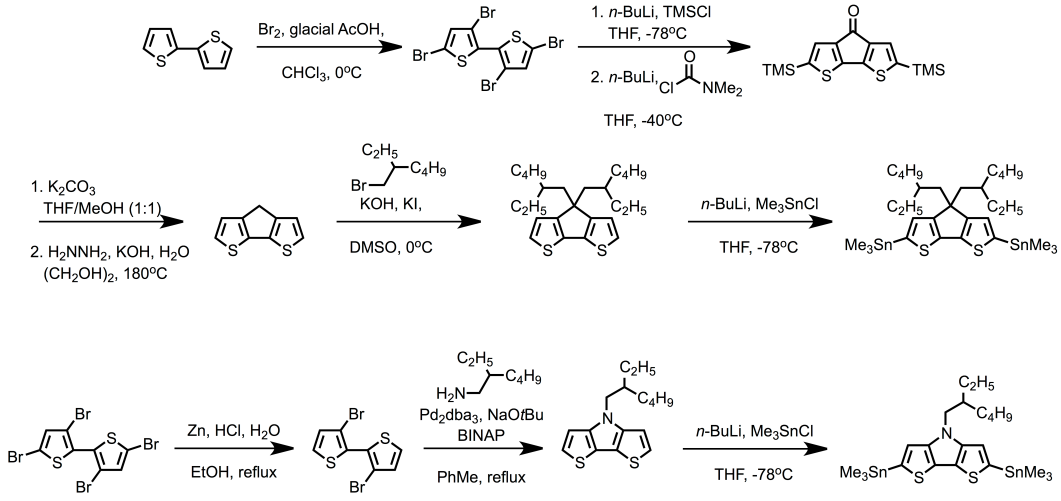

Scheme 2.3: Synthetic scheme detailing synthesis of strong donors, CPDT and DTP.

Synthesis of the strong donors began with bromination of 2,2'-bithiophene to give 3,3',5,5'-tetrabromo-2,2'-bithiophene. For CPDT, the alpha positions were then protected using trimethylsilyl (TMS) groups, followed by condensation with dimethylcabamoyl chloride. Next, the TMS groups were deprotected using basic

conditions, followed by Wolff-Kishner reduction of the ketone bridge to a methylene bridge. The bridgehead carbon was then dialkylated with 2-ethylhexyl bromide. The bis(stannylated)-CPDT was formed using similar conditions described for BDT (Scheme 2.3).[25, 31]

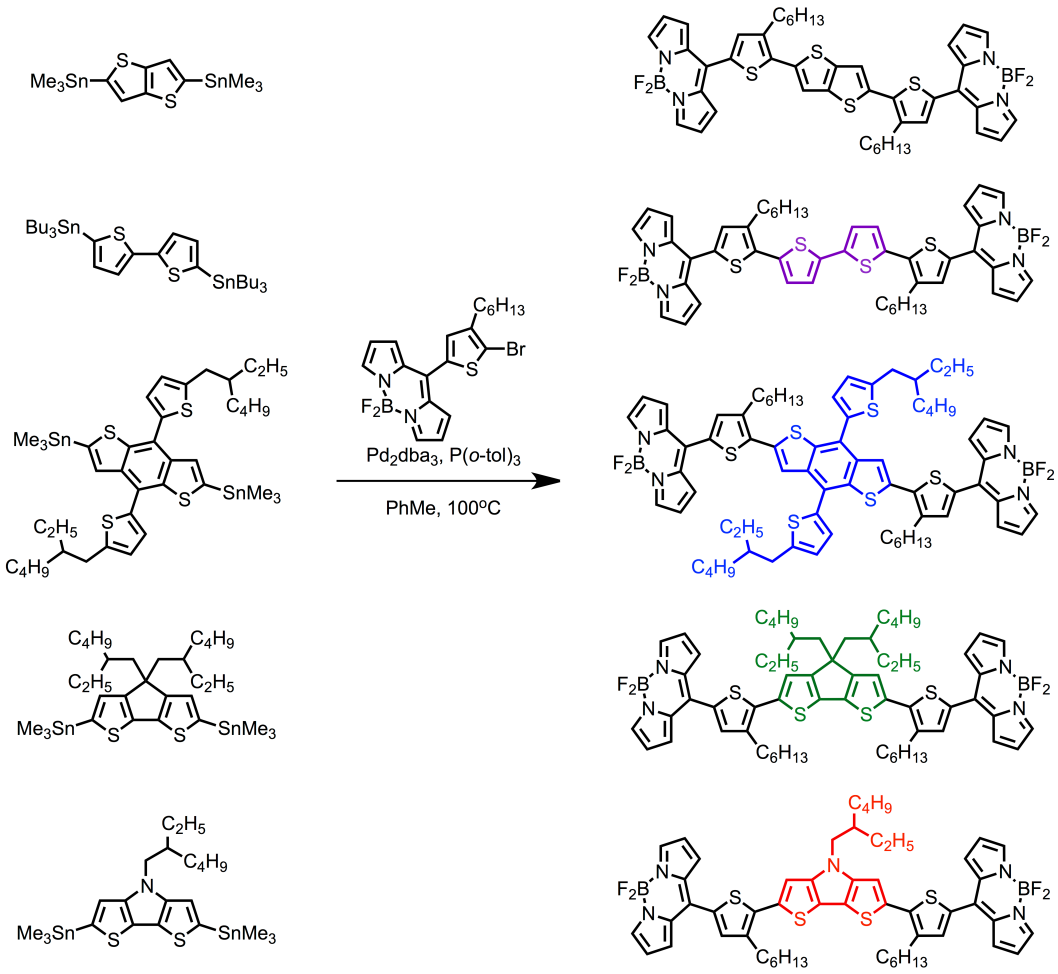

Scheme 2.4: Reaction scheme for Stille coupling conditions to yield final BODIPY acceptors.

For DTP, the alpha positions of 3,3',5,5'-tetrabromo-2,2'-bithiophene were debrominated using zinc metal under acidic conditions. The fused ring was then closed using palladium catalyzed Buchwald coupling conditions. The DTP core was then bis(stannylated) using similar conditions described for CPDT.[32]

Stille coupling between the bistannylated donors and the previously synthesized BODIPY "cap" afforded the targeted molecules in good yields (Scheme 2.4).

2.3.2 Absorption Properties

The solution state and thin film absorption properties for each of the final molecules are shown in Figure 2.3 and summarized in Table 2.1. The absorption spectra all have a similar maximum absorption with variations in the 300-425 nm and 550-850 nm ranges. All molecules exhibit an absorption maximum characteristic of a π-π^* transition in the BODIPY moiety.[20, 33] This is supported by the very similar molar absorptivity values throughout the series, with the "weak donor" cored molecule possess similar absorption coefficients (*ca.* 6 x 10^4 M^{-1} cm^{-1}) while the "strong donor" cores deviate slightly (7.2 x 10^4 and 2.5 x 10^4 M^{-1} cm^{-1} for BDP-CPDT and BDP-DTP, respectively).

BODIPY	λ^{sol}_{max} (nm)	ε (x 10^4 M^{-1} cm^{-1})	λ^{film}_{max} (nm)	λ^{film}_{onset} (nm)	E_g^{opt} (eV)
BDP-TTh	518	6.4	535	728	1.70
BDP-biTh	518	6.0	532	740	1.68
BDP-BDT	518	6.2	532	717	1.73
BDP-CPDT	516	7.6	530	805	1.54
BDP-DTP	516	2.5	532	845	1.47

Table 2.1: Tabulated absorption properties of the BODIPY based molecules. Solution state spectra measured in chlorobenzene. Thin films spin casted from concentrated dichloromethane solutions onto glass substrates and annealed for 30 minutes. Optical band gap estimated from the red edge onset of thin film absorption ($E_g^{opt} = 1240/\lambda^{film}_{onset}$).

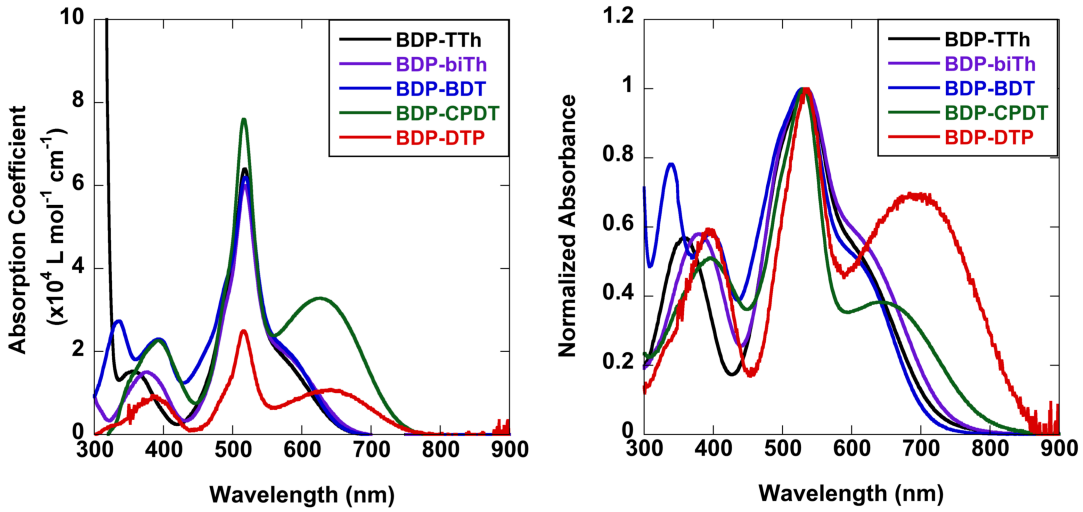

Figure 2.3: Absorption spectra of chlorobenzene solutions (left) and thin films (right) of BDP-TTh (black), BDP-biTh (purple), BDP-BDT (blue), BDP-CPDT (green) and BDP-DTP (red). The solution spectra are plotted with respect molar absorptivity. Thin film absorption spectra measured using films spin cast from concentrated dichloromethane solutions and annealed at 150 °C for 30 minutes (right) and normalized with respect to maximum absorption. Red edge absorption varies with respect to donor strength.

The high energy region shows variations that correspond to the absorption of the core moiety in both shape and intensity.[34-36] The low energy shoulder is attributed to an intramolecular charge transfer process, as its position in the solution state varies with the donor strength. In the case of the "weak donor" cored molecules, BDP-TTh, BDP-biTh, BDP-BDT, the band exists as a shoulder (*ca*. 590 nm). Installation of a "strong donor" core led to a significant red shift in the charge transfer band, yielding a 0.43 and 0.47 eV distance between the λ^{sol}_{max} and the charge transfer band for BDP-CPDT and BDP-DTP, respectively.[37]

Thin film absorption spectra are shown in Figure 2.3. In thin films, the spectra broaden significantly, red shifting both the maximum absorption (*ca.* 530 nm) and charge transfer peaks. From here, we can extract the optical band gap (E_g^{opt}) using the onset of optical absorption. While E_g^{opt} for BDP-TTh, BDP-biTh, and

BDP-BDT are comparable (1.70, 1.68, and 1.73 eV, respectively), BDP-CPDT and BDP-DTP show a significant reduction in band gap (1.54 and 1.47 eV, respectively). We can also see that the relative intensity of the charge transfer peak nearly doubles for BDP-DTP going from solution state to thin film, indicating a great improvement in intermolecular ordering.

2.3.3 Electrochemical Properties

The electrochemical properties of the molecules were examined using cyclic voltammetry. The HOMO and LUMO levels were calculated using the onset of oxidation and reduction, respectively, from the cyclic voltammograms shown in Figure 2.4. The redox potentials were measured against a Ag/Ag^+ reference cell and corrected with respect to the ferrocene/ferrocenium (Fc/Fc^+) redox couple. The extracted values are listed in Table 2.2. Each molecule shows amphoteric behavior, exhibiting two reversible oxidations and at least one reduction, which is consistent with behavior often seen in A-D-A systems.[38] The onset of the first oxidation potential for the dyes containing weak donors are very similar, with BDP-TTh possessing the most stable HOMO (-5.45 eV). Increasing the donor strength of the core moiety destabilized the HOMO energy level, as the strongest donor (BDP-DTP) possesses the least stable HOMO of -5.14 eV. E^{red} values are similar throughout the series, indicating the reduction of the BODIPY moiety within the molecule is relatively unaffected by the donor strength of the core moiety. Since each of these molecules possesses a LUMO significantly lower than that of P3HT (-2.74 eV), it can

be assumed that efficient exciton dissociation is possible, allowing them to be considered as candidates for acceptors in BHJ devices.

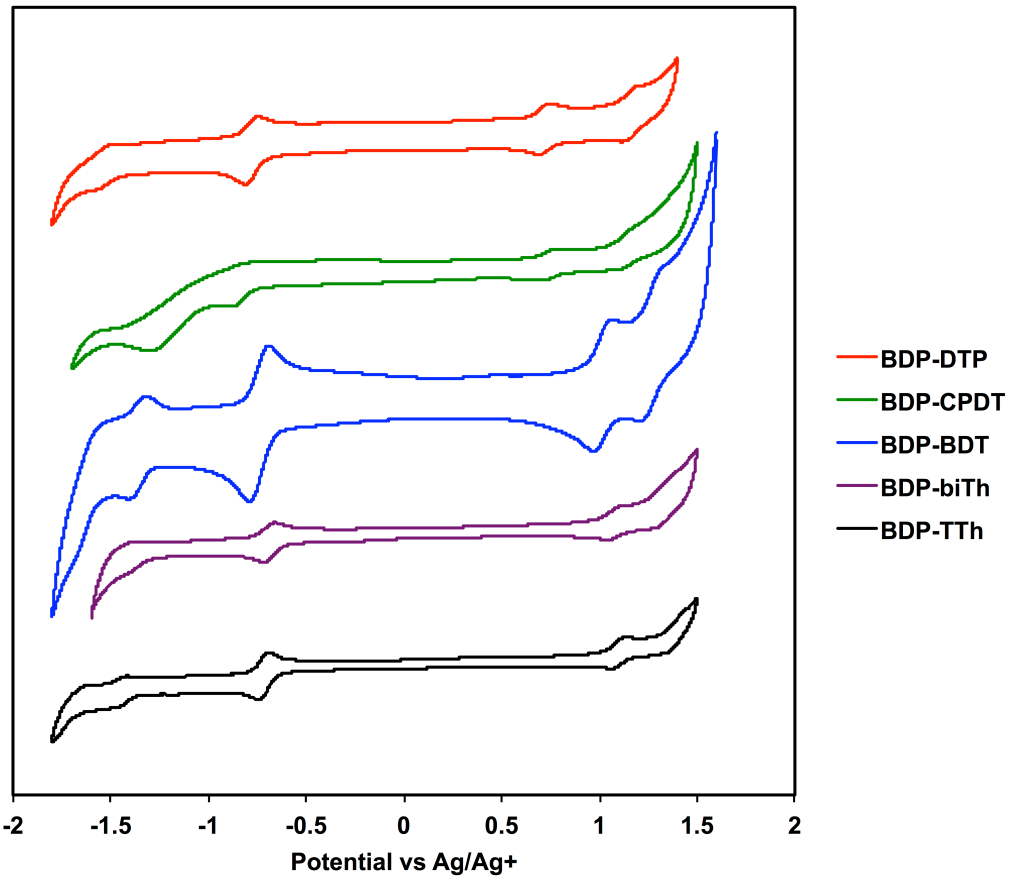

Figure 2.4: Cyclic voltammograms of BDP-TTh (black), BDP-biTh (purple), BDP-BDT (blue), BDP-CPDT (green) and BDP-DTP (red). The spectra were corrected with respect to the Fc/Fc^{+} redox coupled.

BODIPY	E^{ox} (V)	E^{red} (V)	$HOMO^{exp}$ (eV)	$HOMO^{theory}$ (eV)	$LUMO^{exp}$ (eV)	$LUMO^{theory}$ (eV)
BDP-TTh	0.65	-0.91	-5.45	-5.98	-3.89	-3.38
BDP-biTh	0.60	-1.04	-5.40	-5.82	-3.76	-3.36
BDP-BDT	0.60	-0.91	-5.40	-5.71	-3.79	-3.30
BDP-CPDT	0.36	-0.98	-5.16	-5.60	-3.82	-3.30
BDP-DTP	0.34	-1.06	-5.14	-5.30	-3.74	-3.30

Table 2.2: Summarized electrochemical properties of the BODIPY-based molecules. The $HOMO^{exp}$ and $LUMO^{exp}$ values were calculated from the onset of oxidation and reduction potentials ($HOMO = -(E^{ox} + 4.8)$; $LUMO = -(E^{red} + 4.8)$).

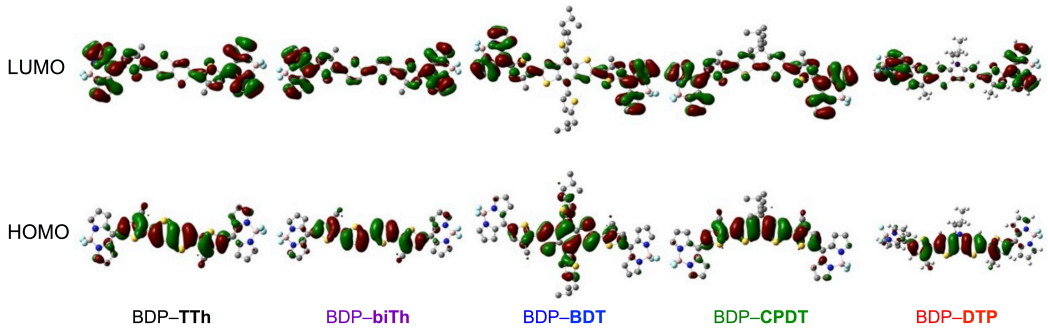

Figure 2.5: Calculated images of frontier molecular orbitals. Each plot shows considerable localization of electron density in HOMO and LUMO.

Density functional theory (DFT) calculations were performed using the B3LYP/6-311G(d,p) level of DFT. Images of the HOMO and LUMO electron density are shown in Figure 2.5. Overall, the HOMO wave function was completely delocalized over the entire core, including the bridging thiophene units, with a slight contribution from one side of each BODIPY moiety. Alternatively, the LUMO is delocalized over the entire backbone of the molecules, with slight localization on the capping BODIPY moieties; BDP-BDT shows no contribution from the flanking thiophenes to the LUMO.[39] Although the relatively electron deficient nature of the BODIPY moieties causes some localization of the LUMO, there is considerable contribution from the core moiety, indicating that the two end units may be electronically coupled through the core moiety.

As shown in Table 2.2, the calculated LUMO level shows great consistency, falling between -3.4 and -3.3 eV in each case. However, the HOMO gradually increases with the following trend BDP-TTh, BDP-biTh, BDP-BDT, BDP-CPDT, BDP-DTP, indicating that the position of the HOMO is primarily dependent on the structure of the donor core, which is in good agreement with the electron density localization, as well as the experimental results observed using CV.

It is well known that electron transport takes place through the LUMO. In this case, the delocalization of the LUMO can greatly benefit intermolecular orbital overlap, potentially facilitating electron transport.

2.3.4 Charge Transport Properties

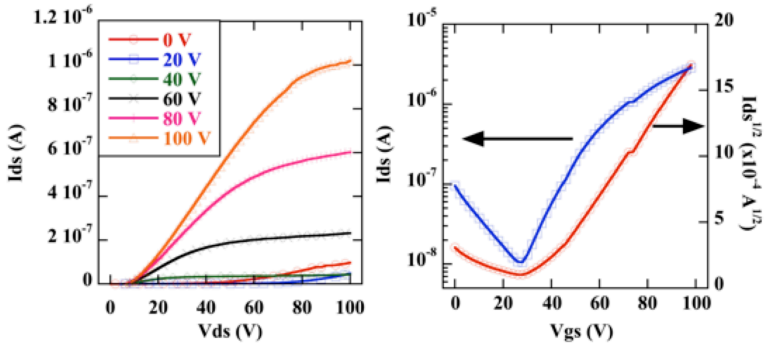

Figure 2.6: Output (left) and transfer (right) characteristics for fabricated bottom gate bottom contact organic field effect transistors using BDP-DTP as the active material.

To investigate the charge transport properties of these molecules, bottom gate bottom contact organic field effect transistors (OFET) were fabricated. Output and transfer characteristics for BDP-DTP are displayed in Figure 2.6. All molecules exhibit only n-type characteristics with mobilities on the order of 10^{-5} cm^2 V^{-1} s^{-1} (Table 2.3). Of the devices, BDP-biTh exhibited the highest electron mobility (9.67 x 10^{-5} cm^2 V^{-1} s^{-1}), while that of BDP-BDT was the lowest (3.30 x 10^{-5} cm^2 V^{-1} s^{-1}). Although the direction of charge transport in OPV devices and OFET devices are orthogonal, the consistent n-type transport observed, independent of the core, suggests that the *meso*-BODIPY cap could be a promising building block of low band gap, small molecule acceptors for OPVs.

BODIPY	Electron Mobility ($x10^{-5}$ cm^2 V^{-1} s^{-1}) Average	Best	$I_{on/off}$	V_T (V)
BDP-TTh	3.34 ± .03	3.38	10^2	28.4
BDP-biTh	8.39 ± .92	9.67	10^1	14.4
BDP-BDT	3.20 ± .06	3.30	10^1	7.3
BDP-CPDT	5.29 ± .28	5.77	10^2	17.7
BDP-DTP	4.59 ± .37	5.39	10^2	27.3

Table 2.3 Summarized electron transport properties of the BODIPY-based molecules

2.3.5 Photovoltaic Studies

2.3.5.1 Initial Direct Cells

To evaluate the potential use of these materials as electron acceptors in BHJ OPV devices, cells were fabricated with a direct device architecture using either BDP-biTh or BDP-BDT (ITO/PEDOT:PSS/P3HT:BDP/Al). In each case, either a 1:1 or 1:2 donor-to-acceptor (D:A) ratio was used. Despite a very low efficiency of 0.102% achieved, the rectifying curves indicate that these materials can be incorporated as the sole electron acceptor. The device properties are summarized in Table 2.4

Acceptor	D:A Ratio	V_{OC} (V)	J_{SC} (mA cm^{-2})	FF	PCE (%)
BDP-BDT	1:1	0.23	0.34	0.27	0.021
	1:2	0.30	0.33	0.27	0.026
BDP-biTh	1:1	0.37	0.51	0.25	0.047
	1:2	0.56	0.73	0.25	0.102

Table 2.4: Photovoltaic device properties of best performing direct cells (ITO/PEDOT:PSS/P3HT:BDP/Al) fabricated using either BDP-BDT or BDP-biTh.

For the BDP-BDT derivative, device performances were very low, reaching 0.026 % for the 1:2 blend. However, the devices did show rectifying curves when placed under illumination. Similarly, when BDP-biTh was used as the acceptor in a 1:2 ratio, rectification was also achieved. Compared to BDP-BDT, the BDP-biTh

device shows a slight enhancement in both V_{OC} and $J_{SC,}$ increasing the efficiency to 0.102%.

It should be noted that a potential source of the poor efficiency could be the device area. The above reported data was extracted from devices with an area of 18 mm^2. Reduction of the device area could greatly benefit device performance. Considering the previous results, the experimental conditions were refined, specifically the device area which was reduced to 8.6 mm^2. Also, the donor to acceptor ratio was varied more drastically (1:0.8, 1:1, 1:1.5, 1:2). Similar to the prior experiment, the 1:2 ratio was found to be optimal for both BDP-TTh, and BDP-CPDT. Reducing the device area greatly benefited the device performance. At this ratio, an efficiency of 0.235% was achieved using BDP-TTh and 0.181% using BDP-CDPT. The device properties at each D:A ratio for these two acceptors are detailed in Table 2.5.

Acceptor	D:A Ratio	V_{OC} (V)	J_{SC} (mA cm^{-2})	FF	PCE (%)	R_S (Ω)	R_{SH} (Ω)
BDP-TTh	1:0.8	0.46	0.53	0.33	0.080	754	1637
	1:1	0.49	0.73	0.41	0.145	345	1987
	1:1.5	0.55	0.95	0.42	0.218	209	2453
	1:2	0.55	0.98	0.44	0.235	190	2151
BDP-CPDT	1:0.8	0.35	0.61	0.39	0.083	229	1105
	1:1	0.49	0.77	0.35	0.131	446	1016
	1:1.5	0.42	0.89	0.39	0.144	190	914
	1:2	0.41	1.08	0.41	0.181	151	833

Table 2.5: Photovoltaic device properties of best performing direct cells (ITO/PEDOT:PSS/P3HT:BDP/Ca/Al) fabricated using either BDP-TTh or BDP-CPDT at various D:A ratios.

For BDP-TTh, increasing the acceptor concentration in the blend led to a gradual increase in V_{OC} from 0.46 V to 0.55 V, as well as improvements in both J_{SC} and FF of 0.45 mA cm^{-2} and 0.11, respectively. The combined improvement in each of these parameters led to the efficiency at the 1:2 ratio nearly three times that at

1:0.8. Increasing the ratio to 1:3 led to a drastic reduction in all of the device properties, indicating 1:2 as the upper limit of this specific combination under these processing conditions. For BDP-CPDT, similar improvements were also observed in the J_{SC}, but improvements in both V_{SC} and FF were significantly less drastic.

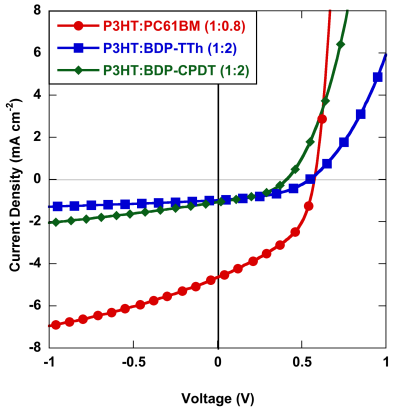

Figure 2.7: *J-V* curves of best performing P3HT devices containing BDP-TTh (blue squares), BDP-CPDT (green diamonds) or $PC_{61}BM$ (red circles) as the electron acceptor. V_{OC} and FF of BODIPY containing devices are comparable to $PC_{61}BM$ containing device, but suffer from low current

2.3.5.2 Revised Direct Cells

While V_{OC} and FF values were comparable to our P3HT:$PC_{61}BM$ reference cells (Figure 2.7), the J_{SC} values are very low, by comparison. The source of the poor current was believed to be due to the film thickness (350-400 nm). While the use of thicker films may be advantageous, resulting in greater light harvesting, free charges are less likely to be efficiently extracted at this thickness. In an effort to produce thinner films, we significantly altered the processing conditions. The active layers were produced from 12 mg mL^{-1} solutions of the 1:2 ratio blends in *o*-dichlorobenzene (*o*-DCB) spin cast at 1500 RPM for 45 s. Under these conditions, the film thickness was drastically reduced to *ca.* 80 nm.

For both BDP-TTh, and BDP-CPDT, reducing the film thickness did in fact lead to an increase in J_{SC} (Figure 2.8). However, the efficiency responded differently in each case. For BDP-TTh, the 0.42 mA cm^{-2} improvement in J_{SC} was accompanied by a 0.23 V and 0.12 reduction in the V_{OC} and FF, respectively. Because of this, the efficiency suffered, only reaching 0.142%. Alternatively, V_{OC}, J_{SC} and FF each improved for BDP-CPDT. The combined enhancement led to an efficiency of 0.401%, more than twice that of the thicker device.

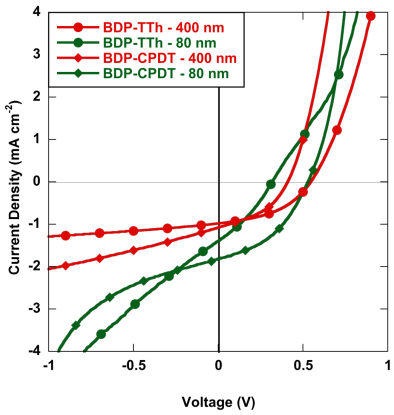

Figure 2.8: *J-V* curves for BDP-TTh (circles) and BDP-CPDT (diamonds) based devices at thicknesses of 400 (red) and 80 nm (green). Reducing the film thickness led to improvements in the current for both acceptors.

In an effort to further improve the device performance, we looked to improve the order of the P3HT donor within the bulk material. P3HT:PCBM devices have been extensively studied in the literature.[34] Various methods have been used to improve the device performance.[40, 41] Two of the most common methods include annealing techniques and the addition of solvent additives to the processing solvent. Both of these approaches are taken with the goal of generating crystalline P3HT domains to better facilitate hole transport.

While the BHJ architecture allows for a facile processing technique to yield the intermixed donor/acceptor active layer, the morphology is essentially spontaneously achieved, within the confines of the processing method.[42] In most cases, simple spin coating leads to an amorphous matrix of P3HT and PCBM. Within this matrix, clusters of both donor and acceptor can be found. The order within these domains may not be optimum for facilitating charge transport, specifically for P3HT where improved order benefits the cofacial interactions between chains, to facilitate charge hopping, as well as the intrachain planarity, which facilitates charge transport along the backbone.

Thermal annealing provides the polymer chains with the energy to planarize and order, generating P3HT crystallite domains in addition to the amorphous P3HT:PCBM matrix.[40] An added benefit of forming these crystalline domains is that they expel the PCBM from the domain, which allows clusters of these acceptors to form.

This tuning of the bulk morphology can also be attempted through the use of solvent additives.[41] This approach has been used with P3HT, as well as systems containing conjugated semiconducting polymers and small molecules other than P3HT, to tune the morphology. In this method, a small amount of a second solvent is included in the processing solvent to drive the formation of crystalline donor domains. This is achieved if the additive is a poor solvent for the donor, but a relatively good solvent for the acceptor. This disparate solubility allows the donor to crystallize during processing while the acceptor is kept in solution to exclude itself from the donor domains.

Since both of these methods are advantageous for P3HT:PCBM systems, given the specific properties of the PCBM molecule, we attempted to improve our devices using these methods. Figure 2.9 shows *J-V* curves for the resulting devices fabricated using BDP-biTh, BDP-CPDT and BDP-BDT. For BDP-CPDT, when 1-chloronapthalene (CN) was added, the best PCE was only 0.192%, due to the poor J_{SC} of 1.03 mA cm^{-2}. Adding CN gradually improved the J_{SC} to 1.79 mA cm^{-2}. V_{OC} and FF also improved, but without following a general trend. At 5 vol% of CN, the efficiency reached 0.389%. Thermal annealing of the P3HT:BDP-CPDT (1:2) device led to a slight decrease in J_{SC} (0.06 mA cm^{-2}), but improvements in V_{OC} and FF (0.07 V and 0.05, respectively). As a result, the efficiency increased to 0.484%.

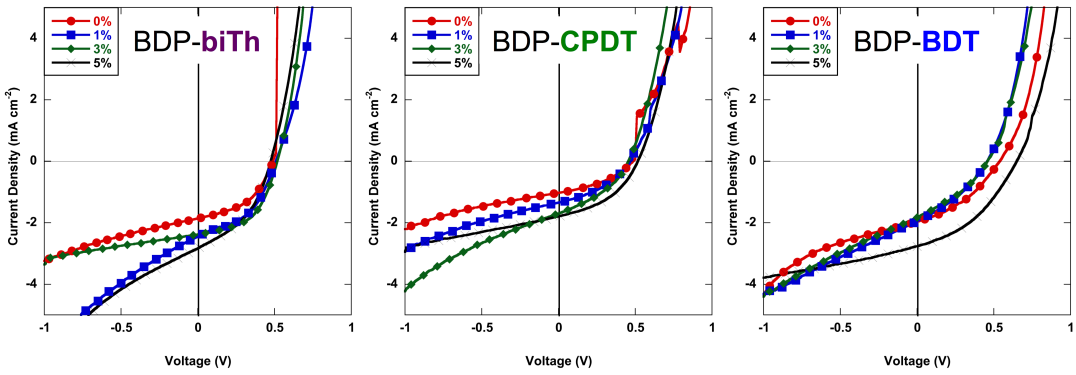

Figure 2.9: *J-V* curves for photovoltaic devices containing BDP-biTh (left), BDP-CPDT (center) or BDP-BDT (right) processed using 0 vol% (red circles), 1 vol% (blue squares), 3 vol% (green diamonds) or 5 vol% (black crosses) 1-chloronapthalene as a solvent additive. Devices showed gradual improvements in current with maximum efficiency achieved at 3 vol% for BDP-biTh and 5 vol% for BDP-CPDT and BDP-BDT.

For BDP-biTh, the gradual incorporation of CN led to an increase in J_{SC}, reaching as high as 2.83 mA cm^{-2} at 5 vol%. However, increasing additive concentration past 3 vol% CN decreased both the V_{OC} and FF, leading to a slight decrease in efficiency to 0.560%. The optimum amount of CN added was found to be 3 vol%, giving a PCE of 0.635%. The most significant improvement was achieved for

BDP-BDT. Using 5 vol% of CN led to a 0.11 V improvement in V_{OC} and 0.79 mA cm^{-2} increase in J_{SC}. A combination of these enhancements, as well as a slight improvement in FF, led to an efficiency of 0.7%.

2.3.5.3 Initial Inverted Cells

With a peak efficiency of 0.7% when BDP-BDT is used as the sole electron acceptor, the efficiency is low compared to the available non-fullerene acceptors used with the P3HT donor.[43] To determine if this efficiency was a limit of the materials we looked towards previously reported NFAs in BHJ devices.

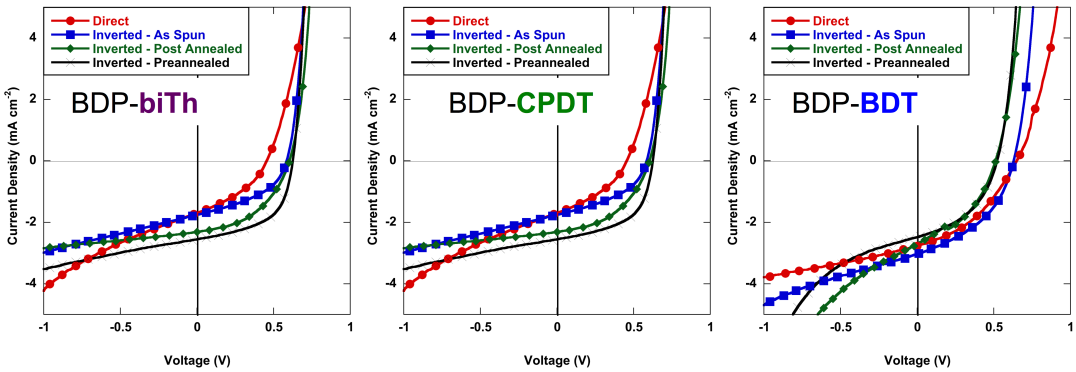

Figure 2.10: *J-V* curves of direct cells (red circles) and as spun (blue squares), post annealed (green diamonds) and preannealed (black crosses) inverted cells (ITO/ZnO/P3HT:BDP (1:2)/MoOx/Ag) for BDP-biTh (left), BDP-CPDT (center) and BDP-BDT (right) acceptors. Devices show better performance in inverted cells, as well as positive effects of annealing prior to electrode deposition.

Tetrafluorene-9,9'-bifluorenylidene (TFBF*)* was reported to achieve an efficiency of 0.26% in direct cells prior to annealing; tapping atomic force microscopy (AFM) to analyze the surface of the film.[44] Before annealing the films, balanced amounts of donor and acceptor were identified, however, after annealing the film the device performance dropped precipitously. AFM illustrated the migration of P3HT towards the surface. This event significantly hinders the ability of

the top electrode to extract electrons due to the high concentration of hole transporting material at the electrode-active layer interface and, alternatively, holes at the bottom electrode given the high concentration of acceptor.

Since this phenomenon could potentially affect our system, we decided to investigate an inverted device architecture (ITO/ZnO/P3HT:BDP (1:2)/MoO_x/Ag). As shown in Figure 2.10, switching to the inverted architecture yielded some consistent improvements across the board with BDP-biTh, BDP-CPDT, and BDP-BDT, namely in fill factor.

BDP-biTh gave optimum performance with the as spun inverted device. While there was a slight sacrifice in J_{sc}, FF improved by 0.10 yielding an efficiency of 0.652%. The improved series and shunt resistances indicate that inverted devices are more suitable for these non-fullerene acceptors. Annealing the active film either before or after deposition of the MoO_x/Ag electrode led to a drastic reduction in efficiency.

BDP-BDT also showed an improvement in efficiency by 0.11%, reaching 0.812%, through a combined increase in J_{sc} (0.27 mA cm^{-2}) and FF (0.04). However, similar to BDP-biTh, annealing the device either before or after deposition of the top electrode led to a decrease in device performance, although to a lesser extent. The most significant performance enhancement was achieved with BDP-CPDT. Improvements in V_{OC}, J_{sc} and FF (0.18 V, 0.86 mA cm^{-2} and 0.17, respectively) gave an efficiency of 0.878% for the preannealed inverted device.

2.3.5.4 Revised Inverted Cells

Given the success of these fabricated devices and the potential of the inverted device architecture with these BODIPY-based NFAs, we proceeded to optimize the processing conditions for this system and further reduce the device area from 8.6 mm^2 to 6 mm^2. We also sought to determine the contribution of the BODIPY dye light harvesting to the photogenerated current. To do so, we selected the BDP-BDT, BDP-CPDT and BDP-DTP derivatives given their varied absorption properties. Similar to the previous devices, we consistently observe open circuit voltages above 0.5 V with each acceptor, however, we see great improvements in the fill factor and, as a result, power conversion efficiencies. Contrary to the direct cells, the optimum P3HT:BODIPY ratio for each of the chosen acceptors was found to be 1:1.5.

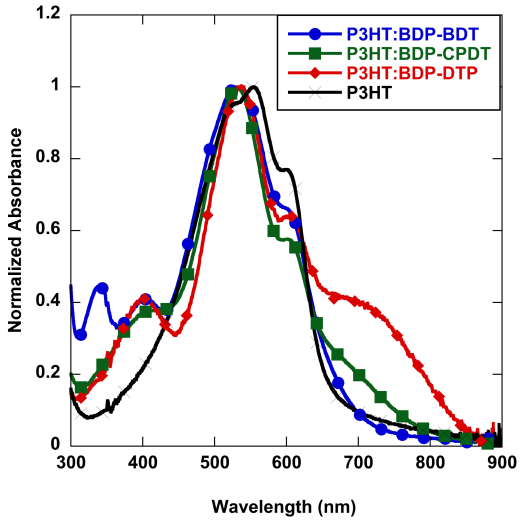

Figure 2.11: Normalized absorption of pristine P3HT (black crosses) film and 1:1 blend of P3HT with BDP-BDT (blue circles), BDP-CPDT (green squares) or BDP-DTP (red diamonds).

Analysis of the estimated absorption properties of P3HT:BODIPY thin films shows that, compared to pristine P3HT, the blended films show significant absorption above 650 nm corresponding to the absorption profile of each BODIPY

acceptor in that same region (Figure 2.11). If incident photon conversion efficiency (IPCE) measurements of the fabricated devices show a signal response in this region, we can confirm the acceptor contribution to device light harvesting. Inverted devices were fabricated using BDP-BDT, BDP-CPDT or BDP-DTP as the electron acceptor. The *J-V* curves and EQE spectra for the 1:1.5 D:A ratio are shown in Figure 2.12; the summarized results from the D:A ratio variation are shown in Table 2.6.

Similar to the previously studied direct and inverted cells, BDP-BDT showed the highest efficiency of 1.21% with a V_{OC} of 0.65 V, J_{SC} of 3.09 mA cm^{-2} and FF of 0.60. IPCE data, in the form of external quantum efficiency (EQE), shows a very slight shoulder above 650 nm matching the absorption of the BDP-BDT molecule. We also see a significant increase in intensity in the 350-500 nm range of the EQE spectrum. This contribution likely lends itself to the improved J_{SC} (3.09 mA cm^{-2}) observed in the 1:1.5 ratio compared to the 1:1 and 1:2 ratios (2.16 and 2.08 mA cm^{-2}, respectively).

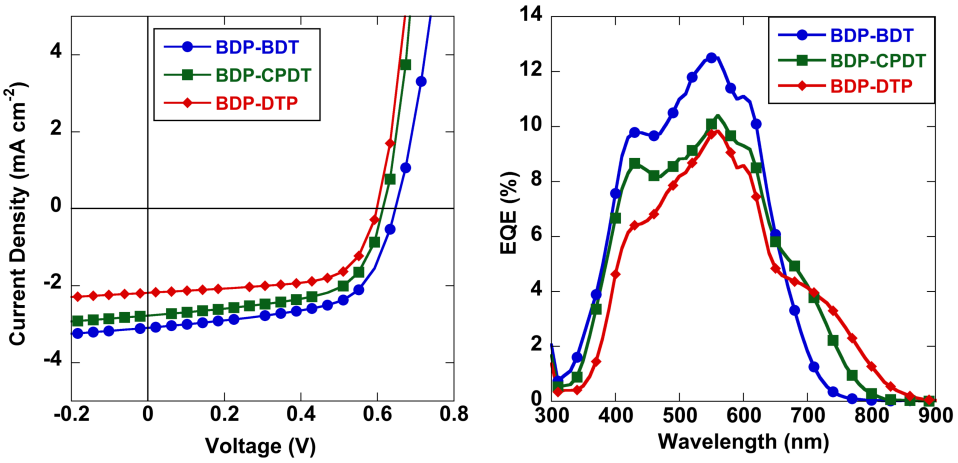

Figure 2.12: *J-V* curves (left) and EQE spectra (right) for the fabricated inverted devices (ITO/ZnO/P3HT:BDP (1:1.5)/MoO_x/Ag) where BDP-BDT (blue circles), BDP-CPDT (green squares) or BDP-DTP (red diamonds) are used as electron acceptors. The BODIPY-based acceptors contribute to photogenerated current above 650 nm.

Acceptor	D:A ratio	V_{OC} (V)	J_{SC} (mA cm^{-2})	FF	PCE (%)
BDP-BDT	1:1	0.62	2.16	0.57	0.76
	1:1.5	0.65	3.09	0.60	1.21
	1:2	0.61	2.08	0.60	0.75
BDP-CPDT	1:1	0.63	2.16	0.61	0.83
	1:1.5	0.61	2.78	0.56	1.02
	1:2	0.58	1.51	0.62	0.54
BDP-DTP	1:1	0.51	1.83	0.52	0.49
	1:1.5	0.60	2.18	0.65	0.84
	1:2	0.52	1.72	0.38	0.34

Table 2.6: Photovoltaic device properties of best performing direct cells (ITO/ZnO/P3HT:BDP/MoO_x/Ag) fabricated using BDP-BDT, BDP-CPDT or BDP-DTP at various D:A ratios.

The concurrent improvement in EQE and J_{SC} was also observed in when BDP-CPDT was used as an acceptor. The red region of the EQE spectra also shows an acceptor specific shoulder extending to 800 nm, given its consistent presence independent of D:A ratio.

Consistent with the previous results, the 1:1.5 ratio performed the best when BDP-DTP was used as the acceptor. Of the series, this acceptor yielded the highest FF (0.65) and comparable V_{OC} (0.60 V), but, due to the low J_{SC} (2.18 mA cm^2), the efficiency achieved (0.84%) was the lowest of the series.

The results for devices processed with CN are shown in Figure 2.13 and summarized in Table 2.7. Introducing solvent additives into the processing solvent yielded positive result, primarily in J_{SC}, similar to the previously studied direct cells. A slight improvement (0.11 mA cm^{-2}) was observed for BDP-BDT at 3 vol% of CN added. However, since this device suffered from decreased and inconsistent V_{OC} and FF, the best performing device was obtained with no additive used. BDP-CPDT and BDP-DTP saw more significant enhancements in J_{SC}, increasing respectively by 0.62

and 1.1 mA cm^{-2}, as well as improved stability in V_{OC} and FF. As a result, the efficiency increased to 1.51% for BDP-CPDT and 1.18% for BDP-DTP.

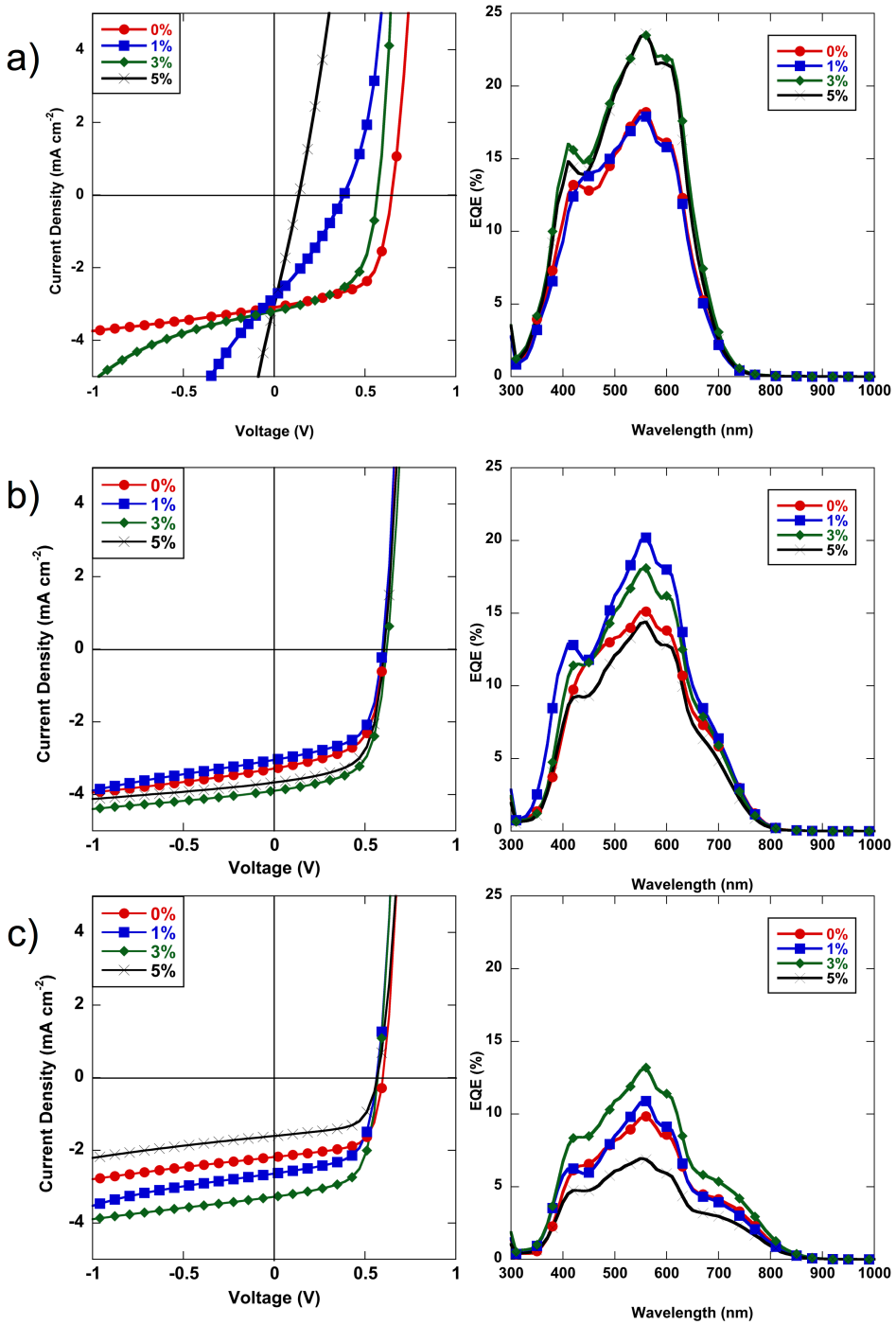

Figure 2.13: *J-V* curves (left) and IPCE plots (right) of devices processed using 0 vol% (red circles), 1 vol% (blue squares), 3 vol% (green diamonds) or 5 vol% (black crosses) of CN as a solvent additive: a) BDP-BDT, b)BDP-CPDT and c)BDP-DTP.

Acceptor	CN (vol %)	V_{OC} (V)	J_{SC} (mA cm^{-2})	FF	PCE (%)
BDP-BDT	0	0.65	3.09	0.60	1.21
	1	0.39	2.73	0.30	0.33
	3	0.57	3.20	0.56	1.01
	5	0.14	3.03	0.26	0.11
BDP-CPDT	0	0.60	3.28	0.61	1.20
	1	0.60	3.04	0.61	1.11
	3	0.62	3.90	0.63	1.51
	5	0.61	3.67	0.63	1.41
BDP-DTP	0	0.60	2.18	0.65	0.84
	1	0.56	2.64	0.62	0.92
	3	0.57	3.28	0.63	1.18
	5	0.57	1.60	0.62	0.56

Table 2.7: Photovoltaic device properties of best performing direct cells (ITO/ZnO/P3HT:BDP (1:1.5)/MoO_X/Ag) fabricated using various amounts of the CN solvent additive. The active layers were spuncase from *o*-DCB solutions (15 mg mL^{-1}) at 1500 RPM for 60 s and annealed at 150 °C for 2 min. While BDP-CPDT and BDP-DTP devices improved, while BDP-BDT devices did not.

To investigate the effect of the solvent additive on the morphology of the active layer, tapping atomic force microscopy (AFM) was used. The height images are shown in Figure 2.14. Scanning of the films showed improved order with smaller domain sizes as the concentration of CN increases. The effect is most pronounced at 3 and 5 vol% CN in the BDP-CPDT containing films, with uniform domains of ~370 nm at 3 vol% and finer domains at 5 vol%. The improvements indicate that the morphology can be effectively tuned with solvent additives, similar to PCBM based devices. Although these results support the experimental data acquired from the fabricated PV devices, further investigation into the bulk morphology is required to determine what role the crystallinity, solubility, etc. of the BODIPY dye play in the bulk structure.

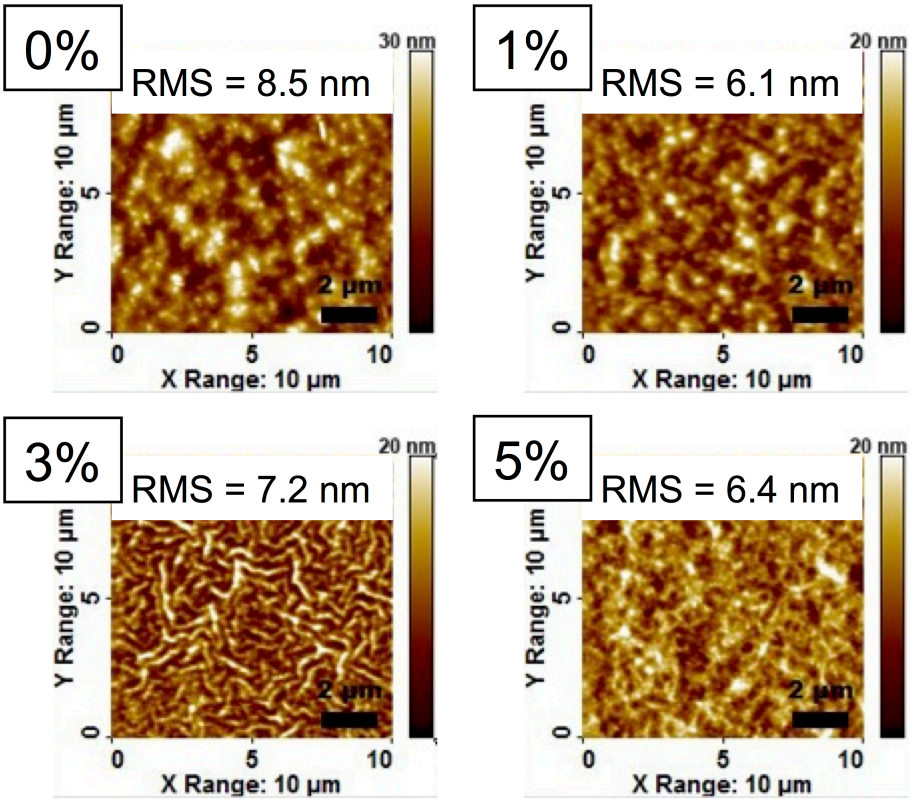

Figure 2.14: AFM images for BDP-CPDT devices. At 3 vol%, long range ordered domains were observed.

2.4 Summary

In summary, a series of n-type small molecules consisting of a thiophene-based donor core conjugated to a BODIPY cap through the *meso* position were synthesized. These molecules exhibited good visible absorption with a common peak between 530-535 nm in thin films, independent of the donor core. Introduction of a stronger donor (BDP-CPDT and BDP-DTP) to the core of the molecule led to a significant red shift in the charge transfer band, resulting in an optical band gap of as low as 1.47 eV. Each of the molecules possessed a low-lying LUMO, between -3.7 eV and -3.9 eV, and decent electron mobility of $\sim 10^{-5}$ $cm^2 V^{-1} s^{-1}$, making them potential light harvesting acceptors for many donor materials.

Direct and inverted bulk heterojunction photovoltaic devices were successfully fabricated, combining these molecules with P3HT as the donor. The P3HT:BDP-BDT active layer yielded an efficiency of 0.70% in the direct architecture and 1.21% in the inverted architecture. The use of CN as a solvent additive improved device efficiency in the P3HT:BDP-BDT direct cell but reduced device performance in the inverted cell at the optimized D:A ratio. BDP-CPDT and BDP-DTP based devices both responded positively to the addition of CN in the inverted architecture, with the best performing cell yielding a PCE of 1.51% (P3HT:BDP-CPDT + 3 vol% CN).

The red edge absorption of the BODIPY acceptor contributes to the photogenerated current, as indicated by IPCE measurements. EQE spectra show features specific to the BODIPY dye above 650 nm.

Analysis of the surface morphology using AFM showed the evolution of more narrow and uniform domain sizes correlating to the improved Jsc values observed experimentally.

We are further investigating the effect of both core, cap and linker modifications on the electronic properties of the resulting materials for optimal pairing with donors other than P3HT. Further device optimization and morphological studies of the blends are currently underway. Through fine-tuning of the molecular structure, we hope to achieve a library of BODIPY based electron acceptors with robust electronic properties for OPV applications.

2.5 Experimental

All reagents were purchased from commercial sources and used as received, unless otherwise mentioned. Tetrahydrofuran (THF) was distilled over sodium and benzophenone 2,5-bis(trimethylstannyl)thieno[3,2-b]thiophene,[45] 2,6-bis (trimethyltin)-4,8-bis(5-(2-ethylhexyl)thiophen-2-yl)benzo[1,2-b:4,5-b'] dithiophe-ne,[4, 30] 4,4-Bis(2-ethylhexyl)-2,6-bis(trimethylstannanyl)-4H-cyclopenta-[2,1-b:3,4-b]dithiophene,[25, 31] *N*-(2-ethylhexyl)-2,6- bis(trimethylstannyl)-dithieno [3,2-*b*:2′,3′-*d*]pyrrole[32] were synthesized according to previously reported procedures.

2.5.1 Instrumentation

^{1}H NMR spectra were recorded on a 400 MHz Bruker NMR spectrometer and the chemical shifts are reported in ppm using deuterated solvent as the internal standard ($CDCl_3$ at 7.26 ppm). When peak multiplicities are given, the following abbreviations are used: s, singlet; d, doublet; t, triplet; m, multiplet. ^{13}C NMR spectra were proton decoupled and recorded on a 100 MHz Bruker NMR spectrometer using the carbon signal of the deuterated solvent as the internal standard ($CDCl_3$ at 77.16 ppm).

2.5.2 Synthesis of 8-(2-bromo-3-hexylthien-5-yl)-4,4-difluoro-4-bora-3a,4a-diaza-s-indacene

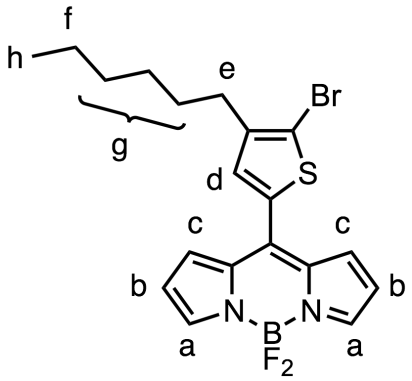

In a dry 250 mL three neck round bottom flask, diisopropylamine (1.7 mL, 12 mmol) was dissolved in THF. The solution was cooled to -78°C using a dry ice/acetone bath. Butyllithium (4.4 mL, 11 mmol) was added dropwise and the mixture was stirred for 30 minutes at -78°C. A solution of 2-bromo-3-hexylthiophene (2 mL, 10 mmol) in THF (5 mL) was added dropwise over 30 min and the reaction was stirred at -78°C for 1 hour. Triisopropylborate (5.8 mL, 25 mmol) was added at once and the reaction was allowed to reach room temperature and stirred overnight. 10% aq. HCl was added and the reaction was stirred for 1 hr. The crude product was extracted with ethyl acetate. The combined organics were washed with water and dried over sodium sulfate. The solvent was removed *in vacuo* to give the crude product to be used without further purification. ^{1}H NMR confirmed a 1:0.6 ratio of starting material to product.

8-(thiomethyl)-4,4,difluoro-3,5-diethyl-4-bora-3a,4a-diaza-*s*-indacene (0.355 g, 1.5 mmol) and the crude (5-bromo-4-hexylthiophen-2-yl) boronic acid (1.30 g, 4.5 mmol) were dissolved in tetrahydrofuran under argon. The mixture was purged with argon for 10 minutes. Copper (I) thiophene-2-carboxylate (0.852 g, 4.5 mmol),

Pd_2dba_3 (34 mg, 2.5 mol%) and tris(2-furyl)phosphine (26 mg, 7.5 mol%) were added as a solid mixture. The reaction was placed into a preheated oil bath and stirred at 55°C for 15 hr. The solvent was removed *in vacuo* and the crude product was purified by silica gel column chromatography using hexanes and ethyl acetate as eluents. The solvents were removed *in vacuo* to give a red solid (0.523 g, 80%). ^{1}H-NMR (400 MHz, $CDCl_3$): δ 7.93 (s, 2H, a), 7.27 (m, 3H, b+d), 6.58 (dd, J = 4.1, 1.1 Hz, 2H, c), 2.66 (t, J = 7.7 Hz, 2H, e), 1.65 (m, 2H, f), 1.41-1.31 (m, 6H, g), 0.91 (t, J = 7.0 Hz, 3H, h). **^{13}C-NMR** (100 MHz, $CDCl_3$): δ 144.13, 144.02, 138.59, 134.13, 134.01, 131.28, 118.73, 116.68, 31.69, 29.76, 29.70, 29.05, 22.73, 14.21. FAB/MS Calculated m/z = 438.06, Found m/z = 438.05

2.5.3 Synthesis of BDP-TTh

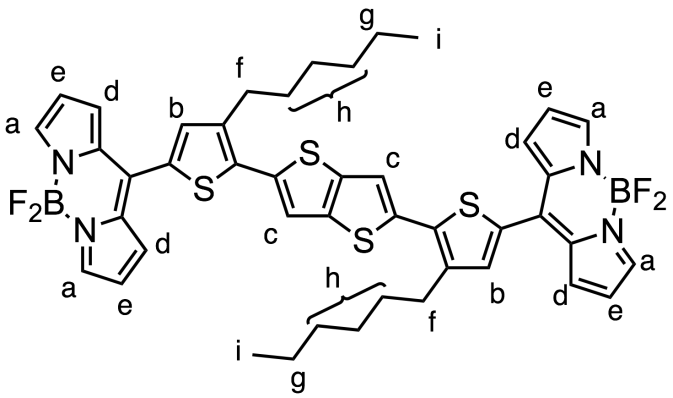

2,5-bis(trimethylstannyl)thieno[3,2-b]thiophene (274 mg, 0.59 mmol) and 8-(2-bromo-3-hexylthien-5-yl)-4,4-difluoro-4-bora-3*a*,4*a*-diaza-*s*-indacene (592 mg, 1.35 mmol) were dissolved in degassed toluene, followed by the addition of Pd_2dba_3 (13 mg, 2.5 mol%) and tri(o-tolyl)phosphine (13 mg, 7.5 mol%). The reaction was heated to 100°C and stirred for 24 hr. The solvents were removed *in vacuo* and the crude product was purified by silica gel column chromatography using hexanes and

ethyl acetate as eluents. The solvents were removed *in vacuo* to give the product as a purple solid (251 mg, 50%). **^{1}H-NMR** (400 MHz, $CDCl_3$): δ 7.94 (s, 4H, a), 7.47 (s, 2H, b), 7.46 (s, 2H, c), 7.38 (d, *J* = 4.1 Hz, 4H, d), 6.61 (dd, *J* = 4.0, 1.5 Hz, 4H, e), 2.92 (t, *J* = 7.8 Hz, 4H, f), 1.76 (dt, *J* = 15.3, 7.6 Hz, 4H, g), 1.48-1.34 (m, 12H, h), 0.91 (t, *J* = 6.9 Hz, 6H, i). **^{13}C-NMR** (100 MHz, $CDCl_3$): δ 143.73, 141.78, 140.60, 138.98, 138.05, 137.25, 136.54, 134.11, 133.23, 131.23, 119.22, 118.61, 118.59, 31.77, 30.75, 29.65, 29.42, 22.78, 14.22. FAB/MS Calculated *m/z* = 852.2, Found *m/z* = 852.1

2.5.4 Synthesis of BDP-biTh

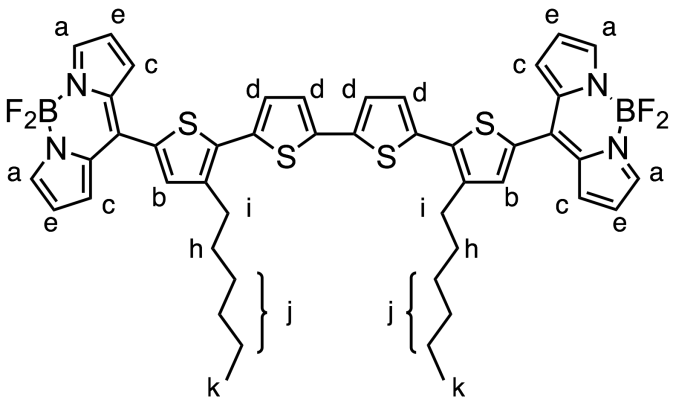

5,5-Bis(tributylstannyl)-2,2-bithiophene (116 mg, 0.16 mmol) and 8-(2-bromo-3-hexylthien-5-yl)-4,4-difluoro-4-bora-3*a*,4*a*-diaza-*s*-indacene (150 mg, 0.343 mmol) were dissolved in degassed toluene, followed by the addition of Pd_2dba_3 (4 mg, 2.5 mol%) and tri(o-tolyl)phosphine (4 mg, 7.5 mol%). The reaction was heated to 100°C and stirred for 24 hr. The solvents were removed *in vacuo* and the crude product was purified by silica gel column chromatography using hexanes and ethyl acetate as eluents. The solvents were removed *in vacuo* to give the product as a purple solid (100 mg, 73%). **^{1}H-NMR** (400 MHz, $CDCl_3$): δ 7.93 (s, 4H, a), 7.46 (s, 2H, b), 7.37 (d, *J* = 4.0 Hz, 4H, c), 7.29-7.23 (m, 4H, d), 6.62-6.60 (m, 4H, e), 2.90 (t,

J = 7.8 Hz, 4H, f), 1.79-1.71 (m, 4H, g), 1.48-1.25 (m, 16H, h), 0.92 (t, *J* = 6.9 Hz, 6H, i). **^{13}C-NMR** (100 MHz, $CDCl_3$): δ 143.58, 141.32, 139.11, 138.20, 137.94, 136.67, 134.27, 134.09, 132.64, 131.18, 128.10, 124.92, 118.54, 118.52, 31.76, 30.58, 29.67, 29.39, 22.78, 14.24. FAB/MS Calculated *m/z* = 878.3, Found *m/z* = 878.2

2.5.5 Synthesis of BDP-BDT

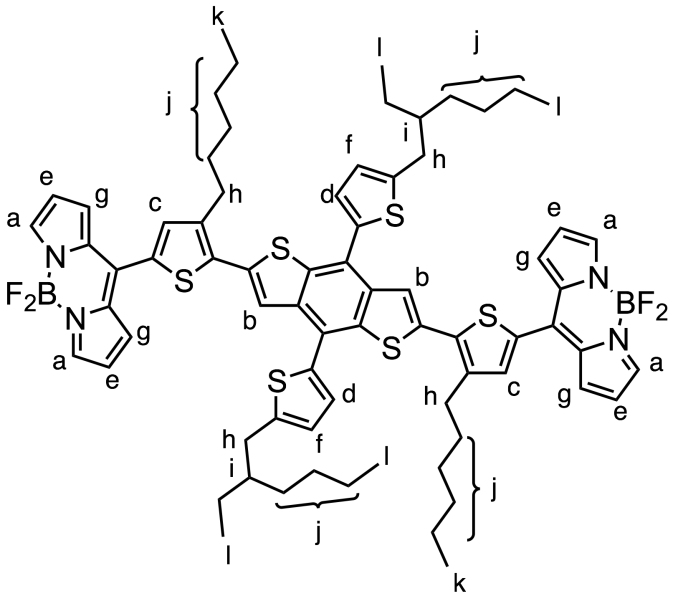

2,6-bis(trimethylstannyl)-4,8-bis(5-(2-ethylhexyl)thiophen-2-yl)benzo[1,2-*b*:4,5- *b'*]dithiophene (108 mg, 0.12 mmol) and 8-(2-bromo-3-hexylthien-5-yl)-4,4-difluoro-4-bora-3*a*,4*a*-diaza-*s*-indacene (120 mg, 0.275 mmol) were dissolved in degassed toluene, followed by the addition of Pd_2dba_3 (8 mg, 2.5 mol%) and tri(*o*-tolyl)phosphine (8 mg, 7.5 mol%). The reaction was heated to reflux and stirred for 24 hr. The solvents were removed *in vacuo* and the crude was purified by silica gel column chromatography using hexanes and ethyl acetate as eluents. The solvents were removed *in vacuo* to give the product as a purple solid (123 mg, 80%). **^{1}H-NMR** (400 MHz, $CDCl_3$): δ 7.93 (s, 4H, a), 7.81 (s, 2H, b), 7.46 (s, 2H, c), 7.38 (d, *J* =

3.5 Hz, 2H, d), 7.36 (d, *J* = 4.2 Hz, 4H, e), 6.95 (d, *J* = 3.5 Hz, 2H, f), 6.60 (m, 4H, g), 2.92 (m, 8H, h), 1.75-1.69 (m, 6H, i), 1.47-1.30 (m, 28H, j), 0.96 (t, *J* = 7.4 Hz, 6H, k), 0.90 (m, 12H, l). **^{13}C-NMR** (100 MHz, $CDCl_3$): δ 146.5, 143.7, 142.4, 139.6, 139.0, 138.2, 137.2, 136.6, 136.5, 136.2, 134.1, 133.7, 131.2, 131.2, 128.1, 125.8, 124.1, 123.2, 122.9, 118.6, 118.5, 41.6, 34.4, 32.6, 31.7, 30.7, 29.7, 29.4, 29.0, 25.8, 23.18, 22.7, 14.3, 14.2, 11.0. MALDI/MS Calculated *m/z* = 1290.5, Found *m/z* = 1291.3.

2.5.6 Synthesis of BDP-CPDT

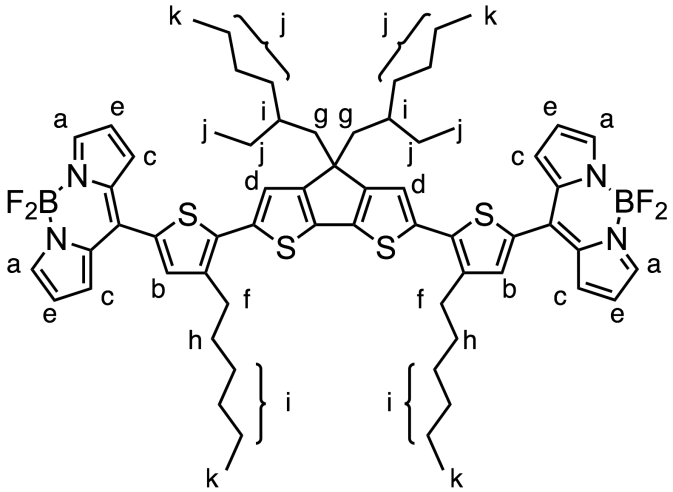

4,4-Bis(2-ethylhexyl)-2,6-bis(trimethylstannyl)-4*H*-cyclopenta-[2,1-*b*:3,4-*b*']dithiophene (73 mg, 0.10 mmol) and 8-(2-bromo-3-hexylthien-5-yl)-4,4-difluoro-4-bora-3*a*,4*a*-diaza-*s*- indacene (100 mg, 0.23 mmol) were dissolved in degassed toluene, followed by the addition of Pd_2dba_3 (3 mg, 2.5 mol%) and tri(o-tolyl)phosphine (3 mg, 7.5 mol%). The reaction was heated to 100°C and stirred for 24 hr. The solvents were removed *in vacuo* and the crude product was purified by silica gel column chromatography using hexanes and ethyl acetate as eluents. The solvents were removed *in vacuo* to give the product as a purple solid (86 mg, 77%). **^{1}H-NMR** (400 MHz, $CDCl_3$): δ 7.92 (s, 4H, a), 7.48 (s, 2H, b), 7.40 (d, *J* = 4.1 Hz, 4H, c),

7.18 (s, 2H, d), 6.62-6.60 (m, 4H, e), 2.90 (t, *J* = 7.9 Hz, 4H, f), 2.03-1.92 (m, 4H, g), 1.82-1.73 (m, 4H, h), 1.50- 1.29 (m, 14H, i), 1.07-0.93 (m, 22H, j), 0.98-0.88 (m, 12H, k). **^{13}C-NMR** (100 MHz, $CDCl_3$): δ 158.8, 143.2, 140.6, 139.7, 139.2, 138.7, 137.0, 135.2, 134.0, 132.1, 131.0, 130.9, 122.3, 118.4, 118.3, 118.3, 54.5, 43.3, 35.4, 34.4, 31.8, 30.6, 29.8, 29.4, 28.8, 27.6, 23.0, 22.8, 14.2, 10.9. FAB/MS Calculated *m/z* = 1114.5, Found *m/z* = 1114.5

2.5.7 Synthesis of BDP-DTP

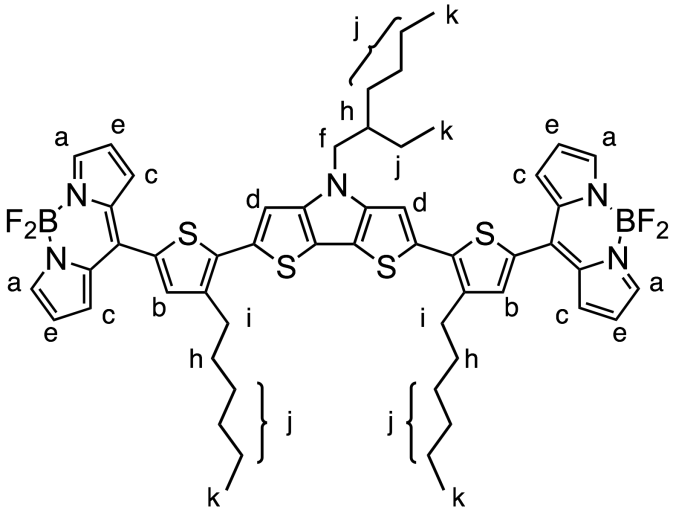

N-(2-ethylhexyl)-2,6-bis(trimethylstannyl)-dithieno[3,2-*b*:2′,3′-*d*]pyrrole (140 mg, 0.23 mmol) and 8-(2-bromo-3-hexylthien-5-yl)-4,4-difluoro-4-bora-3*a*,4*a*-diaza-*s*-indacene (200 mg, 0.46 mmol) were dissolved in degassed toluene, followed by the addition of Pd_2dba_3 (5 mg, 2.5 mol%) and tri(o-tolyl)phosphine (5 mg, 7.5 mol%). The reaction was heated to 100°C and stirred for 24 hr. The solvents were removed *in vacuo* and the crude product was purified by silica gel column chromatography using hexanes and ethyl acetate as eluents. The solvents were removed *in vacuo* to give the product as a purple solid (217 mg, 94%). **^{1}H-NMR** (400

MHz, $CDCl_3$): δ 7.92 (s, 4H, a), 7.48 (s, 2H, b), 7.40 (d, *J* = 4.1 Hz, 4H, c), 7.18 (s, 2H, d), 6.61 (dd, *J* = 4.1, 1.7 Hz, 4H, e), 4.14 (dd, *J* = 7.0, 5.6 Hz, 2H, f), 2.95 (t, *J* = 7.9 Hz, 4H, g), 2.04-1.98 (m, 2H, h), 1.79-1.74 (m, 4H, i), 1.49-1.34 (m, 20H, j), δ 0.99-0.88 (m, 12H, k). **^{13}C-NMR** (100 MHz, $CDCl_3$): δ 145.7, 143.2, 140.9, 140.1, 139.2, 137.1, 134.0, 133.2, 132.4, 131.0, 118.4, 116.5, 110.7, 51.5, 40.6, 31.8, 30.9, 30.7, 29.8, 29.5, 28.6, 24.3, 23.2, 22.8, 14.2, 10.8. ESI-HR Calculated *m/z* = 1003.4, Found *m/z* = 1003.4

2.5.8 Solution and Thin Film Absorption

Solution and thin film UV-vis absorption spectra were recorded on a Cary 100 scan UV-vis spectrophotometer. All extinction coefficients were determined from a linear fit of five data points. Thin films were prepared from dichloromethane solutions spin cast onto a glass substrate, followed by annealing at 150°C for 30 min.

2.5.9 Cyclic Voltammetry

Solution state electrochemical measurements were performed on a BASi Epsilon potentiostat using a Pt disc electrode as a working electrode and a Pt wire as the auxiliary electrode. The potentials were measured against a Ag/Ag^+ reference at a scan rate of 50 mV s^{-1}. Tetrabutylammonium hexafluorophosphate was used as the supporting electrolyte and the recorded spectra were calibrated with respect to an internal standard (ferrocene/ferrocenium (Fc/Fc^+) redox couple).

2.5.10 Field Effect Transistors

Organic field effect transistor (OFET) devices were fabricated using pre-patterned n-doped silicon substrates. Gold electrodes were deposited on the gate layer to yield the bottom contact OFETs. The channel width of all transistors was 10 mm. The channel length was 2.5, 5, 10 or 20 μm. The capacitance of the insulator is 14.9 nF cm^{-2} for 230 nm of SiO_2. The OFET substrates were rinsed with acetone to remove the protective layer before film deposition. Organic thin films were deposited on the surface by spin coating a 10 mg mL^{-1} chlorobenzene solution at 1000 RPM for 60 s. The devices were allowed to dry at room temperature for 1 hr. The devices were measured directly after drying. All measurements were performed under a controlled atmosphere in a glove box using an Agilent 4165C precision semiconductor parameter analyzer.

2.5.11 Solar Cell Fabrication

2.5.11.1 Solar cell fabrication – *Direct cells*

ITO coated glass sheets (10 Ω^2, Kintec) were successively washed in acetone, ethanol and isopropanol in an ultrasonic bath and exposed to UV-ozone for 15 min. PEDOT:PSS suspension (Clevois) was filtered through a 0.2 μm filter and used to spin-coat the clean substrates at 4000 rpm for 60 s, after which the layer was dried in at 110°C in a dynamic primary vacuum for 30 min. The coated substrates were transferred to a glove box with a controlled atmosphere (O_2, H_2O < 0.1 ppm).

Active layer solutions were prepared from stock solutions in o-dichlorobenzene of P3HT (30 mg mL^{-1}), the synthesized acceptor (15 mg mL^{-1}) and

additional solvent. They were heated to 80°C for 1 hr followed by heating at 50°C overnight. The active layer was formed by spin coating the prepared solutions at 1500 rpm for 45 s. After spin coating, the samples were place directly into the thermal evaporator to deposit a 20 nm thick calcium layer (0.1 nm s^{-1}), followed by an 80 nm thick aluminum layer (0.25 nm s^{-1}) under a secondary vacuum (10^{-6} mbar) through a shadow mask to define an 8.6 mm^2 active area. The devices were characterized using a K.H.S SolarCelltest-575 solar simulator with AM1.5G filters set at 100 mW cm^{-1}.

2.5.11.2 Solar cell fabrication – *Inverted cells*

ITO coated glass sheets (10 Ω^2, Kintec) were successively washed in acetone, ethanol and isopropanol in an ultrasonic bath and exposed to UV-ozone for 15 min. Sol gel ZnO solution in ethanol was filtered through a 0.2 μm filter and used to spin-coat the clean substrates at 4000 rpm for 60 s, after which the layer was dried on a hot plate at 150°C for 1 min. The coated substrates were transferred to a glove box with a controlled atmosphere (O_2, H_2O < 0.1 ppm).

Active layer solutions were prepared and deposited as described for direct cells. After spin coating, the samples were either preannealed or placed directly into the thermal evaporator to deposit a 7 nm thick MoO_3 layer (0.1 nm s^{-1}), followed by a 100 nm thick silver layer (0.5 nm s^{-1}) under a secondary vacuum (10^{-6} mbar) through a shadow mask to define an 8.6 mm^2 active area. Preannealed devices were heated to 150°C for 10 min prior to metal deposition. The devices were

characterized using a K.H.S SolarCelltest-575 solar simulator with AM1.5G filters set at 100 mW cm^{-1}.

2.6 References

1. He, Z.; Zhong, C.; Su, S.; Xu, M.; Wu, H.; Cao, Y., Enhanced power-conversion efficiency in polymer solar cells using an inverted device structure. *Nat. Photon.* 2012, 6, 593-597.

2. Chochos, C. L.; Choulis, S. A., How the structural deviations on the backbone of conjugated polymers influence their optoelectronic properties and photovoltaic performance. *Prog. Polym. Sci.* 2011, 36, 1326-1414.

3. Li, Y., Molecular design of photovoltaic materials for polymer solar cells: toward suitable electronic energy levels and broad absorption. *Acc. Chem. Res.* 2012, 45, 723-733.

4. Huo, L.; Zhang, S.; Guo, X.; Xu, F.; Li, Y.; Hou, J., Replacing alkoxy groups with alkylthienyl groups: a feasible approach to improve the properties of photovoltaic polymers. *Angewandte Chemie* 2011, 50, 9697-9702.

5. Lin, Y.; Li, Y.; Zhan, X., Small molecule semiconductors for high-efficiency organic photovoltaics. *Chem. Soc. Rev.* 2012, 41, 4245-4272.

6. Zhou, H.; Yang, L.; You, W., Rational Design of High Performance Conjugated Polymers for Organic Solar Cells. *Macromolecules* 2012, 45, 607-632.

7. Thompson, B. C.; Frechet, J. M., Polymer-fullerene composite solar cells. *Angewandte Chemie* 2008, 47, 58-77.

8. Liu, T.; Troisi, A., What makes fullerene acceptors special as electron acceptors in organic solar cells and how to replace them. *Adv. Mater.* 2013, 25, 1038-1041.

9. Zhou, Y.; Dai, Y. Z.; Zheng, Y. Q.; Wang, X. Y.; Wang, J. Y.; Pei, J., Non-fullerene acceptors containing fluoranthene-fused imides for solution-processed inverted organic solar cells. *Chem. Commun.* 2013, 49, 5802-5804.

10. Bloking, J. T.; Han, X.; Higgs, A. T.; Kastrop, J. P.; Pandey, L.; Norton, J. E.; Risko, C.; Chen, C. E.; Brédas, J.-L.; McGehee, M. D.; Sellinger, A., Solution-Processed Organic Solar Cells with Power Conversion Efficiencies of 2.5% using Benzothiadiazole/Imide-Based Acceptors. *Chem. Mater.* 2011, 23, 5484-5490.

11. Chochos, C. L.; Tagmatarchis, N.; Gregoriou, V. G., Rational design on n-type organic materials for high performance organic photovoltaics. *Rsc Adv* 2013, 3, 7160-7181.

12. Zhao, Y.; Guo, Y.; Liu, Y., 25th anniversary article: recent advances in n-type and ambipolar organic field-effect transistors. *Adv. Mater.* 2013, 25, 5372-91.

13. Lin, Y.; Zhang, Z. G.; Bai, H.; Li, Y.; Zhan, X., A star-shaped oligothiophene end-capped with alkyl cyanoacetate groups for solution-processed organic solar cells. *Chem. Commun.* 2012, 48, 9655-9657.

14. Anthony, J. E., Small-Molecule, Nonfullerene Acceptors for Polymer Bulk Heterojunction Organic Photovoltaics. *Chem. Mater.* 2011, 23, 583-590.

15. Eftaiha, A. F.; Sun, J.-P.; Hill, I. G.; Welch, G. C., Recent advances of non-fullerene, small molecular acceptors for solution processed bulk heterojunction solar cells. *J. Mater. Chem. A* 2014, 2, 1201-1213.

16. Zhou, Y.; Ding, L.; Shi, K.; Dai, Y. Z.; Ai, N.; Wang, J.; Pei, J., A non-fullerene small molecule as efficient electron acceptor in organic bulk heterojunction solar cells. *Adv. Mater.* 2012, 24, 957-961.

17. Benniston, A. C.; Copley, G., Lighting the way ahead with boron dipyrromethene (Bodipy) dyes. *Phys. Chem. Chem. Phys.* 2009, 11, 4124-4131.

18. Hayashi, Y.; Obata, N.; Tamaru, M.; Yamaguchi, S.; Matsuo, Y.; Saeki, A.; Seki, S.; Kureishi, Y.; Saito, S.; Yamaguchi, S.; Shinokubo, H., Facile synthesis of biphenyl-fused BODIPY and its property. *Org. Lett.* 2012, 14, 866-869.

19. Kim, B.; Ma, B.; Donuru, V. R.; Liu, H.; Frechet, J. M., Bodipy-backboned polymers as electron donor in bulk heterojunction solar cells. *Chem. Commun.* 2010, 46, 4148-4150.

20. Lin, H. Y.; Huang, W. C.; Chen, Y. C.; Chou, H. H.; Hsu, C. Y.; Lin, J. T.; Lin, H. W., BODIPY dyes with beta-conjugation and their applications for high-efficiency inverted small molecule solar cells. *Chem. Commun.* 2012, 48, 8913-8915.

21. Bura, T.; Leclerc, N.; Fall, S.; Leveque, P.; Heiser, T.; Retailleau, P.; Rihn, S.; Mirloup, A.; Ziessel, R., High-performance solution-processed solar cells and ambipolar behavior in organic field-effect transistors with thienyl-BODIPY scaffoldings. *J. Am. Chem. Soc.* 2012, 134, 17404-17407.

22. Chi, C.-C.; Huang, Y.-J.; Chen, C.-T., Synthesis and Spectroscopic Characterization of Dual Absorption BODIPY Type Dyes and their Light Harvesting Application in Polymer-Based Bulk Hetrojunction Organic Photovoltaics. *J. Chin. Chem. Soc.* 2012, 59, 305-316.

23. Yoshii, R.; Yamane, H.; Nagai, A.; Tanaka, K.; Taka, H.; Kita, H.; Chujo, Y., π-Conjugated Polymers Composed of BODIPY or Aza-BODIPY Derivatives Exhibiting High Electron Mobility and Low Threshold Voltage in Electron-Only Devices. *Macromolecules* 2014, 47, 2316-2323.

24. Popere, B. C.; Della Pelle, A. M.; Thayumanavan, S., BODIPY-Based Donor–Acceptor π-Conjugated Alternating Copolymers. *Macromolecules* 2011, 44, 4767-4776.

25. Popere, B. C.; Della Pelle, A. M.; Poe, A.; Balaji, G.; Thayumanavan, S., Predictably tuning the frontier molecular orbital energy levels of panchromatic low band gap BODIPY-based conjugated polymers. *Chem. Sci.* 2012, 3, 3093-3102.

26. Benniston, A. C.; Copley, G.; Harriman, A.; Rewinska, D. B.; Harrington, R. W.; Clegg, W., A donor-acceptor molecular dyad showing multiple electronic energy-transfer processes in crystalline and amorphous states. *J. Am. Chem. Soc.* 2008, 130, 7174-7175.

27. Goud, T. V.; Tutar, A.; Biellmann, J.-F., Synthesis of 8-heteroatom-substituted 4,4-difluoro-4-bora-3a,4a-diaza-s-indacene dyes (BODIPY). *Tetrahedron* 2006, 62, 5084-5091.

28. Lager, E.; Liu, J.; Aguilar-Aguilar, A.; Tang, B. Z.; Pena-Cabrera, E., Novel meso-polyarylamine-BODIPY hybrids: synthesis and study of their optical properties. *J. Org. Chem.* 2009, 74, 2053-2058.

29. Pena-Cabrera, E.; Aguilar-Aguilar, A.; Gonzalez-Dominguez, M.; Lager, E.; Zamudio-Vazquez, R.; Godoy-Vargas, J.; Villanueva-Garcia, F., Simple, general, and efficient synthesis of meso-substituted borondipyrromethenes from a single platform. *Org. Lett.* 2007, 9, 3985-3988.

30. Hou, J.; Park, M.-H.; Zhang, S.; Yao, Y.; Chen, L.-M.; Li, J.-H.; Yang, Y., Bandgap and Molecular Energy Level Control of Conjugated Polymer Photovoltaic Materials Based on Benzo[1,2-b:4,5-b′]dithiophene. *Macromolecules* 2008, 41, 6012-6018.

31. Zhu, Z.; Waller, D.; Gaudiana, R.; Morana, M.; Mühlbacher, D.; Scharber, M.; Brabec, C., Panchromatic Conjugated Polymers Containing Alternating Donor/Acceptor Units for Photovoltaic Applications. *Macromolecules* 2007, 40, 1981-1986.

32. Shi, M.-M.; Deng, D.; Chen, L.; Ling, J.; Fu, L.; Hu, X.-L.; Chen, H.-Z., Design and synthesis of dithieno[3,2-b:2′3′-d]pyrrole-based conjugated polymers for photovoltaic applications: consensus between low bandgap and low HOMO energy level. *J. Poly. Sci. A: Poly. Chem.* 2011, 49, 1453-1461.

33. Yin, S.; Leen, V.; Jackers, C.; Beljonne, D.; Van Averbeke, B.; Van der Auweraer, M.; Boens, N.; Dehaen, W., Oligo(p-phenylene ethynylene)-BODIPY derivatives: synthesis, energy transfer, and quantum-chemical calculations. *Chem. Eur. J.* 2011, 17, 13247-13257.

34. Dang, M. T.; Hirsch, L.; Wantz, G., P3HT:PCBM, Best Seller in Polymer Photovoltaic Research. *Adv. Mater.* 2011, 23, 3597-3602.

35. Peet, J.; Heeger, A. J.; Bazan, G. C., "Plastic" solar cells: self-assembly of bulk heterojunction nanomaterials by spontaneous phase separation. *Acc. Chem. Res.* 2009, 42, 1700-1708.

36. Facchetti, A., π-Conjugated Polymers for Organic Electronics and Photovoltaic Cell Applications. *Chem. Mater.* 2011, 23, 733-758.

37. Collado, D.; Casado, J.; Rodriguez Gonzalez, S.; Lopez Navarrete, J. T.; Suau, R.; Perez-Inestrosa, E.; Pappenfus, T. M.; Raposo, M. M., Enhanced functionality for donor-acceptor oligothiophenes by means of inclusion of BODIPY: synthesis, electrochemistry, photophysics, and model chemistry. *Chem. Eur. J.* 2011, 17, 498-507.

38. Dumur, F.; Gautier, N.; Gallego-Planas, N.; Sahin, Y.; Levillain, E.; Mercier, N.; Hudhomme, P.; Masino, M.; Girlando, A.; Lloveras, V.; Vidal-Gancedo, J.; Veciana, J.; Rovira, C., Novel fused D-A dyad and A-D-A triad incorporating tetrathiafulvalene and p-benzoquinone. *J. Org. Chem.* 2004, 69, 2164-2177.

39. Odom, S. A.; Lancaster, K.; Beverina, L.; Lefler, K. M.; Thompson, N. J.; Coropceanu, V.; Bredas, J. L.; Marder, S. R.; Barlow, S., Bis[bis-(4-alkoxyphenyl)amino] derivatives of dithienylethene, bithiophene, dithienothiophene and dithienopyrrole: palladium-catalysed synthesis and highly delocalised radical cations. *Chem. Eur. J.* 2007, 13, 9637-46.

40. Erb, T.; Zhokhavets, U.; Gobsch, G.; Raleva, S.; Stühn, B.; Schilinsky, P.; Waldauf, C.; Brabec, C. J., Correlation Between Structural and Optical Properties of Composite Polymer/Fullerene Films for Organic Solar Cells. *Adv. Funct. Mater.* 2005, 15, 1193-1196.

41. Lee, J. K.; Ma, W. L.; Brabec, C. J.; Yuen, J.; Moon, J. S.; Kim, J. Y.; Lee, K.; Bazan, G. C.; Heeger, A. J., Processing additives for improved efficiency from bulk heterojunction solar cells. *J. Am. Chem. Soc.* 2008, 130, 3619-3623.

42. Moon, J. S.; Takacs, C. J.; Sun, Y.; Heeger, A. J., Spontaneous formation of bulk heterojunction nanostructures: multiple routes to equivalent morphologies. *Nano letters* 2011, 11, 1036-1039.

43. Lin, Y.; Zhan, X., Non-fullerene acceptors for organic photovoltaics: an emerging horizon. *Mater. Horiz.* 2014, 1, 470.

44. Park, O. Y.; Kim, H. U.; Kim, J.-H.; Park, J. B.; Kwak, J.; Shin, W. S.; Yoon, S. C.; Hwang, D.-H., Tetrafluorene-9,9′-bifluorenylidene as a non-fullerene type electron acceptor for P3HT-based bulk-heterojunction polymer solar cells. *Sol. Energ. Mat. Sol. Cells* 2013, 116, 275-282.

45. Subramaniyan, S.; Xin, H.; Kim, F. S.; Jenekhe, S. A., New Thiazolothiazole Copolymer Semiconductors for Highly Efficient Solar Cells. *Macromolecules* 2011, 44, 6245-6248.

CHAPTER 3

LINKER VARIATION FOR ELECTRONIC TUNING OF BODIPY-BASED A-D-A SMALL MOLECULE ORGANIC SEMICONDUCTORS

3.1 Introduction

In Chapter 2 we described a series of BODIPY based acceptor-donor-acceptor (A-D-A) molecules, which behaved as n-type materials and detailed their use as electron transporting materials in OPV devices.[1] We were able to successfully and consistently fabricate working devices when the BODIPY acceptors were matched with the P3HT donor. We also showed that the red edge absorption of the BODIPY acceptor contributed to the photogenerated current of the fabricated devices using external quantum efficiency measurements.

The major selling point of these materials is the fact that their properties are, in fact, tunable. Intelligent design of the molecular structure of donor-acceptor (D-A) molecules is a commonly used method to lower the band gap.[2] We are capable of broadening the absorption of the dyes by substituting "strong" donors at the core of the molecule, generating a more pronounced and red shifted intramolecular charge transfer (ICT) band. This broadening reduces the band gap of the resulting molecules. However, the contribution of light harvested by the BODIPY in the NIR region by this band is relatively small, compared to the dominant peak. Therefore, by improving BODIPY absorption in the red-NIR region, we hope to improve the functionality of this system for P3HT donors, or donors with comparable absorption features.

We were also able to show stabilization of the HOMO through the introduction of relatively “weak” donor cores. However, we were unable to see any substantial modification in the LUMO level, due in a large part to the fact that the LUMO in the A-D-A is largely localized on the BODIPY units. Therefore, any significant perturbation of the LUMO level should come from structural/electronic modification of the BODIPY molecule.

Methods for tuning the electronic properties involve direct structural modification of the BODIPY moiety through extension of conjugation through the α or β positions or the generation of fused BODIPY moieties.[3-5] However, these processes are very synthetically demanding, due to the multiple reactive positions on the BODIPY unit and the need to retain a functional handle for our "plug-and-play" design. As a result, we decided to investigate the linker unit between the donor core and the BODIPY cap, rather than directly attach the BODIPY itself. In our previous study, the alkylthiophene linker was held consistent and was therefore an independent variable.[1] The structure and connectivity of the linker can greatly affect the extent of donor-acceptor (D-A) interactions, providing a useful method to tune the electronic properties of the resulting molecule.[6]

Previously in our group, we have demonstrated the importance of tuning conjugation in donor-bridge-acceptor complexes and how it can affect the rates of forward and backward electron transfer processes, as well as the optical properties.[7] While the structure of the linker was chosen to be a phenylene unit, the connectivity (*meta* vs. *para*) was chosen to allow either (*a*) balanced forward and backward charge transfer (*para*) or (*b*) unbalanced charge transfer favoring the

forward electron transfer process (*meta*). The results of this study show that the *m*-phenylene linker is insulating in the ground state. For this reason, we chose the *m*-phenylene linker for our control molecule. We should expect that the absorption onset should be the furthest blue shifted due to the lack of charge transfer character in the system.

Linker connectivity is also a very valuable tool in the modulation of the electronic properties of conjugated polymers, as well as the morphological properties. A recent report by Nakazumi, et. al. showed that variation in the connectivity of a phenylene linker in a squaraine based conjugated polymer can play an important role in tuning the photovoltaic properties of the resultant devices.[8] This structural modification led to perturbed polymer aggregation and phase segregation, as well as changes in the absorption and electrochemical properties.

Linkers also played an important role in enforcing rigidity in conjugated backbones, facilitating interchain interactions[9] in porphyrin-dithienothiophene alternating copolymers. In a report by Huang, et. al., a series of polymers were synthesized with the two units either directly conjugated or connected through a triple bond linker.[10] The absorption properties greatly benefitted from the introduction of the triple bond, reducing the optical band gap by *ca.* 0.45 eV. When directly conjugated, the two alternating units twist significantly out of plane with one another. However, bridging the units with an ethynyl linker planarized the polymer backbone, promoting polymer aggregation and benefitting light harvesting for photovoltaic devices. This planarizing effect has also been shown in BODIPY based small molecules used as donors in inverted OPV devices.[11] In this case,

introducing an ethynyl linker between a 1,3,4,5,7-pentamethyl BODIPY and a thiophene unit reduced the dihedral angle between the two by nearly 50°.

Given the extensive modifications possible in our BODIPY based, A-D-A type system, which has already been successfully used as non-fullerene acceptors in OPV devices, we decided to investigate how various conjugated linkers affected the absorption properties, frontier molecular orbitals, and charge carrier mobility. If successful, modifications at this point in the molecular structure will yield control over these properties, allowing us to obtain complementary properties to a specific donor material, on demand.

3.2 Molecular Design

For consistency with our previous studies, the core unit was chosen to be DTP and the cap remains an unsubstituted BODIPY unit. Being the strongest donor, we should be able to effectively monitor the ICT band in each absorption spectrum.

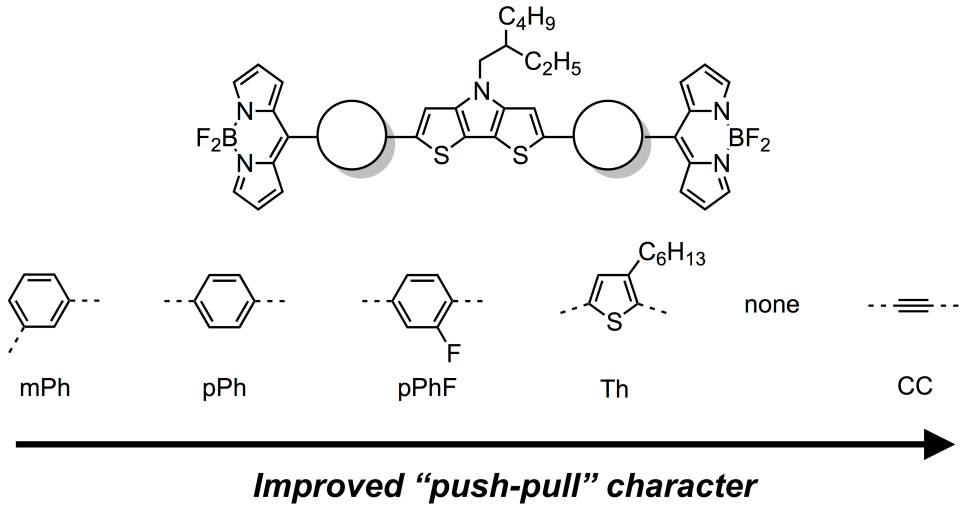

Figure 3.1: Molecular design of proposed linker variation on BODIPY A-D-A architecture. The linkers were selected to show a systemic improvement in the electronic communication between the DTP donor core and the BODIPY cap.

The use of the DTP unit also benefits from the fact that it is fully conjugated and should act as an effective conduit between the two BODIPY moieties, if they are in fact in communication. This should allow the structure and properties of the linker to act as the dominant limiting factor in the effective conjugation of the series.

To investigate this modification to the molecular design, we chose a series of linkers, shown in Figure 3.1. We expect the linker quality to follow the trend *m*-phenylene (mPh) < *p*-phenylene (pPh) < 2-fluoro-*p*-phenylene (pPhF) < 3-hexylthiophene (Th) < directly linked < ethynyl (CC), where *m*-phenylene will be the most insulating and ethynyl provide the strongest electronic communication.

In Chapter 2, we observed a significant distance between the maximum absorption and ICT band (0.47 eV) when a thiophene unit was chosen as the linker. In this study, we hope to not only observe an blue shift in ICT band when "push-pull" character is decreased in the system through the introduction of an electronically insulating linker moiety (*m*-phenylene), but also a red shift in the ICT band due to improved D-A communication when either no linker is used or an ethynyl linker is introduced. We also expect variation in the intensity of the ICT band, dependent on the extent of communication between the donor core and BODIPY acceptor cap. The thin film absorption properties will also be investigated, as well as the electrochemical properties, to determine the effect of D-A communication on both the optical band gap and the redox properties of the BODIPY molecules.

When phenylene units are installed at the *meso* position of the BODIPY moiety, a significant twist is often observed between the two units in crystal

structure analysis and computational modeling. This is most commonly seen in 3,5-alkylated derivatives, where the twist approaches 90°.[3, 4] This twist, however, could potentially be eliminated through the used of an ethynyl unit as a linker. Rod-like ethynyl linkers have successfully been used in conjugated polymers to instill planarity across several units. We have previously reported a series of conjugated polymers incorporating such units based on the BODIPY dye.[12, 13] These polymers were found to be very rigid, which allowed for great delocalization of the frontier molecular orbitals, as well as a low optical band gap. While the BODIPY unit was conjugated through the β position, we expect the planarizing effect to hold true in this system. Modifying the planarity of the molecule may also lead to altered charge transport properties, due to the need for favorable intermolecular packing for effective charge transport in organic semiconductors.

3.3 Results and Discussion

3.3.1 Synthesis

Synthesis of the molecules follow a similar method as those developed in Chapter 2, essentially building a functional BODIPY cap to be coupled with a DTP core with a compatible functionality for a palladium catalyzed aryl-aryl cross coupling reaction. For detailed synthesis of the thiophene-linked molecule, see Chapter 2.9.2 and Chapter 2.9.7.

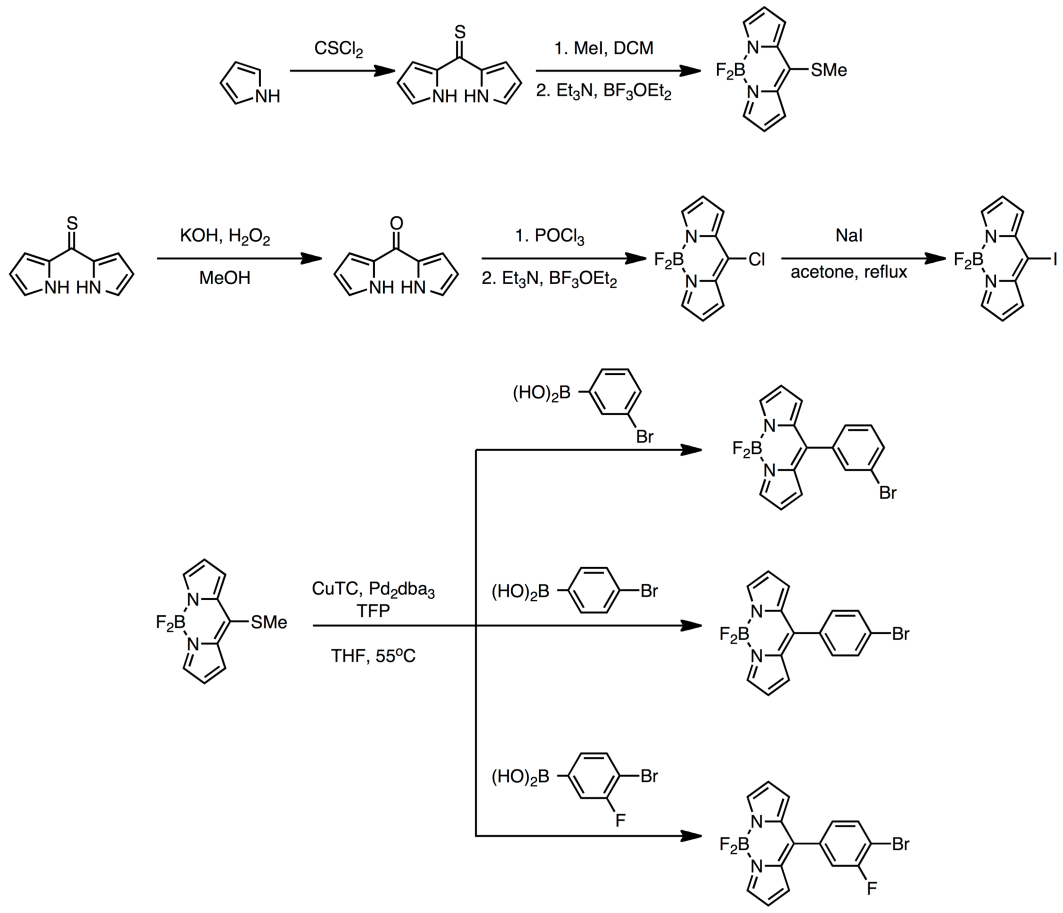

Scheme 3.1: Synthetic scheme for thiomethyl-BODIPY, *meso*-iodo BODIPY, as well as caps containing brominated phenylene units for subsequent coupling with DTP.

The phenylene-linked molecules were synthesized similar to the BDP-Th-DTP linked molecule from a previously described method.[14, 15] The thiomethyl BODIPY was synthesized starting from pyrrole, which was condensed with thiophosgene, followed by methylation and introduction of the boron difluoride group in the presence of triethylamine (Scheme 3.1). Next, the BODIPY was subjected to Liebeskind-Srögl coupling conditions with 3-phenylboronic acid, 4-bromophenylboronic acid or 3-fluoro-4-bromophenylboronic acid to give each of the brominated BODIPY caps, as shown in Scheme 3.1. Each prepared phenylene

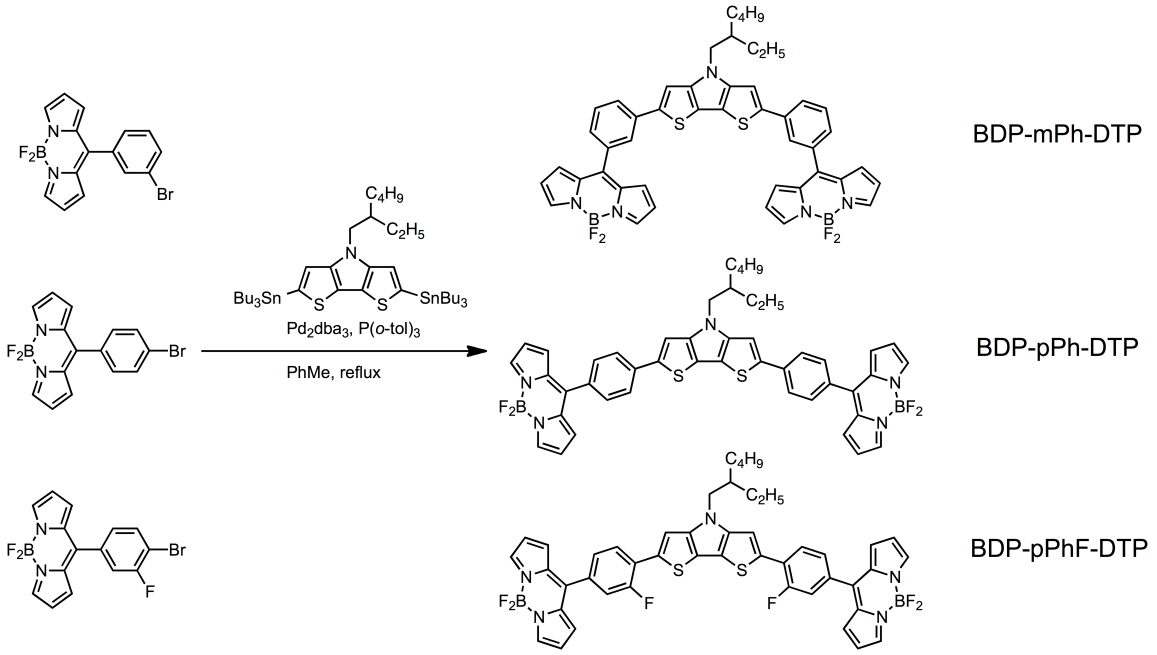

Scheme 3.2: Synthesis of the phenylene-linked molecules.

containing BODIPY was coupled to the stannylated DTP molecule to yield BDP-mPh-DTP, BDP-pPh-DTP and BDP-pPhF-DTP (Scheme 3.2).

A *meso*-iodo BODIPY was also synthesized using a previously reported method (Scheme 3.1).[16] The thioketone was oxidized using potassium hydroxide and hydrogen peroxide in methanol. The resulting ketone was used to generate a *meso*-chloro BODIPY with phosphorous oxychloride, triethylamine and boron trifluoride diethyl etherate. A halogen exchange reaction using sodium iodide in acetone yielded the *meso*-iodo BODIPY. To synthesize the directly linked molecule (BDP-DTP), *meso*-iodo BODIPY and the stannylated DTP were subjected to Stille coupling conditions (Scheme 3.3).

The synthesis of BDP-CC-DTP required linker installation onto the donor core, rather than the BODIPY cap. To do so, the DTP core was synthesized as mentioned in Chapter 2.3, followed by bromination with N-bromosuccinimide

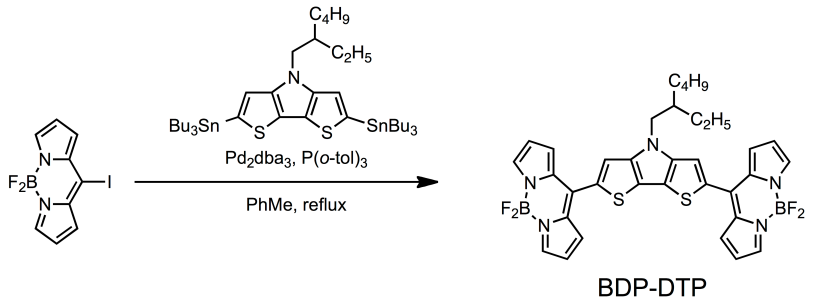

Scheme 3.3: Synthesis of BDP-DTP. Stille coupling conditions with a stannylated DTP derivative yielded the shown final molecule.

(NBS). Sonogashira coupling with trimethylsilylacetylene gave the TMS-protected, bisacetylated DTP molecule. The TMS groups were deprotected using aqueous potassium hydroxide in methanol and a second Sonogashira coupling reaction using the *meso*-chloro BODIPY molecule was done to yield CC. While iodinated molecules are often used in Sonagshira coupling reactions to better facilitate oxidative addition of the Pd(0) species,[17] the *meso*-iodo BODPIY derivative reacts poorly under these conditions,[16] making purification of the product very difficult.

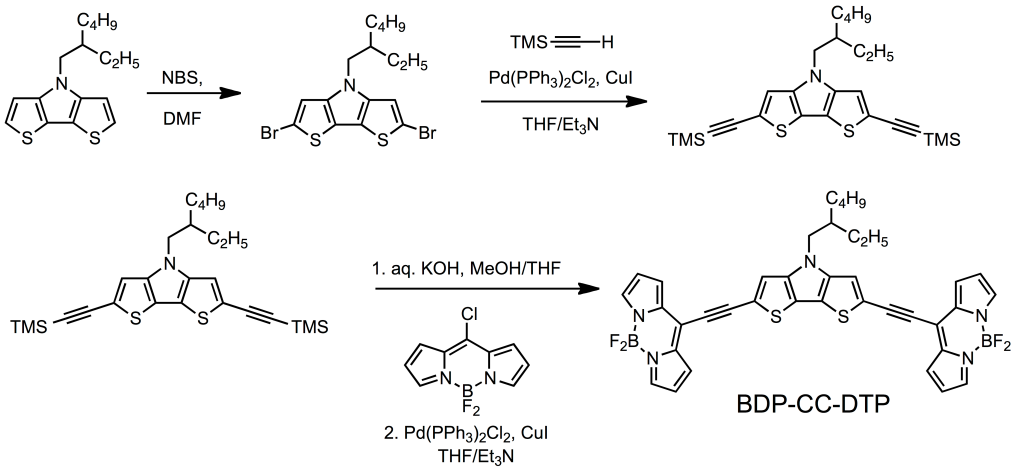

Scheme 3.4: Synthesis of BDP-CC-DTP.

3.3.2 Absorption Properties

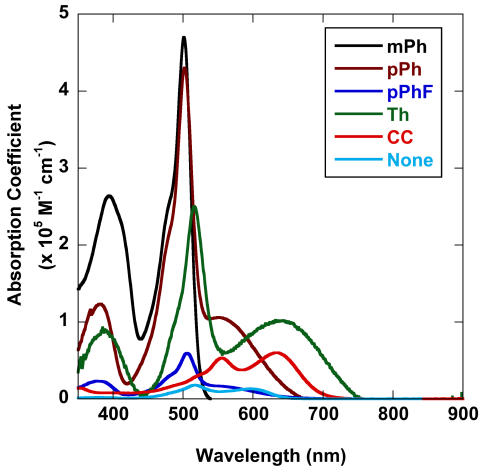

Figure 3.2: Absorption spectra of BDP-mPh-DTP (black), BDP-pPh-DTP (brown), BDP-pPhF-DTP (blue), BDP-Th-DTP (green), BDP-DTP (light blue) and BDP-CC-DTP (red).

	λ_{BDP} (nm)	ϵ_{max} (x 10^5 M^{-1} cm^{-1})	λ_{CT} (nm)	ε_{CT} (x 10^5 M^{-1} cm^{-1})	Relative intensity
BDP-mPh-DTP	501	4.7	-	-	-
BDP-pPh-DTP	502	4.3	540	1.0	0.23
BDP-pPhF-DTP	506	0.59	547	0.17	0.29
BDP-Th-DTP	516	2.5	631	1.0	0.40
BDP-DTP	517	0.18	596	0.13	0.72
BDP-CC-DTP	555	0.53	634	0.60	1.13

Table 3.1: Summarized absorption properties of the BODIPY dyes

The optical properties of the BODIPY dyes were measured using solution state UV-Vis absorption spectroscopy. The solution spectra are shown in Figure 3.2, plotted with respect to their absorption coefficient; Table 3.1 shows the extracted absorption coefficients of the λ_{BDP} and the ICT peak, as well as the relative peak intensity between them. Analysis of the BODIPY π-π^* peak shows a consistent red shift as the donor-acceptor communication is increased starting from BDP-mPh-DTP (501 nm). BDP-pPh-DTP increases by 1 nm, while BDP-pPhF-DTP increases to 506 nm. Replacing the phenylene linker with thiophene (BDP-Th-DTP) or removing the linker altogether (BDP-DTP) yielded a more significant red shift of 15 nm and 16

nm, respectively. Introducing the ethynyl linker (BDP-CC-DTP) resulted in a drastic red shift of 54 nm. This evidence indicates the properties of the BODIPY moiety are effectively modulated to a varying extent as the linker between the donor core and the BODIPY facilitates conjugation extension.

Analysis of the ICT band also offers valuable information regarding the improved D-A character of the resulting molecules as the communication is increased. Figure 3.3a shows the absorption spectra normalized with respect to the BODIPY peak. Comparing the relative intensity of the ICT and BODIPY peaks (Figure 3.2) shows that, just as the BODIPY peak red shifts with increasing communication, the intensity of the ICT peak also gradually increases. BDP-mPh-DTP shows no band or shoulder above 510 nm, indicating that the donor core and BODIPY are completely isolated by the *meta* linkage. The *p*-phenylene linked molecules (BDP-pPh-DTP, BDP-pPhF-DTP) show a band at *ca*. 545 nm with comparable relative intensities (0.23 and 0.29, respectively). Replacement of the phenylene linker with thiophene nearly doubled the relative intensity to 0.40 compared to BDP-pPh-DTP. BDP-DTP yields a substantial increase in relative intensity to 0.72. It is important to note that while communication between the two units is improved, the red edge absorption onset is blue shifted compared to the BDP-Th-DTP since the conjugation length is decreased. Introduction of the ethynyl linker led to the ICT band overtaking the BODIPY peak due to a combined extended conjugation and improved coupling between the donor and BODIPY moieties.

Thin film absorption was measured for spin cast film from concentrated chloroform solutions and annealed at 150 °C for 30 minutes. The spectra are shown

in Figure 3.4 and the results are summarized in Table 3.2. The absorption generally red shifted and broadened compared to the solution state absorption. We can also see a significant increase in the relative intensity of the charge transfer band, indicating increased planarity in the thin film compared to the solution state.

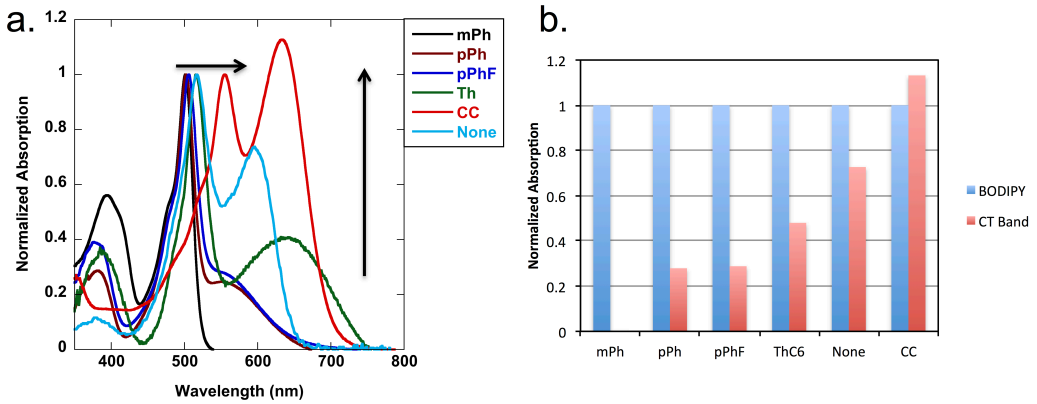

Figure 3.3: a) Solution state absorption spectra of BDP-mPh-DTP (black), BDP-pPh-DTP (brown), BDP-pPhF-DTP (blue), BDP-Th-DTP (green), BDP-DTP (light blue) and BDP-CC-DTP (red) normalized with respect to the BODIPY π-π* band; b) relative intensity of the intramolecular charge transfer band plotted with respect to the BODIPY π-π* band intensity. BDP-DTP (None) is shown in light blue.

Maximum absorption of BDP-mPh-DTP red shifted by 18 nm and no charge transfer band is observed, similar to the solution spectrum. Also similar to the solution state, BDP-pPh-DTP and BDP-pPhF-DTP have very similarly shaped charge transfer bands, yielding comparable optical band gaps (1.60 and 1.59 eV, respectively). While the maximum absorption red shifted by 16 nm in BDP-pPh-DTP, BDP-pPhF-DTP showed a less significant 4 nm red shift. Given the broadening of the absorption spectra, the charge transfer band exists as a shoulder at *ca*. 570 nm for each molecule. The relative intensity also significantly increases compared to the solution state spectra, indicating an increase in planarity, given the domination of the charge transfer band.

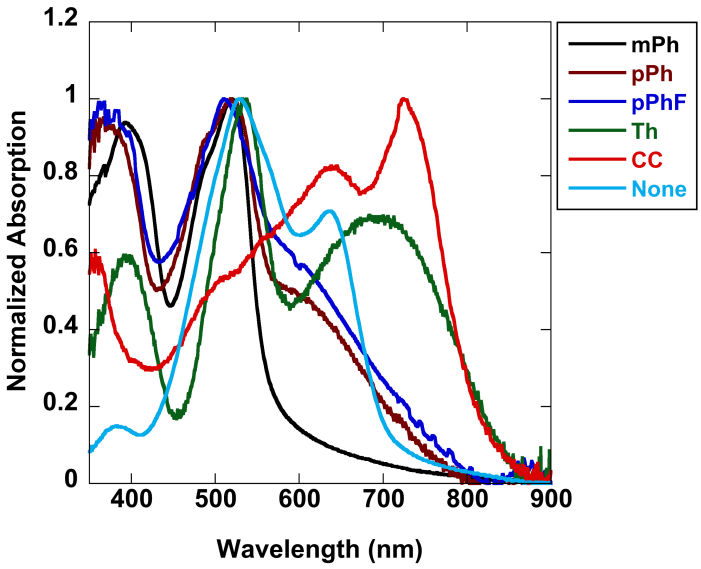

Figure 3.4: Absorption spectra of BODIPY thin films spun cast from concentrated chloroform solutions and annealed at 150 °C for 30 minutes. BDP-DTP (None) is shown in light blue.

	λ_{BDP} (nm)	λ_{ICT} (nm)	λ_{onset} (nm)	E_g^{opt} (eV)	Relative intensity
BDP-mPh-DTP	519	-	580	2.14	-
BDP-pPh-DTP	518	570	775	1.60	0.53
BDP-pPhF-DTP	510	570	780	1.59	0.65
BDP-Th-DTP	532	706	845	1.47	0.70
BDP-DTP	529	636	710	1.75	0.71
BDP-CC-DTP	645	724	845	1.47	1.21

Table 3.2: Summarized data extracted from the thin film absorption spectra.

Absorption of BDP-Th-DTP and BDP-DTP also red shifts comparatively by 16 and 15 nm, respectively. While the relative intensity in BDP-Th-DTP increases to 0.7, BDP-DTP remains consistent with the solution state spectrum. This could be due to a combination of the short conjugation length and the BODIPY-donor twist. The short conjugation length is also the source for the relatively large optical band gap that is only superseded by BDP-mPh-DTP. BDP-Th-DTP has the lowest band gap of the series (1.47 eV).

Again, BDP-CC-DTP has the most significant change in the series, as with the solution spectra. Both the BODIPY and charge transfer peaks red shift by 90 nm, but the relative intensity only slightly increases by 0.07. The optical band gap matches that of BDP-Th-DTP, indicating that there may be a lower limit to the optical band gap for this specific architecture, if we consider the ethynyl linker to best promote D-A communication. Part of this may be a result of the meso conjugation being relatively insulating. Attachment using the α or β positions may yield a lower band gap.

3.3.3 Electrochemical Properties

The electrochemical properties of the molecules were examined using cyclic voltammetry. The redox potentials were measured against a Ag/Ag^+ reference cell and corrected with respect to the ferrocene/ferrocenium (Fc/Fc^+) redox couple. The optical band gap extracted redox potentials of the BODIPY dyes are listed in Table 3.3. The measured voltammograms are shown in Figure 3.5. The HOMO and LUMO were calculated using the following equations.

$$\text{HOMO} = -(E^{ox} + 4.8)$$

$$\text{LUMO} = E^{ox} + E_g^{opt}$$

E^{ox} is the onset of the first oxidation peak and E_g^{opt} is the optical band gap as extracted from the red edge onset of thin film absorption ($E_g^{opt} = 1240/\lambda_{onset}$).

For each molecule, we observed a reversible oxidation event, with the exception of BDP-DTP and BDP-CC-DTP that showed no reversibility. For BDP-mPh-

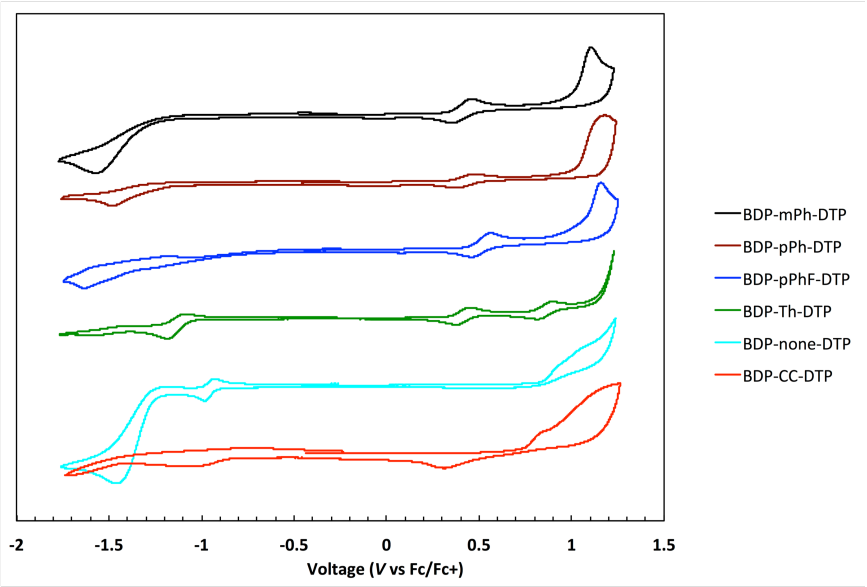

Figure 3.5: Cyclic voltammograms of BDP-mPh-DTP (black), BDP-pPh-DTP (brown), BDP-pPhF-DTP (blue), BDP-Th-DTP (green), BDP-DTP (light blue), BDP-CC-DTP (red).

BODIPY	E_g^{opt} (eV)	E^{ox} (V)	E^{red} (V)
BDP-mPh-DTP	2.14	0.36	-1.30
BDP-pPh-DTP	1.60	0.36	-1.24
BDP-pPhF-DTP	1.59	0.42	-1.08
BDP-Th-DTP	1.47	0.34	-1.12
BDP-DTP	1.75	0.82	-0.92
BDP-CC-DTP	1.47	0.73	-0.86

Table 3.3: Summarized electrochemical redox potentials.

DTP and BDP-pPh-DTP, we can see a single, identical oxidation event at 0.36 V. These results show that the two BODIPY moieties are independent and electronically equivalent in these phenylene derivatives. While BDP-pPhF-DTP also shows only one oxidation event, the reversibility is maintained and the voltage shifts positive because of the introduction of two fluorine atoms. The electrochemical properties were previously discussed in Chapter 2.3.3. BDP-none-DTP and BDP-CC-DTP both yield an oxidation potential more positive than that of each of the phenylene or thiophene linked molecules. Therefore, the ethynyl linker

improves "push-pull" communication and stabilizes the oxidation of the dye. This indicates that the HOMO, which is largely dependent on the donor core, is effectively modulated when the communication between the donor and acceptor is improved.

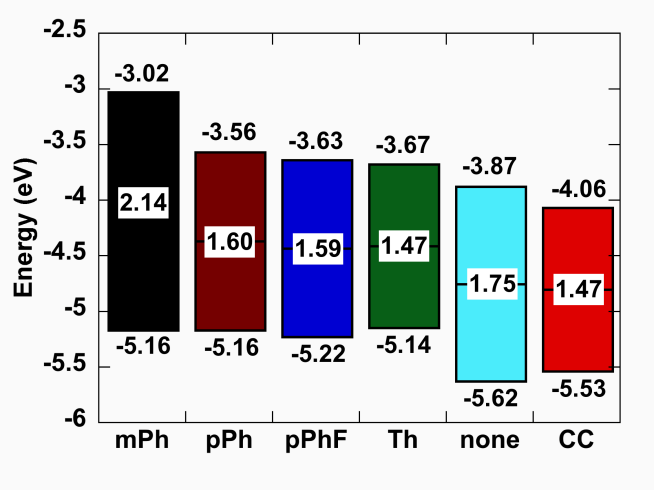

Figure 3.6: Experimentally determined band gap and HOMO and LUMO energy levels of BDP-mPh-DTP (black), BDP-pPh-DTP (brown), BDP-pPhF-DTP (blue), BDP-Th-DTP (green), BDP-DTP (light blue), BDP-CC-DTP (red).

The reduction potentials show a much more gradual positive shift following the previously described trend, BDP-mPh-DTP< BDP-pPh-DTP < BDP-pPhF-DTP < BDP-Th-DTP < BDP-DTP < BDP-CC-DTP. The reversibility of the reduction event is only seen in BDP-Th-DTP and BDP-DTP, with BDP-Th-DTP showing only a quasi-reversible peak.

The frontier molecular orbitals extracted from the CV spectra using the onset of oxidation and the optical band gap are plotted in Figure 3.6. While the HOMO level does not seem to follow a general trend, we can see a trending stabilization in the LUMO level correlating to the increasing D-A communication. The weakest linker (*m*-phenylene) gives a LUMO of -3.02 eV. Replacement with the *p*-phenylene linker led to a 0.54 eV stabilization of the LUMO, because of the reduced band gap. Further stabilization in the LUMO due to the introduction of the fluorine atoms was

achieved in BDP-pPhF-DTP, although the reduction was not as drastic (0.07 eV). The HOMO was also stabilized by 0.06 eV.

Introduction of the thiophene linker further stabilized the LUMO to -3.67 eV, coupled with a reduction in band gap. Eliminating the linker and directly conjugating the DTP and BODIPY units yielded a significant LUMO stabilization of 0.2 eV. This stabilization likely comes because of the increased delocalization of electron density and increased modulation of the electronic properties of the BODIPY moieties. Finally, BDP-CC-DTP possesses the lowest lying LUMO of -4.06 eV, as it benefits from good communication between donor and acceptor, matched with a reduced band gap due to the extended conjugation length.

3.3.4 Theoretical Calculations

To better understand the trends observed in the optical and electrochemical measurements, theoretical calculations were done using density functional theory (DFT). Figure 3.7 shows the surface plots of the calculated HOMO and LUMO energy levels estimated using the B3LYP functional and 6-311G(d,p) basis set.[18]

The increase in the ICT band correlates well with the theoretical calculations, if we observe the overlap between HOMO and LUMO orbitals. The HOMO of BDP-mPh-DTP is completely localized on the donor core and phenylene linker, since the *meta* linkage and the BODIPY twist break the conjugation between the DTP donor and the BODIPY acceptors. For this reason, the BODIPY unit is very independent and the absorption spectra looks as such, with a significant high energy absorption specific to the BODIPY π-π^* transition. While BDP-pPh-DTP and BDP-pPhF-DTP still

show localization of the HOMO on the donor core and phenylene linker, as well as a significant twist at the BODIPY-phenylene bond in the optimized structure, the LUMO begins to slightly extend into the DTP core. This correlates to evolution of an ICT band with low intensity. The additional fluorine atoms in BDP-pPhF-DTP do not seem to greatly affect the intensity of this ICT band, which agrees with the very similar HOMO and LUMO localization, compared to BDP-pPh-DTP.

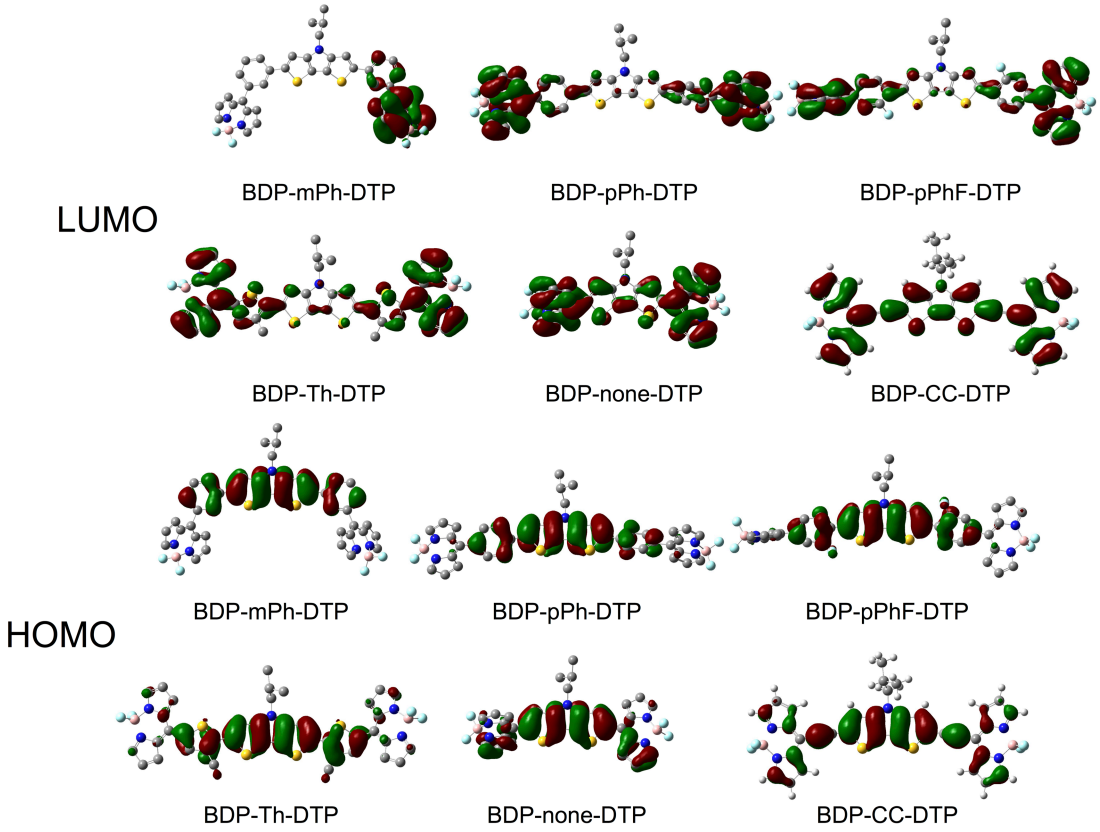

Figure 3.7: Surface plots of the calculated HOMO and LUMO energy levels calculated using B3LYP/6-31G(d,p).

As discussed in Chapter 2.5, the presence of the "strong" donor core is able to affect the absorption properties significantly. This is seen by the slight contribution of the DTP unit to the LUMO, increasing HOMO/LUMO overlap in BDP-Th-DTP, compared to the phenyl-linked molecules. Also, there is a slight contribution from a

single pyrrole unit of the BODIPY moieties in the HOMO, which correlates to the red shift in the BODIPY π-π^* absorption peak. Removing the linker completely in BDP-DTP generates much more overlap between HOMO and LUMO, since the BODPY and the donor are in direct conjugation. This results in a near doubling of the ICT band relative intensity compared to BDP-Th-DTP. Although the calculated molecular orbitals show improved communication between DTP and BODIPY moieties in BDP-DTP, the red edge absorption is blue shifted compared to BDP-Th-DTP due to a reduction in conjugation length.

As expected, BDP-CC-DTP shows the greatest delocalization in both HOMO and LUMO, with electron density balanced across both pyrrole units of the BODIPY moieties in the HOMO and consistent electron density across the entire molecule in the LUMO. The improved contribution from the sulfur atoms in the LUMO could also contribute to the stabilization of the experimentally determined LUMO level; greater contribution was also observed in BDP-DTP, which also exhibited a significant LUMO stabilization. There also seems to be a gain in planarity compared to BDP-DTP. The great overlap between the HOMO and LUMO support drastic red shift of the BODIPY π-π^* transition and the intense charge transfer band observed in solution and thin film absorption spectra.

Figure 3.8 shows the calculated values for the HOMO and LUMO energy levels. We can see that the trend in LUMO stabilization observed in the experimentally determined LUMO levels is in good agreement with the theoretically calculated values. BDP-mPh-DTP shows the highest LUMO of -3.07 eV, which gradually decreases to BDP-DTP (-3.48 eV). While the most stable LUMO should

belong to BDP-CC-DTP, the calculated values are very close and likely within experimental error.

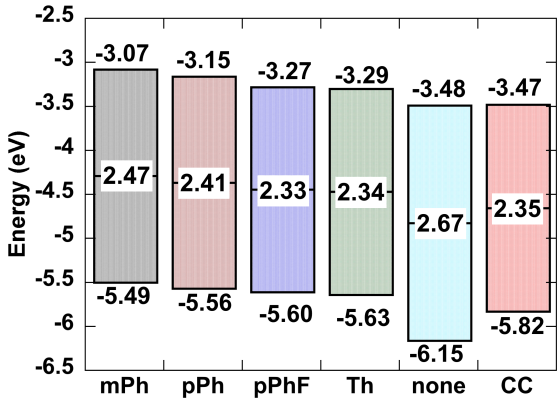

Figure 3.8: Plot of theoretically (B3LYP/6-31G(d,p) basis set) calculated HOMO and LUMO energy levels for BDP-mPh-DTP (black), BDP-pPh-DTP (brown), BDP-pPhF-DTP (blue), BDP-Th-DTP (green), BDP-DTP (light blue) and BDP-CC-DTP (red).

	Energy (eV)	*f*
BDP-mPh-DTP	2.09	0.004
BDP-pPh-DTP	2.13	0.759
BDP-pPhF-DTP	2.05	0.856
BDP-Th-DTP	1.99	1.173
BDP-DTP	2.36	0.872
BDP-CC-DTP	2.16	2.035

Table 3.4: Calculated excited state energy of ICT bands and oscillator strengths determined using TDDFT (B3LYP/6-31G(d,p)).

To gain insight into the excited state of these molecules, time-dependent density functional theory (TDDFT) calculations were carried out using the optimized ground state structure for each BODIPY dye. Table 3.3 shows the energies and oscillator strengths of the calculated long wavelength band for each molecule. The calculated oscillator strengths seem to be directly related to the planarity of the geometry optimized ground state structure and the overlap between the HOMO and LUMO electron densities. The near nonexistent HOMO/LUMO overlap in BDP-mPh-DTP is represented by the oscillator strength of the low energy excited state

(f=0.004), indicating that this transition could be forbidden.[19] The low energy transitions for all of the other molecules are allowed, which is consistent with the fact that they each show a low energy band in their experimental absorption spectra. While each of the molecules, excluding BDP-mPh-DTP, yielded oscillator strengths greater than 0.75, the oscillator strengths of BDP-Th-DTP and BDP-CC-DTP were much higher. This is likely due to their more planar geometries better delocalizing electron density in both the HOMO and LUMO.

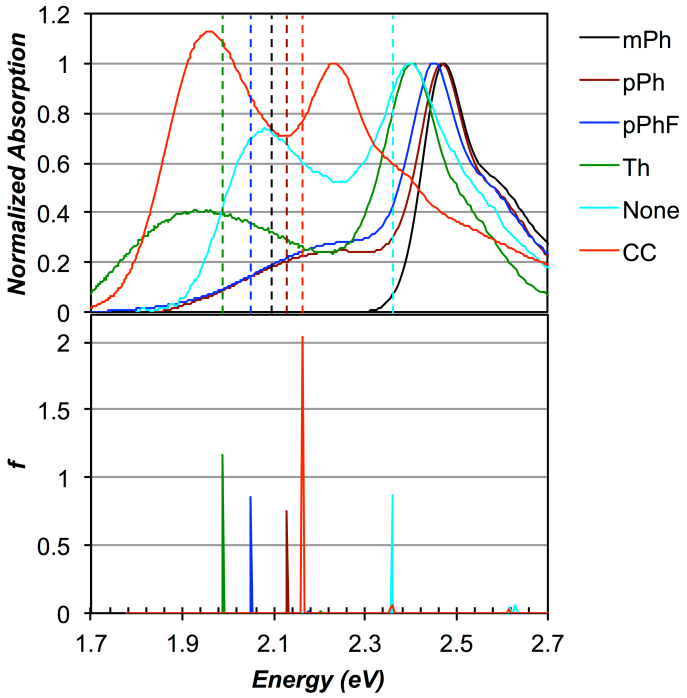

Figure 3.9: Solution state absorption spectra (top) for BDP-mPh-DTP (black), BDP-pPh-DTP (brown), BDP-pPhF-DTP (blue), BDP-Th-DTP (green), BDP-DTP (light blue), BDP-CC-DTP (red) and line plot of the energy and oscillator strengths of the first six excited states of each dye. Dashed lines in the absorption spectrum corresponds to the energy of the lowest energy band.

The calculated energy of the low energy transition also seemed to greatly depend on the identity of the linker, specifically aromaticity and charge delocalization in the linker unit. The dominant calculated energy band for each

molecule increases in energy as follows: BDP-Th-DTP < BDP-pPhF-DTP < BDP-mPh-DTP < BDP-pPh-DTP < BDP-CC-DTP < BDP-DTP. BDP-Th-DTP shows the lowest calculated energy band, which aligns with the ICT peak of the experimental solution state absorption spectrum, due to the relatively high electron density on the 5-membered heteroaromatic thiophene ring. BDP-pPhF-DTP follows BDP-Th-BDP, due to the fluorine atoms attached to the phenylene linkers contributing to the electron density of the unit. While BDP-mPh-DTP should have the next highest energy, followed by BDP-pPh-BDP, the reliability of this energy is questionable, given the forbidden nature of the transition.

Figure 3.9 shows the plotted energies and oscillator strengths of the first six lowest energy excited states. However, due to the low oscillator strengths of the subsequent excited states (N=2-6), the first excited state (HOMO → LUMO) is the most pronounced. With the exception of BDP-mPh-DTP, each molecule possessing aromatic linkers shows good alignment between calculated and experimental low energy bands. Alternatively, the calculated bands for BDP-DTP and BDP-CC-DTP are much closer to the BODIPY π-π^* peak of the experimental spectra. The lower energy of the BDP-CC-DTP band is likely due to the extended conjugation of this molecule, compared to BDP-DTP.

3.3.5 Charge Carrier Mobility

With such disparate LUMO energies, we went on to evaluate the molecules' electron transporting capabilities using bottom gate, bottom contact field effect transistors to determine the correlation between their LUMO levels and the charge

carrier mobility, if any. The devices were prepared using similar methods to those discussed in Chapter 2.6, where the active material was spin casted from a filtered (0.45 μm) 10 mg mL^{-1} solution onto prefabricated devices on top of the gold source and drain electrodes. We evaluated the charge transport characteristics at W/L ratios of 4000, 2000, 1000 and 500 to determine both the charge carrier type and the long-range mobility. The best mobilities are shown in Figure 3.10 and the device properties are detailed in Table 3.4. In each case, the semiconductors performed best in devices where the channel length was 2.5 μm (W/L = 4000). Increasing the channel length resulted in a moderate decrease in device performance, but increasing channel length further yielded a less significant decrease in electron mobility, depending on the semiconductor. In spite of this mobility decrease, we were able to observe trends in electron mobility dependent on the linker unit.

Similar to the molecules discussed in Chapter 2, each semiconductor showed only n-type characteristics with varying degrees of electron mobility. The best

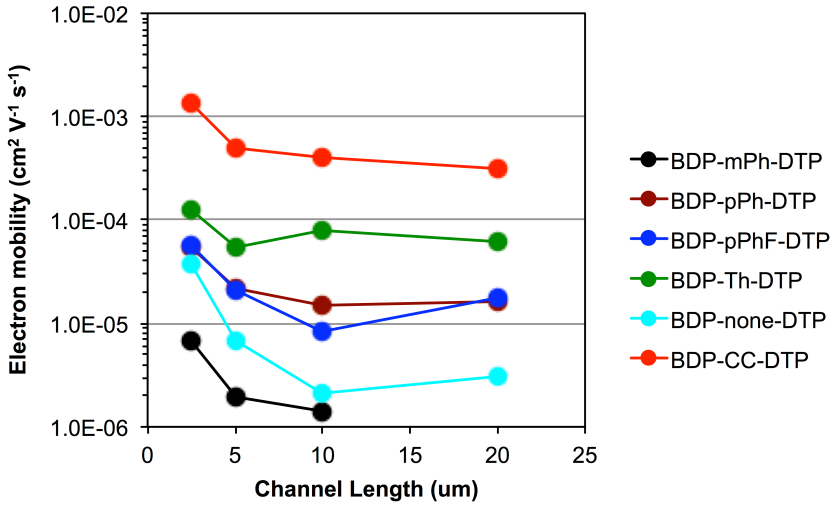

Figure 3.10: Best electron mobility values for the BODIPY dyes with respect to the channel length.

		Electron Mobility ($cm^2 V^{-1} s^{-1}$)			
	W/L	*Average*	*Best*	$I_{on/off}$	V_T *(V)*
BDP-mPh-DTP	4000	$6.79 (\pm.14) \times 10^{-6}$	6.86×10^{-6}	10^2	48.9
	2000	$1.97 (\pm.07) \times 10^{-6}$	1.96×10^{-6}	10^2	50.0
	1000	$1.35 (\pm.08) \times 10^{-6}$	1.42×10^{-6}	10^2	48.3
	500	-	-	-	-
BDP-pPh-DTP	4000[a]	$5.12 (\pm.62) \times 10^{-5}$	5.39×10^{-5}	10^3	53.5
	2000[a]	$2.14 (\pm.08) \times 10^{-5}$	2.19×10^{-5}	10^3	45.2
	1000[a]	$1.43 (\pm.16) \times 10^{-5}$	1.48×10^{-5}	10^4	51.4
	500[a]	$1.43 (\pm.18) \times 10^{-5}$	1.66×10^{-5}	10^3	48.3
BDP-pPhF-DTP	4000	$3.25 (\pm1.9) \times 10^{-5}$	5.71×10^{-5}	10^3	36.9
	2000	$1.78 (\pm.25) \times 10^{-5}$	2.10×10^{-5}	10^3	29.1
	1000[a]	$8.21 (\pm1.9) \times 10^{-6}$	0.82×10^{-5}	10^3	29.5
	500	$1.36 (\pm.56) \times 10^{-5}$	1.80×10^{-5}	10^3	37.3
BDP-Th-DTP	4000	$1.16 (\pm.07) \times 10^{-4}$	1.24×10^{-4}	10^4	33.3
	2000	$5.02 (\pm.32) \times 10^{-5}$	0.54×10^{-4}	10^3	27.3
	1000	$7.87 (\pm.09) \times 10^{-5}$	0.80×10^{-4}	10^3	50.9
	500	$4.38 (\pm1.8) \times 10^{-5}$	0.62×10^{-4}	10^3	49.1
BDP-DTP	4000	$3.69 (\pm.10) \times 10^{-5}$	3.78×10^{-5}	10^3	27.6
	2000[a]	$4.32 (\pm1.5) \times 10^{-6}$	0.69×10^{-5}	10^3	45.0
	1000[a]	$1.91 (\pm.11) \times 10^{-6}$	0.21×10^{-5}	10^4	39.7
	500	$2.97 (\pm.09) \times 10^{-6}$	0.31×10^{-5}	10^3	2.01
BDP-CC-DTP	4000	$1.27 (\pm.09) \times 10^{-3}$	1.38×10^{-3}	10^3	35.7
	2000	$3.76 (\pm1.3) \times 10^{-4}$	0.50×10^{-3}	10^3	24.1
	1000	$3.71 (\pm.30) \times 10^{-4}$	0.41×10^{-3}	10^4	23.3
	500	$2.81 (\pm.29) \times 10^{-4}$	0.31×10^{-3}	10^3	21.8

Table 3.3: Detailed device properties obtained from bottom gate bottom contact field effect transistors. [a]Device annealed at 80°C for 30 min before measurement.

electron mobilities for each semiconductor are plotted in Figure 3.11, along with their experimentally determined HOMO and LUMO levels.

The poorest performing material was BDP-mPh-DTP, showing electron mobility of 6.86×10^{-6} cm^2 V^{-1} s^{-1} at *W/L* = 4000. The observed n-type characteristics of BDP-mPh-DTP were surprising, given the relatively high LUMO level (-3.02 eV). Thermodynamically, the large gap between the LUMO and the Fermi level of the gold source electrode (-5.1 eV) should make electron injection very difficult.[20, 21] However, it is feasible that the boron difluoride units on the BODIPY moieties

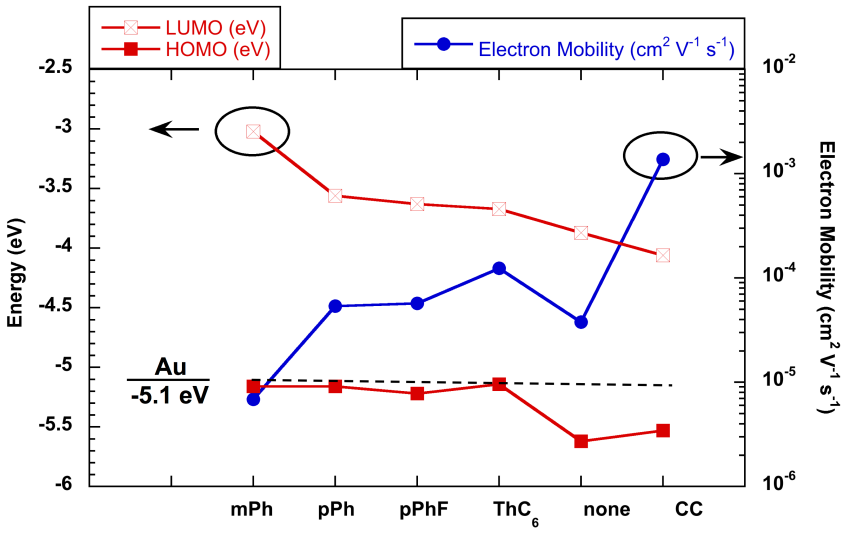

Figure 3.11: Plot of the HOMO (red, closed squares) and LUMO (red, open squares) energy levels and the best electron mobilities (blue). As the LUMO level stabilizes, an improvement in electron mobility is observed.

permit electron transport in spite of the unstable LUMO.[22] However, the molecular architecture could also hinder electron mobility, given its asymmetry and the potential for the BODIPY units to be either *syn* or *anti* in the solid state. This could negatively affect the molecular ordering in the solid state and account for the poor electron mobility.

Altering the connectivity from *meta* to *para* yielded an improvement in electron mobility by nearly an order of magnitude to 5.39 x 10^{-5} cm^2 V^{-1} s^{-1} at the same *W/L* ratio. Mobility on this order was maintained as the *W/L* ratio was decreased, yielding a mobility of 1.66x10^{-5} cm^2 V^{-1} s^{-1} at a channel length of 20 μm. This indicates that the structural tuning allowed for improved molecular ordering in the solid state considering that BDP-mPh-DTP shows no electron mobility at 20 μm.

Asymmetry seems to be the dominating factor in the poor charge transport properties. This carries over to BDP-pPhF-DTP, as the mobilities are nearly identical

to those of BDP-pPh-DTP, despite the stabilized LUMO of BDP-pPhF-DTP (-3.63 eV) compared to BDP-pPh-DTP (-3.56 eV).

BDP-Th-DTP showed electron mobilities nearly double that of BDP-pPh-DTP, reaching 1.24 x 10^{-4} cm^2 V^{-1} s^{-1} at W/L = 4000. While the thiophene units makes the BDP-Th-DTP molecule susceptible to similar *syn*/*anti* asymmetry that affects BDP-mPh-DTP and BDP-pPhF-DTP, the conformation between the thiophene linker and the DTP thiophenes are likely *anti* due to steric interactions between the thiophene hexyl chain and the DTP ethylhexyl unit. This interaction, combined with the smaller size of the thiophene unit compared to the phenylene unit, allowing for better planarity across the entire molecule and the more stable and delocalized LUMO, benefit the charge transport properties.

BDP-DTP shows mobilities on the order of ~10^{-5} cm^2 V^{-1} s^{-1} at W/L = 4000. At longer channel lengths, the mobility drops 10^{-6} cm^2 V^{-1} s^{-1}. The relatively low mobility compared to BDP-Th-DTP, in spite of the LUMO stabilization, could be due to the shortened conjugation length and poorer solid state ordering as a result. Introduction of the ethynyl liker drastically increases the charge transport, yielding electron mobilities consistently on the order of 10^{-4} cm^2 V^{-1} s^{-1} across the entire range of W/L values and reaching as high as 1.38 x 10^{-3} cm^2 V^{-1} s^{-1} at W/L = 4000. The source of the improved mobility is a combination of the increased crystallinity instilled by the rigid, rod-like linker and the delocalized LUMO; stabilization of the LUMO to -4.06 eV could also be a factor.

The thin film surface topography was measured using tapping mode atomic force microscopy (AFM) measurements of spun cast films. Analyses of the height

images show very low surface roughness for each of the phenylene-linked molecules, with RMS values of 0.267 nm (BDP-mPh-DTP), 0.389 nm (BDP-pPh-DTP) and 0.369 (BDP-pPhF-DTP). The RMS nearly doubles for BDP-DTP, giving a value of 0.792 nm with slight evidence of nanostructures being formed. The most significant ordering is seen in BDP-CC-DTP, matching the improved charge carrier mobility. The surface roughness increases drastically to 28.9 nm due to the formation of large crystallites (*ca.* 160 nm). As expected, the crystallinity was best in BDP-CC-DTP due to the rigid ethynyl linker, allowing for the consistently high mobility across channel lengths as high as 20 μm.

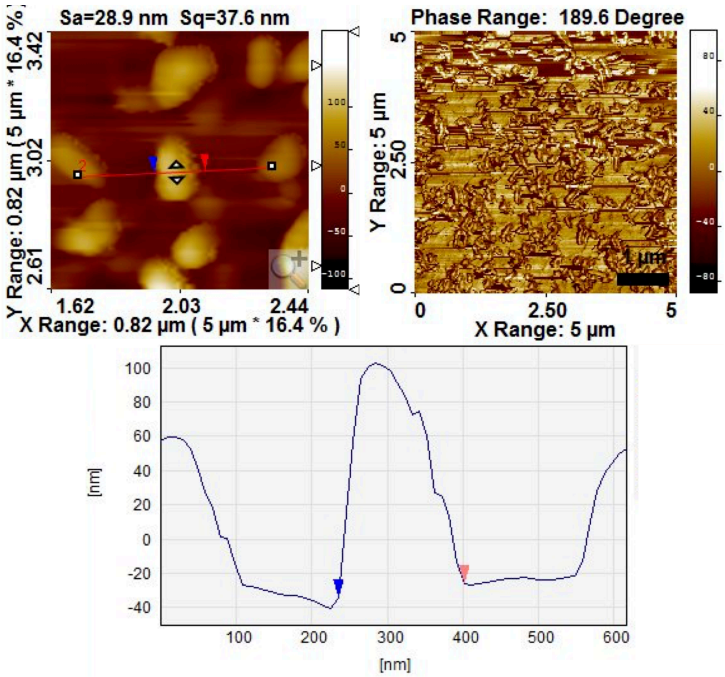

Figure 3.12: Height (top-left), phase (top-right) and surface profile (bottom) images for BDP-CC-DTP thin film obtained by tapping atomic force microscopy. The height and surface profile images highlight an observed aggregated *ca.* 160 nm wide.

Although the mobility values are widely varied through structural modifications, we still consistently see n-type characteristics using this architecture,

showing that the BODIPY capping strategy could be very useful for generating n-type materials with mobilities as high as 10^{-3} cm^2 V^{-1} s^{-1}.

3.4 Summary

In summary, the previously designed BODIPY based A-D-A architecture was expanded through systemic modification of the linker between the donor core and the BODIPY capping moiety. The linker unit was varied in such a way that a gradient of "push-pull" character was achieved, with the linker acting as the gateway. Relatively insulating phenylene linkers (*m*-phenylene) gave narrow absorption properties and a substantially destabilized LUMO level, while installation of an ethynyl linker, or removal of the linker altogether, led to red shifted absorption properties with a well pronounced charge transfer band, as well as significant stabilization both HOMO and LUMO energy levels.

Theoretical DFT calculations were used to examine the optimized ground state energetics, while TDDFT was used to examine the excited states of these molecules. A combination of these methods allowed us to see that the localized electron density of the linker, as well as the delocalization of the HOMO and LUMO across the entire A-D-A molecule, play a significant role in the stabilization of the energy levels. Also, analysis of the optimized geometries showed that planarization of the A-D-A molecules greatly benefit the charge delocalization in the ground and excited states.

Field effect transistors were used to show the consistent n-type characteristics, independent of the LUMO level. The best performing material was

found to be BDP-CC-DTP, given its planar structure, its low-lying, delocalized LUMO and its ability to form large crystallites in the solid state. All of these factors allowed a mobility on the order of 10^{-3} cm^2 V^{-1} s^{-1} to be achieved and short channel lengths and 10^{-4} cm^2 V^{-1} s^{-1} $W/L > 500$.

3.5 Experimental

All reagents were purchased from commercial sources and used as received, unless otherwise mentioned. Tetrahydrofuran (THF) was distilled over sodium and benzophenone. *N*-(2-ethylhexyl)-2,6-bis(trimethylstannyl)-dithieno[3,2-*b*:2′,3′-*d*]pyrrole and *N*-(2-ethylhexyl)-2,6-bis(tributylstannyl)-dithieno[3,2-*b*:2′,3′-*d*]pyrrole were synthesized according to the previously described method. 8-(thiomethyl)-4,4,difluoro-4-bora-3a,4a-diaza-*s*-indacene,[15] 8-chloro-4,4-difluoro-4-bora-3a,4a-diaza-s-indacene, 8–iodo-4,4-difluoro-4-bora-3a,4a-diaza-s-indacene,[16] and *N*-(2-ethylhexyl)-2,6-dibromo-dithieno[3,2-*b*:2′,3′-*d*]pyrrole[12] were synthesized according to previously reported methods. Liebskind-Srogl cross coupling reaction methods were adapted from previously reported procedures.[14]

3.5.1 Instrumentation

^{1}H NMR spectra were recorded on a 400 MHz Bruker NMR spectrometer and the chemical shifts are reported in ppm using deuterated solvent as the internal standard ($CDCl_3$ at 7.26 ppm). When peak multiplicities are given, the following abbreviations are used: s, singlet; d, doublet; t, triplet; m, multiplet. ^{13}C NMR spectra were proton decoupled and recorded on a 100 MHz Bruker NMR spectrometer

using the carbon signal of the deuterated solvent as the internal standard ($CDCl_3$ at 77.16 ppm).

3.5.2 Solution and Thin Film Absorption

Solution and thin film UV-vis absorption spectra were recorded on a Cary 100 scan UV-vis spectrophotometer. All extinction coefficients were determined from a linear fit of five data points. Thin films were prepared from dichloromethane solutions spin cast onto a glass substrate, followed by annealing at 150 °C for 10 min.

3.5.3 Cyclic Voltammetry

Solution state electrochemical measurements were performed on a BASi Epsilon potentiostat using a Pt disc electrode as a working electrode and a Pt wire as the auxiliary electrode. The potentials were measured against a Ag/Ag^+ reference at a scan rate of 50 mV s^{-1}. Tetrabutylammonium hexafluorophosphate was used as the supporting electrolyte and the recorded voltammograms were calibrated with respect to an internal standard (ferrocene/ferrocenium (Fc/Fc+) redox couple).

3.5.4 Field Effect Transistors

Organic field effect transistor (OFET) devices were fabricated using pre-patterned n-doped silicon substrates. Gold electrodes were deposited on the gate layer to yield the bottom contact OFETs. The channel width of all transistors was 10 mm. The channel length was 2.5, 5, 10 or 20 μm. The capacitance of the insulator is 14.9 nF cm^{-2} for 230 nm of SiO_2. The OFET substrates were rinsed with acetone to

remove the protective layer before film deposition. Organic thin films were deposited on the surface by spin coating a filtered (0.45 μm) 10 mg mL^{-1} chloroform solution at 1000 RPM for 60 s. The devices were allowed to dry at room temperature for 1 hour. The devices were measured directly after drying. All measurements were performed under a controlled atmosphere in a glove box using an Agilent 4165C precision semiconductor parameter analyzer.

3.5.5 Synthesis of 8-(3-bromophenyl)-4,4,difluoro-4-bora-3a,4a-diaza-*s*-indacene

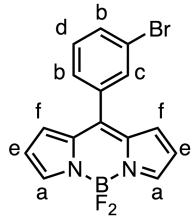

8-(thiomethyl)-4,4,difluoro-4-bora-3a,4a-diaza-*s*-indacene (238 mg, 1 mmol) and 3-bromophenylboronic acid (600 mg, 3 mmol) were dissolved in THF under argon. The mixture was purged with argon for 10 minutes. Copper (I) thiophene-2-carboxylate (570 mg, 3 mmol), Pd_2dba_3 (24 mg, 2.5 mol%) and tris(2-furyl)phosphine (25 mg, 7.5 mol%) were added as a solid mixture. The reaction was placed into a preheated sand bath and stirred at 55°C for 3 hr. The solvent was removed *in vacuo* and the crude product was purified by silica gel column chromatography using hexanes and ethyl acetate as eluents. The solvents were removed *in vacuo* to give a red solid (306 mg, 87%). **^{1}H-NMR** (400 MHz, $CDCl_3$): δ 7.96 (s, 2H, a), 7.74-7.72 (m, 2H, b), 7.50 (d, J = 7.7 Hz, 1H, c), 7.43-7.39 (m, 1H, d), 6.92 (d, J = 4.1 Hz, 2H, e), 6.57 (d, J = 3.9 Hz, 2H, f).

3.5.6 Synthesis of 8-(4-bromophenyl)-4,4,difluoro-4-bora-3a,4a-diaza-*s*-indacene

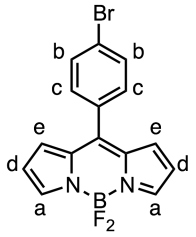

8-(thiomethyl)-4,4,difluoro-4-bora-3a,4a-diaza-*s*-indacene (238 mg, 1 mmol) and 4-bromophenylboronic acid (600 mg, 3 mmol) were dissolved in THF under argon. The mixture was purged with argon for 10 minutes. Copper (I) thiophene-2-carboxylate (570 mg, 3 mmol), Pd_2dba_3 (24 mg, 2.5 mol%) and tris(2-furyl)phosphine (25 mg, 7.5 mol%) were added as a solid mixture. The reaction was placed into a preheated sand bath and stirred at 55°C for 3 hr. The solvent was removed *in vacuo* and the crude product was purified by silica gel column chromatography using hexanes and ethyl acetate as eluents. The solvents were removed *in vacuo* to give a red solid (322 mg, 91%). **^{1}H-NMR** (400 MHz, $CDCl_3$): δ 7.96 (s, 2H, a), 7.70-7.67 (m, 2H, b), 7.46-7.43 (m, 2H, c), 6.91 (d, J = 4.2 Hz, 2H, d), 6.57-6.56 (m, 2H, e).

3.5.7 Synthesis of 8-(3-fluoro-4-bromophenyl)-4,4,difluoro-4-bora-3a,4a-diaza-*s*-indacene

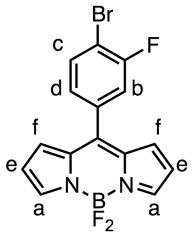

8-(thiomethyl)-4,4,difluoro-4-bora-3a,4a-diaza-*s*-indacene (318 mg, 1.34 mmol) and 3-fluoro-4-bromophenylboronic acid (670 mg, 2.2 mmol) were dissolved

in THF under argon. The mixture was purged with argon for 10 minutes. Copper (I) thiophene-2-carboxylate (572 mg, 2.2 mmol), Pd_2dba_3 (23 mg, 1.9 mol%) and tris(2-furyl)phosphine (18 mg, 5.6 mol%) were added as a solid mixture. The reaction was placed into a preheated sand bath and stirred at 55°C for 3.5 hr. The solvent was removed *in vacuo* and the crude product was purified by silica gel column chromatography using hexanes and ethyl acetate as eluents. The solvents were removed *in vacuo* to give a red crystalline solid (169 mg, 35%). **^{1}H-NMR** (400 MHz, $CDCl_3$): δ 7.97 (s, 2H, a), 7.76-7.72 (m, 1H, b), 7.37-7.34 (m, 1.9 Hz, 1H, c), 7.24 (d, J = 1.4 Hz, 1H, e), 6.92 (d, J = 4.1 Hz, 2H, f), 6.58 (d, J = 3.9 Hz, 2H, g). **^{13}C-NMR** (100 MHz, $CDCl_3$): δ 160.25, 157.77, 145.24, 144.15, 134.82, 134.75, 134.63, 134.03, 131.37, 127.25, 127.21, 119.24, 118.64, 118.40, 112.44, 112.23. FAB/MS Calculated *m/z* = 364.0, Found *m/z* = 364.0.

3.5.8 Synthesis of BDP-mPh-DTP

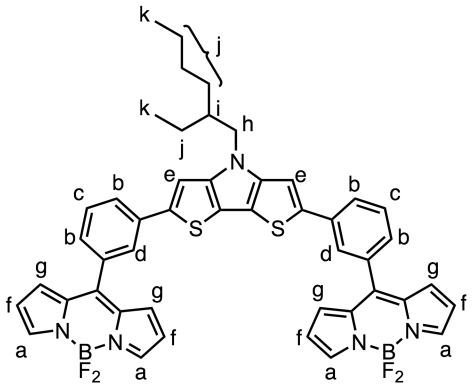

N-(2-ethylhexyl)-2,6-bis(trimethylstannyl)-dithieno[3,2-b:2′,3′-d]pyrrole (150 mg, 0.243 mmol) and 8-(3-bromophenyl)-4,4-difluoro-4-bora-3a,4a-diaza-s-indacene (178 mg, 0.512 mmol) were dissolved in degassed toluene, followed by the addition of Pd_2dba_3 (23 mg, 10 mol%) and tri(o-tolyl)phosphine (23 mg, 30 mol%).

The reaction was heated to reflux and stirred for 24 hr. The solvents were removed *in vacuo* and the crude product was purified by silica gel column chromatography using hexanes and ethyl acetate as eluents. The solvents were removed *in vacuo* to give the product as a red solid (28 mg, 14 %). **^{1}H-NMR** (400 MHz, $CDCl_3$): δ 7.98 (s, 4H, a), 7.85-7.82 (m, 4H, b), 7.55 (t, J = 7.6 Hz, 2H, c), 7.45 (d, J = 7.7 Hz, 2H, d), 7.27 (s, 2H, e), 7.02 (d, J = 3.9 Hz, 4H, f), 6.58 (t, J = 1.9 Hz, 4H, g), 4.10 (4.11-4.08, 2H, h), 2.03-1.97 (m, 1H, i), 1.40-1.27 (m, 8H, j), 0.94-0.83 (m, 6H, k). **^{13}C-NMR** (100 MHz, $CDCl_3$): δ 146.97, 145.77, 144.57, 140.72, 136.04, 135.11, 134.71, 131.77, 131.70, 129.30, 129.16, 127.52, 127.08, 118.88, 118.85, 118.83, 115.20, 107.97, 51.62, 40.55, 30.71, 28.69, 24.13, 23.17, 14.17, 10.88. FAB/MS Calculated m/z = 823.3, Found m/z = 823.4.

3.5.9 Synthesis of BDP-pPh-DTP

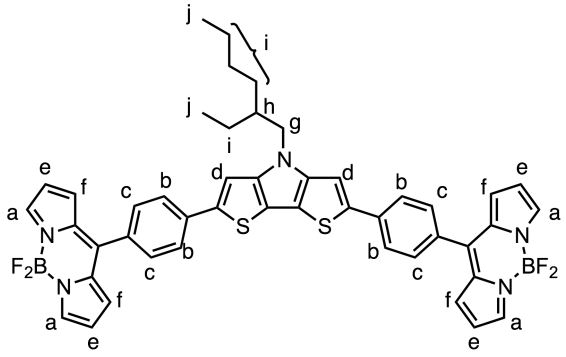

N-(2-ethylhexyl)-2,6-bis(trimethylstannyl)-dithieno[3,2-b:2′,3′-d]pyrrole (100 mg, 0.138 mmol) and 8-(4-bromophenyl)-4,4-difluoro-4-bora-3a,4a-diaza-s-indacene (100 mg, 0.275 mmol) were dissolved in degassed toluene, followed by the addition of Pd_2dba_3 (10 mg, 8 mol%) and tri(o-tolyl)phosphine (10 mg, 23 mol%). The reaction was heated to reflux and stirred for 24 hr. The solvents were removed

in vacuo and the crude product was purified by silica gel column chromatography using hexanes and ethyl acetate as eluents. The solvents were removed *in vacuo* to give the product as a purple solid (46 mg, 40 %). **^{1}H-NMR** (400 MHz, $CDCl_3$): δ 7.96 (s, 4H, a), 7.81 (d, J = 8.3 Hz, 4H, b), 7.63 (d, J = 8.2 Hz, 4H, c), 7.38 (s, 2H, d), 7.04 (d, J = 4.1 Hz, 4H, e), 6.59-6.57 (m, 4H, f), 4.15 (t, J = 6.4 Hz, 2H, g), 2.06-2.03 (m, 1H, h), 1.45-1.29 (m, 8H, i), 0.99-0.92 (m, 6H, j). **^{13}C-NMR** (100 MHz, $CDCl_3$): δ 146.92, 146.27, 144.05, 141.05, 138.31, 134.89, 132.66, 131.64, 131.40, 125.18, 118.67, 115.86, 108.26, 51.66, 40.66, 30.83, 28.83, 27.99, 26.98, 24.25, 23.19, 17.63, 14.22, 13.76, 10.91. FAB/MS Calculated m/z = 823.3, Found m/z = 823.3.

3.5.10 Synthesis of BDP-pPhF-DTP

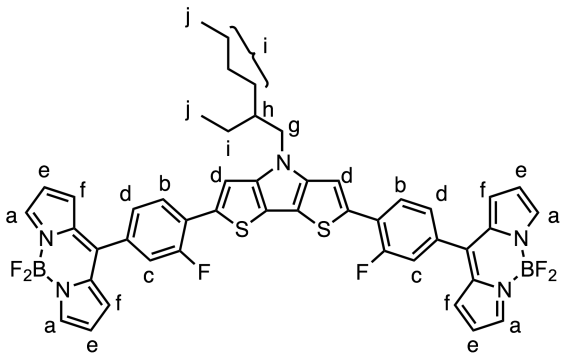

N-(2-ethylhexyl)-2,6-bis(tributylstannyl)-dithieno[3,2-b:2′,3′-d]pyrrole (174 mg, 0.200 mmol) and 8-(3-fluoro-4-bromophenyl)-4,4-difluoro-4-bora-3a,4a-diaza-s-indacene (150 mg, 0.410 mmol) were dissolved in degassed toluene, followed by the addition of Pd_2dba_3 (9 mg, 5 mol%) and tri(o-tolyl)phosphine (7 mg, 10 mol%). The reaction was heated to reflux and stirred for 24 hr. The solvents were removed *in vacuo* and the crude product was purified by silica gel column chromatography using hexanes and ethyl acetate as eluents. The solvents were removed *in vacuo* to give the product as a purple solid (72 mg, 42 %). **^{1}H-NMR** (400 MHz, $CDCl_3$): δ 7.98

(s, 4H, a), 7.84 (t, J = 7.9 Hz, 2H, b), 7.60 (s, 2H, c), 7.46-7.43 (m, 4H, d), 7.05 (d, J = 4.0 Hz, 4H, e), 6.60 (t, J = 2.0 Hz, 4H, f), 4.18 (t, J = 6.5 Hz, 2H, g), 2.05-2.02 (m, 1H, h), 1.44-1.26 (m, 8H, i), 0.99-0.86 (m, 6H, j). **^{13}C-NMR** (100 MHz, $CDCl_3$): δ 159.83, 157.32, 146.72, 145.05, 144.63, 142.97, 134.71, 134.55, 133.51, 133.42, 132.73, 131.36, 129.59, 127.97, 127.16, 126.22, 126.10, 122.66, 121.67, 119.01, 118.76, 116.01, 112.10, 111.99, 64.16, 51.51, 40.69, 30.81, 28.81, 26.96, 24.24, 23.13, 14.19, 13.76, 10.89. FAB/MS Calculated m/z = 859.3, Found m/z = 859.3.

3.5.11 Synthesis of BDP-DTP

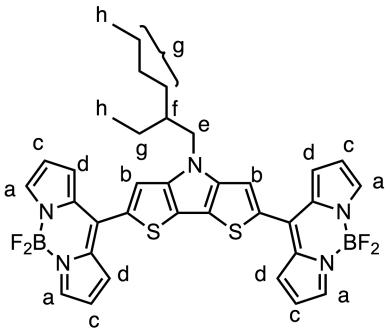

N-(2-ethylhexyl)-2,6-bis(trimethylstannyl)-dithieno[3,2-b:2′,3′-d]pyrrole (596 mg, 0.97 mmol) and 8–iodo-4,4-difluoro-4-bora-3a,4a-diaza-s-indacene (605 mg, 1.9 mmol) were dissolved in degassed toluene, followed by the addition of Pd_2dba_3 (45 mg, 5 mol%) and tri(o-tolyl)phosphine (45 mg, 15 mol%). The reaction was heated to reflux and stirred for 24 hr. The solvents were removed *in vacuo* and the crude product was purified by silica gel column chromatography using hexanes and ethyl acetate as eluents. The solvents were removed *in vacuo* to give the product as a purple solid (495 mg, 76 %). ^{1}H-NMR (400 MHz, $CDCl_3$): δ 7.98 (s, 4H, a), 7.84 (t, J = 7.9 Hz, 2H, b), 7.60 (s, 2H, c), 7.46-7.43 (m, 4H, d), 7.05 (d, J = 4.0 Hz, 4H, e), 6.60 (t, J = 2.0 Hz, 4H, f), 4.18 (t, J = 6.5 Hz, 2H, g), 2.05-2.02 (m, 1H, h), 1.44-1.26 (m,

8H, i), 0.99-0.86 (m, 6H, j). ^{13}C-NMR (101 MHz, $CDCl_3$): δ 159.83, 157.32, 146.72, 145.05, 144.63, 142.97, 134.71, 134.55, 133.51, 133.42, 132.73, 131.36, 129.59, 127.97, 127.16, 126.22, 126.10, 122.66, 121.67, 119.01, 118.76, 116.01, 112.10, 111.99, 64.16, 51.51, 40.69, 30.81, 28.81, 26.96, 24.24, 23.13, 14.19, 13.76, 10.89. FAB/MS ($C_{34}H_{31}B_2F_4N_5S_2$) Calculated m/z = 671.2, Found m/z = 671.2.

3.5.12 Synthesis of N-(2-ethylhexyl)-2,6-bis(trimethylsilylethynyl)-dithieno[3,2-b:2′,3′-d]pyrrole

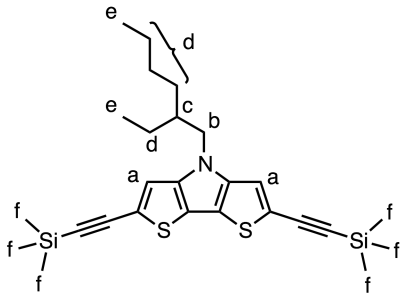

N-(2-ethylhexyl)-2,6-dibromo-dithieno[3,2-b:2′,3′-d]pyrrole (413 mg, 0.92 mmol) was dissolved under argon in a degassed solvent/base mixture (10 mL, toluene/diisopropylamine (2:1)). Ethynyltrimethylsilane (0.42 mL, 2.94 mmol) was added and the mixture was purged with argon for 10 minutes. $Pd(PPh_3)_2Cl_2$ (32 mg, 5 mol%) and copper (I) iodide (5 mg, 5 mol%) were added and the yellow solution gradually turned brown. The mixture was heated to 60°C and stirred overnight. The reaction mixture was cooled to room temperature. The crude was filtered over Celite and washed with toluene. The solvent was removed *in vacuo* and the crude solid was dissolved in dichloromethane and purified by silica gel chromatography using hexanes as the eluent. The solvent was removed *in vacuo* to give a brown oil that solidifies when cooled (425 mg, 95%). **^{1}H-NMR** (400 MHz, $CDCl_3$): δ 7.11 (s, 2H, a),

4.00-3.89 (m, 2H, b), 1.92-1.85 (m, 1H, c), 1.30-1.23 (m, 8H, d), 0.87 (t, J = 7.3 Hz, 6H, e), 0.28-0.26 (m, 18H, f). **^{13}C-NMR** (126 MHz, $CDCl_3$): δ 144.94, 121.00, 116.20, 115.91, 100.00, 99.32, 51.60, 40.43, 30.80, 28.86, 24.15, 23.13, 14.16, 10.79, 0.07. FAB/MS Calculated m/z =483.2, Found m/z = 483.3.

3.5.13 Synthesis of BDP-CC-DTP

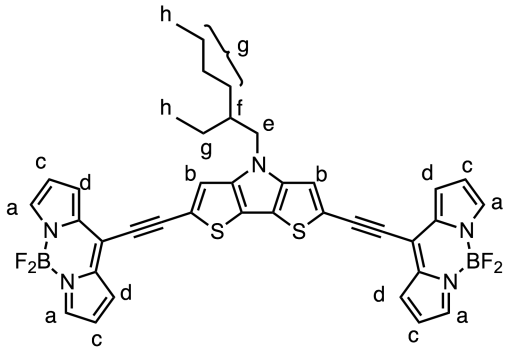

N-(2-ethylhexyl)-2,6-bis(trimethylsilylethynyl)-dithieno[3,2-b:2′,3′-d]pyrrole (425 mg, 0.88 mmol) was dissolved in THF under argon, followed by the addition of methanol (9 mL). 20% Aqueous potassium hydroxide (0.6 mL) was added and the mixture was stirred for 3 hours. The mixture was poured into water and extracted with dichloromethane (3 x 50 mL). The combined organic layer were washed with water and dried over anhydrous sodium sulfate. The solvents were removed *in vacuo* without heat using rotary evaporation. The crude was used without further purification.

The crude N-(2-ethylhexyl)-2,6-bis(ethynyl)-dithieno[3,2-b:2′,3′-d]pyrrole was dissolved under argon in a degassed solvent/base mixture (15 mL, toluene/triethylamine (2:1)). 8-chloro-4,4-difluoro-4-bora-3a,4a-diaza-s-indacene (279 mg, 1.23 mmol) was added and the mixture was cooled in an ice bath and

purged with argon for 20 minutes. $Pd(PPh_3)_2Cl_2$ (22 mg, 0.031 mmol) and copper (I) iodide (7 mg, 0.064 mmol) were added and the red solution quickly turned blue. The mixture was raised to room temperature and stirred overnight. The solvents were removed *in vacuo* and the crude solid was dissolved in dichloromethane and purified by silica gel chromatography using hexanes and ethyl acetate as the eluents. The solvents were removed *in vacuo* to give a crystalline purple solid (48 mg, 8% over 2 steps). **^{1}H-NMR** (400 MHz, $CDCl_3$): δ 7.82 (s, 4H), 7.38 (s, 2H), 7.34 (d, J = 3.9 Hz, 4H), 6.57-6.54 (m, 4H), 4.06-3.98 (m, 2H), 1.98-1.92 (m, 1H), 1.39-1.25 (m, 8H), 0.96-0.89 (m, 6H). **^{13}C-NMR** (100 MHz, $CDCl_3$): δ 147.50, 143.08, 135.73, 128.37, 126.51, 120.81, 120.35, 118.98, 118.35, 102.04, 92.49, 51.90, 40.51, 30.75, 28.72, 24.23, 23.14, 14.19, 10.85. FAB/MS Calculated m/z = 719.2, Found m/z = 719.4.

3.6 References

1. Poe, A. M.; Della Pelle, A. M.; Subrahmanyam, A. V.; White, W.; Wantz, G.; Thayumanavan, S., Small molecule BODIPY dyes as non-fullerene acceptors in bulk heterojunction organic photovoltaics. *Chem. Commun.* **2014**, 50, 2913-2915.

2. Kim, J.; Cho, N.; Ko, H. M.; Kim, C.; Lee, J. K.; Ko, J., Push-pull organic semiconductors comprising of bis-dimethylfluorenyl amino benzo[b]thiophene donor and various acceptors for solution processed small molecule organic solar cells. *Sol. Energ. Mat. Sol. Cells* **2012**, 102, 159-166.

3. Bura, T.; Leclerc, N.; Fall, S.; Leveque, P.; Heiser, T.; Retailleau, P.; Rihn, S.; Mirloup, A.; Ziessel, R., High-performance solution-processed solar cells and ambipolar behavior in organic field-effect transistors with thienyl-BODIPY scaffoldings. *J. Am. Chem. Soc.* **2012**, 134, 17404-17407.

4. Singh, S.; Venugopalan, V.; Krishnamoorthy, K., Organic soluble and uniform film forming oligoethylene glycol substituted BODIPY small molecules with improved hole mobility. *Phys. Chem. Chem. Phys.* **2014**, 16, 13376-82.

5. Hayashi, Y.; Obata, N.; Tamaru, M.; Yamaguchi, S.; Matsuo, Y.; Saeki, A.; Seki, S.; Kureishi, Y.; Saito, S.; Yamaguchi, S.; Shinokubo, H., Facile synthesis of biphenyl-fused BODIPY and its property. *Org. Lett.* **2012**, 14, 866-869.

6. Homnick, P. J.; Tinkham, J. S.; Devaughn, R.; Lahti, P. M., Engineering frontier energy levels in donor-acceptor fluoren-9-ylidene malononitriles versus fluorenones. *J. Phys. Chem. A* **2014**, 118, 475-486.

7. Thompson, A. L.; Ahn, T. S.; Thomas, K. R.; Thayumanavan, S.; Martinez, T. J.; Bardeen, C. J., Using meta conjugation to enhance charge separation versus charge recombination in phenylacetylene donor-bridge-acceptor complexes. *J. Am. Chem. Soc.* **2005**, 127, 16348-16349.

8. Maeda, T.; Tsukamoto, T.; Seto, A.; Yagi, S.; Nakazumi, H., Synthesis and Characterization of Squaraine-Based Conjugated Polymers With Phenylene Linkers for Bulk Heterojunction Solar Cells. *Macromol Chem Phys* **2012**, 213, 2590-2597.

9. Ashraf, R. S.; Shahid, M.; Klemm, E.; Al-Ibrahim, M.; Sensfuss, S., Thienopyrazine-Based Low-Bandgap Poly(heteroaryleneethynylene)s for Photovoltaic Devices. *Macromol. Rapid. Commun.* **2006**, 27, 1454-1459.

10. Huang, X.; Zhu, C.; Zhang, S.; Li, W.; Guo, Y.; Zhan, X.; Liu, Y.; Bo, Z., Porphyrin-Dithienothiophene π-Conjugated Copolymers: Synthesis and Their Applications in Field-Effect Transistors and Solar Cells. *Macromolecules* **2008**, 41, 6895-6902.

11. Lin, H. Y.; Huang, W. C.; Chen, Y. C.; Chou, H. H.; Hsu, C. Y.; Lin, J. T.; Lin, H. W., BODIPY dyes with beta-conjugation and their applications for high-efficiency inverted small molecule solar cells. *Chem. Commun.* **2012**, 48, 8913-5.

12. Popere, B. C.; Della Pelle, A. M.; Poe, A.; Balaji, G.; Thayumanavan, S., Predictably tuning the frontier molecular orbital energy levels of panchromatic low band gap BODIPY-based conjugated polymers. *Chem. Sci.* **2012**, 3, 3093-3102.

13. Popere, B. C.; Della Pelle, A. M.; Thayumanavan, S., BODIPY-Based Donor–Acceptor π-Conjugated Alternating Copolymers. *Macromolecules* **2011**, 44, 4767-4776.

14. Pena-Cabrera, E.; Aguilar-Aguilar, A.; Gonzalez-Dominguez, M.; Lager, E.; Zamudio-Vazquez, R.; Godoy-Vargas, J.; Villanueva-Garcia, F., Simple, general, and efficient synthesis of meso-substituted borondipyrromethenes from a single platform. *Org. Lett.* **2007**, 9, 3985-3988.

15. Goud, T. V.; Tutar, A.; Biellmann, J.-F., Synthesis of 8-heteroatom-substituted 4,4-difluoro-4-bora-3a,4a-diaza-s-indacene dyes (BODIPY). *Tetrahedron* **2006**, 62, 5084-5091.

16. Leen, V.; Yuan, P.; Wang, L.; Boens, N.; Dehaen, W., Synthesis of meso-halogenated BODIPYs and access to meso-substituted analogues. *Org. Lett.* **2012**, 14, 6150-6153.

17. Silvestri, F.; Marrocchi, A., Acetylene-based materials in organic photovoltaics. *International journal of molecular sciences* **2010**, 11, 1471-1508.

18. Frisch, M. J.; Trucks, G. W.; Schlegel, H. B.; Scuseria, G. E.; Robb, M. A.; Cheeseman, J. R.; Scalmani, G.; Barone, V.; Mennucci, B.; Petersson, G. A.; Nakatsuji, H.; Caricato, M.; Li, X.; Hratchian, H. P.; Izmaylov, A. F.; Bloino, J.; Zheng, G.; Sonnenberg, J. L.; Hada, M.; Ehara, M.; Toyota, K.; Fukuda, R.; Hasegawa, J.; Ishida, M.; Nakajima, T.; Honda, Y.; Kitao, O.; Nakai, H.; Vreven, T.; Montgomery, J., J. A.; Peralta, J. E.; Ogliaro, F.; Bearpark, M.; Heyd, J. J.; Brothers, E.; Kudin, K. N.; Staroverov, V. N.; Kobayashi, R.; Normand, J.; Raghavachari, K.; Rendell, A.; Burant, J. C.; Iyengar, S. S.; Tomasi, J.; Cossi, M.; Rega, N.; Millam, J. M.; Klene, M.; Knox, J. E.; Cross, J. B.; Bakken, V.; Adamo, C.; Jaramillo, J.; Gomperts, R.; Stratmann, R. E.; Yazyev, O.; Austin, A. J.; Cammi, R.; Pomelli, C.; Ochterski, J. W.; Martin, R. L.; Morokuma, K.; Zakrzewski, V. G.; Voth, G. A.; Salvador, P.; Dannenberg, J. J.; Dapprich, S.; Daniels, A. D.; Farkas, O.; Foresman, J. B.; Ortiz, J. V.; Cioslowski, J.; Fox, D. J., Gaussian 09. Gaussian, Inc.: Wallingford CT, 2009; Vol. Revision A.1.

19. Guo, H.; Jing, Y.; Yuan, X.; Ji, S.; Zhao, J.; Li, X.; Kan, Y., Highly selective fluorescent OFF-ON thiol probes based on dyads of BODIPY and potent intramolecular electron sink 2,4-dinitrobenzenesulfonyl subunits. *Organic & biomolecular chemistry* **2011**, 9, 3844-3853.

20. Huang, J. D.; Wen, S. H.; Han, K. L., First-principles investigation of the electronic and conducting properties of oligothienoacenes and their derivatives. *Chem. Asian J.* **2012**, 7, 1032-1040.

21. Anthony, J. E.; Facchetti, A.; Heeney, M.; Marder, S. R.; Zhan, X., n-Type organic semiconductors in organic electronics. *Adv. Mater.* **2010**, 22, 3876-3892.

22. Reddy, J. S.; Kale, T.; Balaji, G.; Chandrasekaran, A.; Thayumanavan, S., Cyclopentadithiophene-Based Organic Semiconductors: Effect of Fluorinated Substituents on Electrochemical and Charge Transport Properties. *J. Phys. Chem. Lett.* **2011**, 2, 648-654.

CHAPTER 4

SUMMARY AND FUTURE DIRECTIONS

4.1 Summary

Considerable effort has been put into optimizing organic photovoltaic (OPV) devices through tuning the properties of conjugated and small molecule electron donors, yielding a wide variety of high performance materials. However, by comparison, electron acceptors suffer from a lack of diversity with fullerene based materials (PCBM, C_{60}, etc.) being the primary option. Although fullerene based materials have many desirable properties, their absorption spectra suffer from poor overlap with the solar spectrum, limiting their ability to harvest light. The development of non-fullerene based acceptors with broad absorption in the visible region of the electromagnetic spectrum can limit our reliance on the donor material for light absorption and expand the library of available electron acceptors for OPV devices.

In Chapter 2 the molecular design and properties of five A-D-A small molecules based on the BODIPY dye were described. Though these molecules differ in the structure of their variable core unit, the λ_{max} is consistent (~535 nm) due to the relatively insulating *meso* connectivity of the BODIPY caps. Through tuning of the "donor" strength of the core moiety, the red edge absorption can be selectively modified, where stronger donors (BDP-CPDT, BDP-DTP) yield a more red shifted charge transfer band and, as a result, a lower band gap (1.54, 1.47 eV), while the weak donors (BDP-TTh, BDP-biTh, BDP-BDT) have significantly larger band gaps

(*ca*. 1.70 eV). These molecules also show low comparable LUMOs (-3.7 to -3.9 eV), due to the localization of electron density on the BODIPY capping moieties. Analysis of the charge transport properties using field effect transistors showed that these molecules consistently show n-type behavior ($\mu_{ele} \sim 10^{-5}$ cm^2 V^{-1} s^{-1}). These properties make these materials prime candidates for electron acceptors in bulk heterojunction photovoltaic devices when paired with poly(3-hexylthiophene) (P3HT).

We fabricated direct and inverted bulk heterojunction photovoltaic devices using these molecules as the sole electron acceptor for the P3HT donor. Preliminary device optimization showed that the acceptor can work well even through annealing and the use of solvent additives, methods traditionally used for fullerene based acceptors. Topographical analysis revealed that the active layer morphology shows a significant improvement in the persistence of regular domain sizes over long ranges under the optimum conditions (P3HT:BDP-CPDT (1:1.5) + 3 vol% CN). From the external quantum efficiency measurements, we were able to determine that the light harvesting of the BODIPY acceptors contribute to the photogenerated current in the devices, motivating the improvement in the red edge absorption of the A-D-A architecture through structural modification.

In Chapter 3, we looked towards the linker unit between the donor core and the BODIPY acceptor cap as a means to improve red edge absorption and tune the energy levels of these electron transporting materials. We were able to show perturbation in the absorption and electrochemical properties by treating the linker unit as a valve for electronic communication, tuning the "push-pull" character in the

system (*m*-phenylene < *p*-phenylene < fluoro-*p*-phenylene < thiophene < directly linked < ethynyl). Doing so allowed for the systemic broadening and red shifting of the absorption spectra (λ_{onset}^{film} = 580-845 nm), as well as the LUMO level (-3.02 eV to -4.06 eV). Theoretical calculations of the HOMO and LUMO in the geometry optimized state showed that the localization of the frontier molecular orbitals was affected by the structure of the linker unit. The ethynyl linked molecule (BDP-CC-DTP) showed the most significant HOMO/LUMO overlap, which caused the significant enhancement in the charge transfer band. Analysis of the charge transport properties showed that the delocalized LUMO of BDP-CC-DTP, as well as its ability to form nanoscale aggregates in the thin film, contributed to its high electron mobility ($\sim 10^{-3}$ cm^2 V^{-1} s^{-1})

4.2 Future Directions

The A-D-A architectures explored in this dissertation have shown great potential as light harvesting materials, showing the significance of the BODIPY moiety as a capping unit in electron transporting materials with broad light absorption. Since the molecules reported in Chapter 2 were successful when blended with P3HT, their use with other acceptors is an obvious first approach. The LUMO of P3HT is ~1 eV higher than that of the BODIPY molecules, indicating that significant energy is lost during the charge transfer process. Choosing a donor with a more stable LUMO level could limit these losses. Also, the high electron mobility and crystallinity of BDP-CC-DTP (Chapter 3), as well as the improved absorption in the NIR region, makes it another viable choice for use in BHJ OPV devices. However,

the ethynyl groups will likely reduce the solubility of the acceptor, indicating that optimization of the processing conditions is imperative.

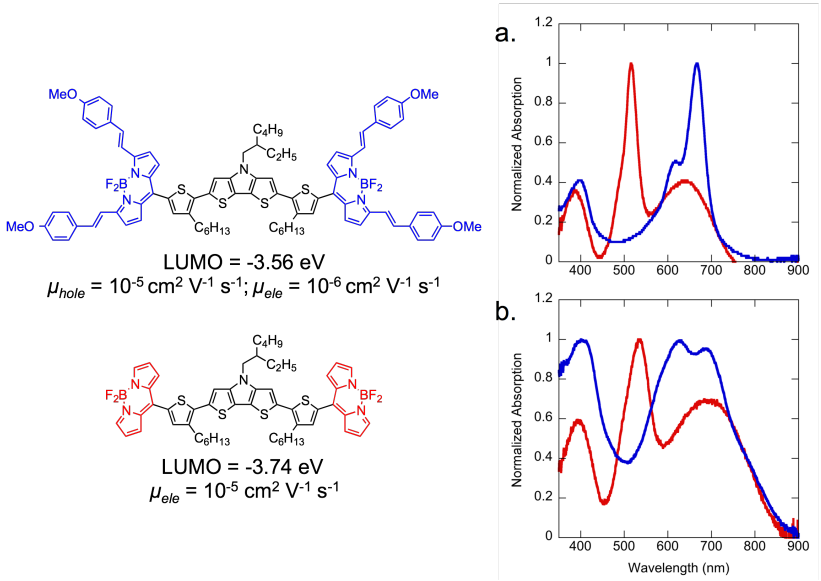

Figure 4.1: Molecular structures and electronic properties of BDP-DTP and ExBDP-DTP.

The BODIPY-cap is also ripe for further exploration. One possible modification includes extension of the molecule through the α position of the BODIPY unit. By installing α-methyl groups onto the BODIPY caps, we can further functionalize the molecule using Knoevenagel condensation with an aldehyde functionalized moiety, forming an ethylene bond, as shown in Figure 4.1. As a result, we will be able to tune the absorption properties of the BODIPY peak, red shifting it from its otherwise pinned position, to generate a localized D-A-D system on either end of the core moiety. Given the altered electronic structure through this modification, we also observe a change in charge carrier type, generating a p-type material and a potential donor for BHJ OPV devices. Considering the success of other BODIPY-based donors and the tunability of these systems, BODIPY dye based materials could make a significant impact in the field of OPVs.[14, 47, 63, 104]

4.3 References

1. Bura, T.; Leclerc, N.; Fall, S.; Leveque, P.; Heiser, T.; Retailleau, P.; Rihn, S.; Mirloup, A.; Ziessel, R., High-performance solution-processed solar cells and ambipolar behavior in organic field-effect transistors with thienyl-BODIPY scaffoldings. *J. Am. Chem. Soc.* **2012**, 134, 17404-17407.

2. Hayashi, Y.; Obata, N.; Tamaru, M.; Yamaguchi, S.; Matsuo, Y.; Saeki, A.; Seki, S.; Kureishi, Y.; Saito, S.; Yamaguchi, S.; Shinokubo, H., Facile synthesis of biphenyl-fused BODIPY and its property. *Org. Lett.* **2012**, 14, 866-869.

3. Kim, B.; Ma, B.; Donuru, V. R.; Liu, H.; Frechet, J. M., Bodipy-backboned polymers as electron donor in bulk heterojunction solar cells. *Chem. Commun.* **2010**, 46, 4148-4150.

4. Rousseau, T.; Cravino, A.; Ripaud, E.; Leriche, P.; Rihn, S.; De Nicola, A.; Ziessel, R.; Roncali, J., A tailored hybrid BODIPY-oligothiophene donor for molecular bulk heterojunction solar cells with improved performances. *Chem. Commun.* **2010**, 46, 5082-5084.

APPENDIX

HYDROCARBON/FLUOROCARBON BLOCK COPOLYMERS FOR ANHYDROUS PROTON TRANSPORT

A.1 Introduction

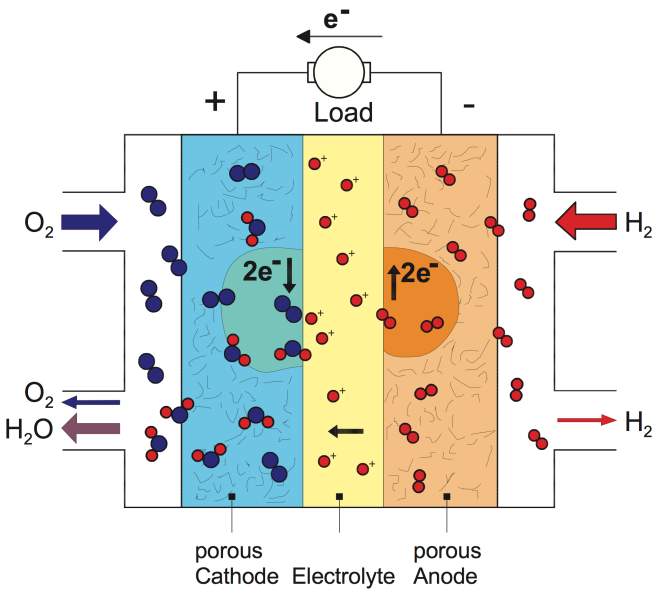

Figure A.1: Illustration of the basic processes of a proton exchange membrane fuel cell.[1]

The environmental benefits of fuel cells are very attractive as a replacement for conventional heat engines due to their clean operation.[1] There are a variety of different fuel cells available including cationic and anionic fuel cells, phosphoric acid fuel cells (PAFC), solid oxide fuel cells (SOFC), Alkaline fuel cells (AFC), molten carbon fuel cells (MCFC), and proton exchange membrane fuel cells (PEMFC), each with their own electrolyte matrix for ion transport. PEMFC technology is continually improving with regards to popularity as evidenced by increased relative worldwide shipments, due to the wide range of both small and large scale applications

including portable electronics, small home power generator or other stationary systems, or in vehicular propulsion systems, as well as other applications.[2-4]

As shown in Figure A.1, proton exchange membranes fuel cells (PEMFCs) are electrochemical cells in which hydrogen fuel is introduced and oxidized by a catalytic anode into free protons and electrons. The electrons are free to generate the electrical current, while the proton is transported through a polymeric network capable of shuttling the protons to the cathode, where they are combined with the conducted electrons and oxygen to form water, the only exhaust of the process. Given the mechanism of current generation in PEMFCs, there are many opportunities for improvements in the fuel generation, catalyst stability, ion transport and overall operation stability.[4, 5]

A.1.1 Hydrous Proton Transport

Nafion® is a perfluorinated ethylene based polymer possessing sulfonate functionalities for hydrated proton transport. While derivatives and variations on this type of polymer structure have been reported, the system was popularized by the DuPont company in the 1960s and is currently the most commonly used material in PEMFCs.[6] The hydrophilic-lipophilic incompatibility between the fluorinated polymer backbone and the pendant sulfonate groups allow for the formation of hydrated channels which facilitate efficient proton conductivity due to the self-assembled inverse micellar morphology achieved, as shown in Figure A.2.[6-8]

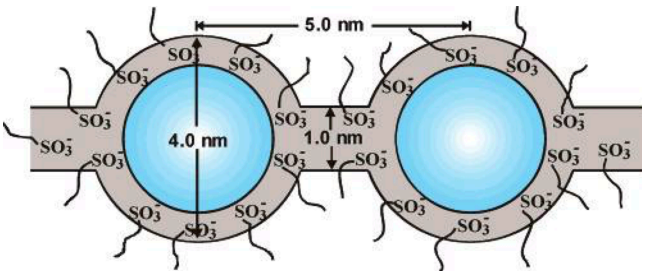

Figure A.2: Representation of the hydrated channels formed in Nafion® membrane stabilized by sulfonate pendant units from the polymer.[6]

The source of the high proton conductivity in hydrated Nafion® (~10^{-1} S cm^{-1}) is contingent on the humidity during both preparation and operation, due to the hydrated channels. This is clearly shown in Figure A.3, which compares the proton conductivity over time to the relative humidity of the operation chamber.[9] This is true for many proton exchange membranes. Unfortunately, of the available polymer membranes for PEMFC applications, the most common reason for poor performance is dehumidification.[10] This issue is a primary concern in the field, considering that the processing of these materials, as well as the operating conditions, often exceed 100 °C, eliminating the water from the system. Because of this, anhydrous proton transport has become an emerging topic in the field of PEMFCs.

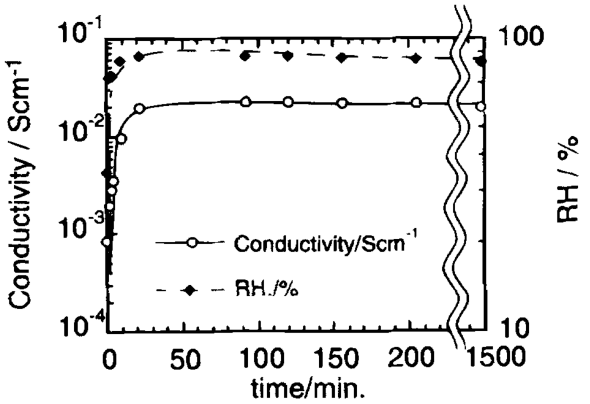

Fig. 3. Change in conductivity after the heat-treatment at 80°C under an RH of 80%.

Figure A.3: Plot of impedance measurements made over time of a heat treated (80 °C) PEMFC device under humid conditions where Nafion 117 is used as the proton exchange membrane.[9]

A.1.2 Anhydrous Proton Transport

To eliminate water as the conducting medium in PEMFCs, many materials have been explored including phosphoric acid, polymer complexes, and Nafion® swollen with non-aqueous media.[11-13] Transport in these systems are generally facilitated by the "Grotthuss mechanism", which involves the ionization of the transporting functionality followed by reorganization of hydrogen bonds.[14-16] Figure A.4 shows two examples of proton conduction under the Grotthuss mechanism.[12] The benefits of these systems are in (a) the ability of the polymer to organize in such a way that the transporting moieties are in close proximity to form the hydrogen bonded network and (b) the high thermal and structural stability of the polymer backbone. Nafion® has been shown to be applicable in anhydrous systems as well by replacing the hydrated domains with alternative solutions through swelling of the polymer network with acid (H_3PO_4) or molten salts (imidazole), which are significantly less susceptible to evaporation at elevated temperatures.[13]

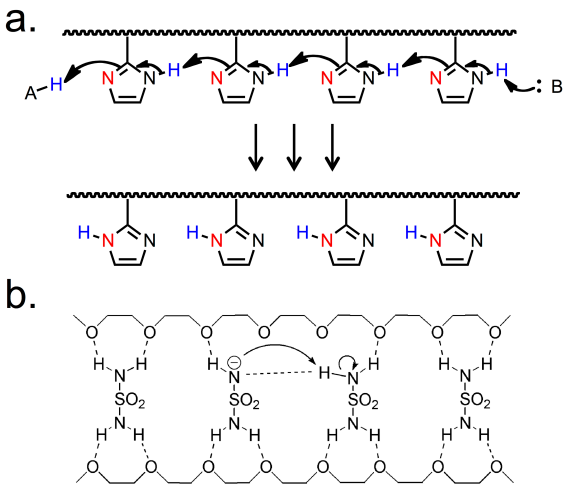

Figure A.4: Representative examples of the Grotthuss mechanism in a (a) polyimidizole based system and a (b) proton deficient guanidine-doped PEO/sulfamide blend.[11, 12]

To address this concern, Thayumanavan and coworkers recently reported a polystyrene based system containing imidazole and benzotriazole proton-transporting moieties.[17] The driving force for the micellar-like self-assembly in this system is the amphiphilic nature of the comb-like homopolymer structure. As shown in Figure A.5, this organization within the polymer membrane yielded a significant enhancement in proton conductivity by three orders of magnitude to ~10^{-3} S cm^{-1}, compared to the model polymer containing no lipophilic side chain on the homopolymer, in spite of the addition of an equal concentration of insulating units onto the polymer structure. The effectiveness of this system is more impressive when you consider that the operating temperature of the devices were as high as 200 °C, at which the proton conductivity approaches that of Nafion® at significantly lower temperatures. These results led to further investigation into the fundamental mechanism of polymeric triazole based proton transport,[18] and the use of other polymeric phenols as proton transporting materials[19] as well as self-assembling block copolymer systems.

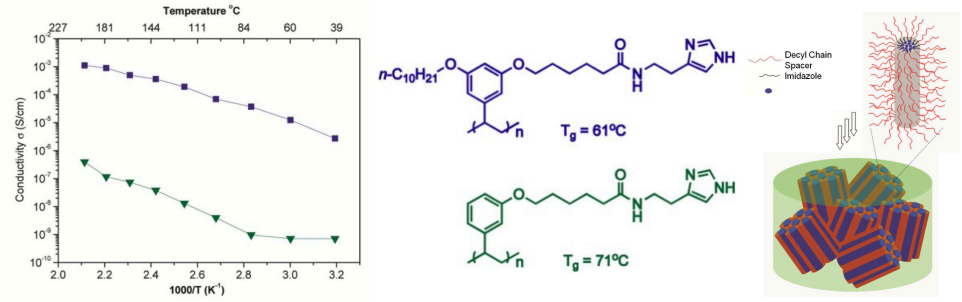

Figure A.5: The polymer structure of amphiphilic comb polymer (blue) and the control polymer (green), which showed no self-assembling characteristics. The proton conductivity results for each polymer are shown, with respect to the operating temperature. The self-assembled cylindrical structure of the imidazole-based comb polymer is also shown (far right).

A.2 Molecular Design

Significant research into the synthesis of block copolymer polymer systems by various methods, including cationic and anionic polymerization, nitroxide mediated polymerization (NMP), reverse addition-fragmentation chain-transfer polymerization (RAFT), atom transfer radical polymerization (ATRP), and others.[20, 21] Block copolymers are well established systems in the field of self-assembling polymer assemblies, such as micelles, vesicles, bicontinuous polymer networks, etc., with applications in drug delivery and biomedical imaging.[22-24] Extensive control of the morphological characteristics are possible through systemic modification of the volume fraction of each block.[22, 23, 25] Examples of the potential microstructures available in block copolymer systems with chemically distinct homopolymers depending on the volume fraction, *f*, of each block and the incompatibility factor, χN (Flory-Huggins parameter), are shown in Figure A.6.[23]

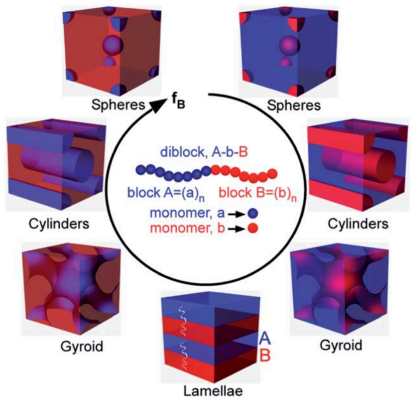

Figure A.6: Illustration of available microstructures of A-*b*-B type diblock copolymers obtained as the volume fraction of block B (*f*B) is increased.[23]

The hydrocarbon/fluorocarbon phase segregation is well established in aliphatic block copolymers; the incompatibility is driven by a combination of entropic effects and the unfavorable energetic interactions between each block.[26]

For this reason, we investigated a polystyrene-*b*-poly(2,3,4,5,6-pentafluorostyrene) (PS-*b*-P(PFS)) block copolymer grafted with a proton transporting histamine moiety for use as a proton exchange membrane. Synthesis of P(PFS) homopolymer and (PS-*b*-P(PFS)) was achieved through ATRP using an *α*-methyl benzyl bromide macroinitiator, as shown in Figure A.7. The P(PFS) homopolymer is very useful for functionalization due to its availability for aromatic nucleophilic substitution at the *para* fluorine position under relatively facile methods.[27-30] In this system, both the homopolymer and block copolymers were subjected to reflux conditions in the presence of histamine and triethylamine for the substitution of pentafluorostyrene.

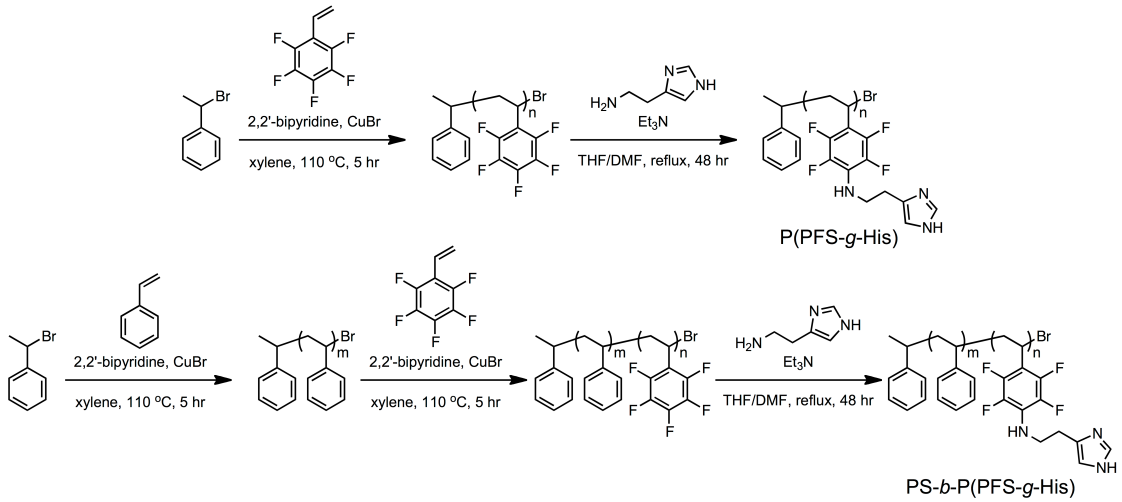

Figure A.7: Synthesis of the grafted homopolymer, P(PFS-*g*-His), and block copolymers, PS-*b*-P(PFS-*g*-His).

Polymer	M_n (g mol^{-1})	*Đ*	wt_{PS}%	$wt_{P(PFS)}$%	T_g (°C)
P(PFS-*g*-His)	8.5k	1.21	0	100	121
PS_{25}-*b*-P(PFS-*g*-His)$_{75}$	22k	1.28	25	75	99
PS_{50}-*b*-P(PFS-*g*-His)$_{50}$	11k	1.22	50	50	98, 108

Table A.1: Summarized properties of synthesized homo- and block copolymers.

The polymers were synthesized and characterized by gel permeation chromatography (GPC) to estimate the molecular weight compared to a PS standard

and differential scanning calorimetry (DSC) to identify the glass transition temperature(s) (T_g). Two weight ratios (1:3 and 1:1) of the grafted BCPs were synthesized with relatively narrow dispersity (1.2-1.3). The glass transition temperature also seems to be contingent on the block weight fraction, with the highest T_g observed in P(PFS-*g*-His), while PS_{50}-*b*-$P(PFS\text{-}g\text{-}His)_{50}$ shows two transitions given its balanced weight fraction.

A.3 Results and Discussion

To investigate the affect of bulk morphology and BCP composition on the proton conductivity, small-angle X-ray scattering (SAXS) and transmission electron microscopy (TEM) were used in an attempt to characterize the morphology. While P(PFS-*g*-His) showed no phase segregation or order, the following Section A.3.1 describes the results of the block copolymers. Section A.3.2 will discuss the proton conductivity results.

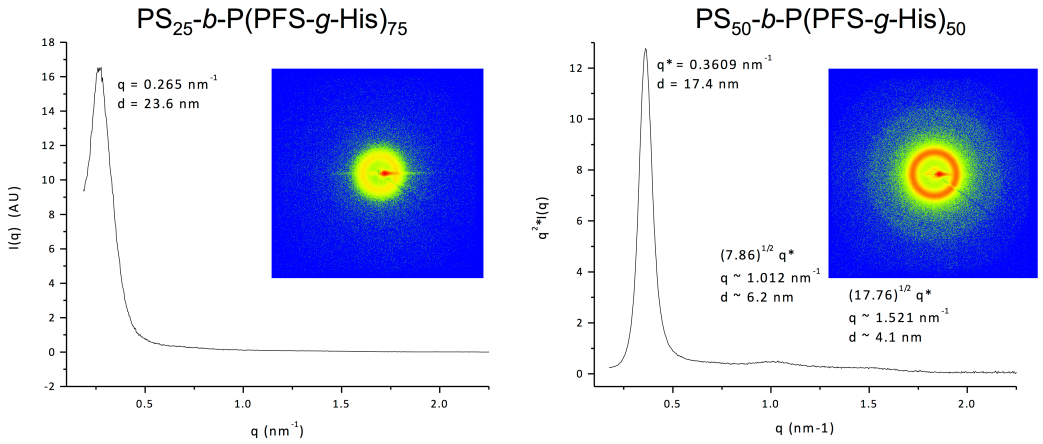

Figure A.8: Small-angle X-ray scattering (SAXS) profiles and patterns (insets) of block copolymers. In the SAXS profile for PS_{50}-*b*-$P(PFS\text{-}g\text{-}His)_{50}$, the wave vector ($q$) is plotted against q^2I for easier visualization of the higher ordered peaks.

A.3.1 Morphology Characterization

The order in the block copolymer systems was measured using SAXS. While both block ratios showed diffraction patterns with strong first ordered peaks, the size scales were slightly different. The wave vector of PS_{25}-*b*-P(PFS-*g*-His)$_{75}$ showed domain sizes at about 24 nm, while PS_{50}-*b*-P(PFS-*g*-His)$_{50}$ showed domain sizes at about 17 nm and significantly less intense higher ordered peaks (6.2 and 4.1 nm), as shown in Figure A.8. However, the ratio of peaks are somewhat meaningless, as they are not indicative of a specific morphology. The order observed is confirmation that the PS/P(PFS-*g*-His) block incompatibility is significant enough to drive the phase segregation, even at high concentration of the P(PFS-*g*-His) block. To confirm phase segregation through out the bulk, tunneling electron microscopy (TEM) was used. The TEM images are shown in Figure A.9 and are stained with iodic acid to identify the regions contain imidazole units, which are capable of quartanization by the stain. These regions are the histamine rich regions or the portion of polymer that rich with the proton transporting moiety. TEM showed domains that approximately agree with the polymer volume fraction and the domain sizes obtained using SAXS. Unfortunately, just as with SAXS, no distinct morphology is observable. In PS_{25}-*b*-P(PFS-*g*-His)$_{75}$, the volume fraction seems to yield a mixture of spheres or cylinders of the fluorinated domains. In PS_{50}-*b*-P(PFS-*g*-His)$_{50}$, the morphology seems to shift towards a mixture of lamellar and cylinders.

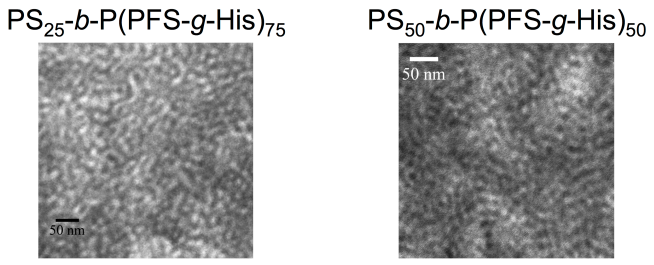

Figure A.9: TEM images of each block copolymer in dry powder epoxy stained with HI (aq).

A.3.2 Proton Conductivity

The conductivity of the polymers were measured under vacuum. During measuremenpt, the devices were subjected to a heating-cooling cycle which involved gradually heating to 160 °C, remaining at 160 °C for 10 hr to observe the conductivity stability, followed by measurements during the gradual return to room temperature. In each polymer we can see the proton conductivity gradually increases with temperature (Figure A.10a), however the thermal stability of the device operation is not very high, decreasing by an order of magnitude in each case when measured over 18 hr at 160 °C (Figure A.10b). The measured conductivity of the homo- and block copolymers at 160 °C (0 hr) and after 18 hr, at temperature, are shown in Table A.2.

	σ (S cm^{-1})	
Polymer	0 hr	18 hr
P(PFS-g-His)	7 x 10^{-7}	1 x 10^{-7}
PS_{25}-b-P(PFS-g-His)$_{75}$	7 x 10^{-6}	1 x 10^{-6}
PS_{50}-b-P(PFS-g-His)$_{50}$	1 x 10^{-8}	-

Table A.2: Maximum proton conductivity for each polymer once resting temperature is reached and after 18 hr at the resting temperature.

As shown in Figure A.10, the proton conductivity of each polymer gradually increased with temperature. However, prolonged operation at 160 °C led to a

decrease of an order of magnitude in PS_{25}-*b*-P(PFS-*g*-His)$_{75}$, and elimination of conductivity for PS_{50}-*b*-P(PFS-*g*-His)$_{50}$. However, we can see that there is a benefit in the use of the BCP architecture. The homopolymer gives mobilities on the order of 10^{-7} S cm^{-1}, but introduction of the non-conducting PS block one-third that of the transporting block yielded an improvement in device performance by an order of magnitude, as shown in Table A.2.

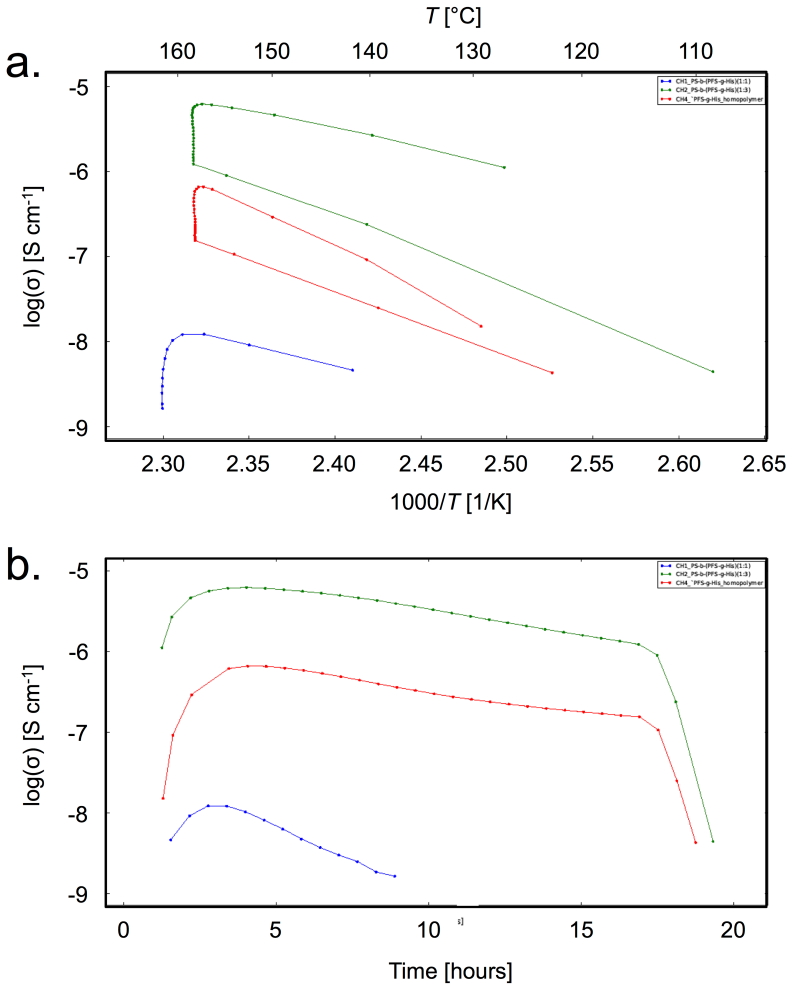

Figure A.10: Proton conductivity of P(PFS-*g*-His) (red), PS_{25}-*b*-P(PFS-*g*-His)$_{75}$ (green) and PS_{50}-*b*-P(PFS-*g*-His)$_{50}$ (blue) with respect to (*a*) temperature and (*b*) resting time at 160 °C.

The stability of the devices with respect to the operation at 160 °C over 18 hr were comparable for the homopolymer and PS_{25}-*b*-P(PFS-*g*-His)$_{75}$, however PS_{50}-*b*-

P(PFS-*g*-His)$_{50}$ does not perform nearly as well with both a low peak conductivity and a more rapid decline over time. The source of of the poor conductivity compared to PS$_{25}$-*b*-P(PFS-*g*-His)$_{75}$ is likely the dilution of the proton transporting moieties, as the weight of the PS block was held constant, while the weight of the P(PFS) block was reduced, limiting the available moieties for substitution. While the morphology of the system was shown to be ordered by SAXS and TEM, the limited histamine moieties likely make the formation of the networked system necessary for efficient proton shuttling through the Grotthuss mechanism very difficult.

A.4 Summary and Future Directions

A PS-*b*-P(PFS-*g*-His) system developed for use as a PEM with fuel cell applications was synthesized with two different block weight fractions, as well as the P(PFS-*g*-His) homopolymer, were synthesized. PS$_{25}$-*b*-P(PFS-*g*-His)$_{75}$ showed an enhancement proton conductivity compared to the homopolymer due to the improved order given by the insulating polystyrene block system showed an enhancement in proton conductivity compared

While the introduction of the non-conducting block to improve the morphology and proton conductivity, a clear structure-property relationship must be established. This can be done by investigating the affect that molecular weight of the polymer and the weight fraction of each block have on the morphology. With a more gradual introduction of the PS block, we may be able to elucidate a more specific phase diagram. Also, increasing the molecular weight may allow for a more persistent morphological structure and better thermal stability.

A.5 Experimental

All chemicals were purchased from commercial sources and used as received, unless otherwise mentioned. Tetrahydrofuran (THF) was distilled over sodium and benzophenone. ^{1}H NMR spectra were recorded on a 400 MHz Bruker NMR spectrometer and the chemical shifts are reported in ppm using deuterated solvent as the internal standard ($CDCl_3$ at 7.26 ppm; DMSO-d_6 at 2.50 ppm). When peak multiplicities are given, the following abbreviations are used: s, singlet; d, doublet; t, triplet; m, multiplet; bs, broad singlet; bm, broad multiplet. The molecular weights of the polymers were determined by gel permeation chromatography (GPC) using THF as the eluent and toluene as the internal reference. Polystyrene standards were used for calibration and the output was received and analyzed using RI detector.

A.5.1. Differential Scanning Calorimeter (DSC)

Glass transition temperature (T_g) of the polymers were obtained using TA instruments Dupont DSC 2910. The samples (~10 mg) were loaded into aluminum pans and were heated from room temperature to 320 °C with a rate of 10 °C min^{-1} under a flow of nitrogen.

A.5.2 Electrochemical Impedance Measurements

A.5.2.1 Membrane Preparation

Kapton tape with a hole thickness of 125 μm and an area of 0.0792 cm^2 was placed onto the gold coated electrode and polymer films were drop cast from a

concentrated THF/DMF solution onto the electrode for controlled area. Another gold coated blocking electrode was placed on top of the film and assembled and transferred to a vacuum oven to carry out the measurement.

A.5.2.2 Device Measurement

Prepared films were characterized by impedance spectroscopy. The samples were initially heated from room temperature from room temperature to 160 °C and held at 160 °C for 18 hr. The samples were then slowly cooled from 160 °C to room temperature. During this entire cycle, the conductivity was measured periodically under vacuum.

The bulk proton conductivity was determined by fitting the impedance spectrum to an equivalent circuit model using Zview software. The data in a high frequency regime fit to a parallel resistor-capacitor subcircuit, appearing as a semicircular impedance arc feature in a Nyquist plot (a parametric plot of the imaginary component of impedance, Z'', versus the real component, Z'). The resistance determined by this fit correlates inversely to bulk conductivity of the material. Conductivity computed as $\sigma = L/RA$, where L is the sample thickness (limited by the Kapton spacer) and A is the area of the sample disk.

A.5.3 Synthesis

A.5.3.1 Polystyrene macroinitiator

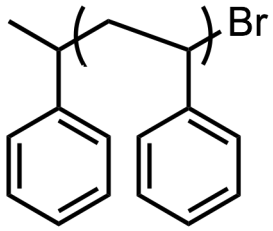

Copper (I) bromide (37 mg, 0.51 mmol) and 2,2'-bipyridine (37 mg, 0.255 mmol.) were combined in a 10 mL shlenk flask. Air was removed from the system through flash purging followed by the addition of the *alpha*-methyl bromobenzene (35 uL, 0.255 mmol). Under argon, styrene (1.6 mL, 13.75 mmol) was added. Any air was removed through three freeze-pump-thaw cycles. The mixture was heated to 110 °C in a prewarmed oil bath and stirred until polymer is formed (4 hr). The mixture was cooled and diluted in THF, followed by filtration to remove copper salt. The solvents were removed *in vacuo* and the polymer was redissolved in THF and precipitated in methanol, collected, and placed under vacuum overnight. Yielded 1.17 g of a white solid (97% conversion). GPC (THF) Mn: 5600 g mol^{-1}; *Đ*: 1.24. **^{1}H-NMR** (400 MHz, $CDCl_3$): δ 7.07 (bm, 3H), 6.48 (bm, 2H), 1.85 (bs, 1H), 1.44 (bs, 2H).

A.5.3.2 Polystyrene-*b*-poly(pentafluorostyrene)

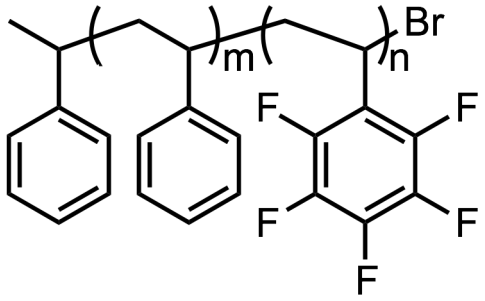

Copper (I) bromide (8.7 mg, 0.06 mmol) and 2,2'-bipyridine (18.8 mg, 0.12 mmol.) were combined in an 10 mL shlenk flask. Air was removed from the system through flash purging followed by the addition of the PS macroinitiator (300 mg, 0.06 mmol) and 3 ml of dry xylene. Under argon, 2,3,4,5,6-pentaflurorostyrene (0.83 mL, 6 mmol) was added. Any air was removed through three freeze-pump-thaw cycles. The mixture was heated to 110 °C in a prewarmed oil bath and stirred until polymer is formed (18 hr). The mixture was cooled and diluted in THF, followed by filtration to remove copper salt. The solvents were removed *in vacuo* and the polymer was redissolved in THF and precipitated in methanol, collected, and placed under vacuum overnight.

PS25-b-P(PFS)75: From 100 eq. Pentaflurostyrene, a white solid was obtained (57% conversion). GPC (THF) Mn: 16800 g mol^{-1}; *Đ*: 1.28.

PS50-b-P(PFS)50: From 30 eq pentaflurostyrene, 0.49 g of a white solid was obtained (64% conversion). GPC (THF) Mn: 9400 g mol^{-1}; *Đ*: 1.22

A.5.3.3 Poly(pentafluorostyrene)

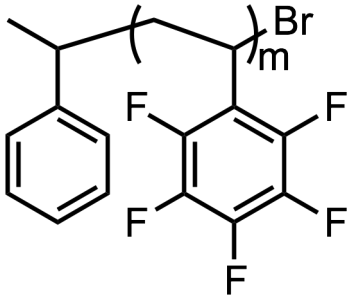

Copper (I) bromide (37 mg, 0.51 mmol) and 2,2'-bipyridine (37 mg, 0.255 mmol.) were combined in an 10 mL shlenk flask. Air was removed from the system through flash purging followed by the addition of the *α*-methyl bromobenzene (35

uL, 0.255 mmol). Under argon, 2,3,4,5,6-pentaflurorostyrene (1.6 mL, 5.9 mmol) was added. Any air was removed through three freeze-pump-thaw cycles. The mixture was heated to 110 °C in a prewarmed oil bath and stirred until polymer is formed (4 hr). The mixture was cooled and diluted in THF, followed by filtration to remove copper salt. The solvents were removed *in vacuo* and the polymer was redissolved in THF and precipitated in methanol, collected, and placed under vacuum overnight. Yielded 1.91 g of a white solid (100% conversion). GPC (THF) Mn: 5800 g mol^{-1}; *Đ*: 1.21.GPC (THF) Mn: 5800 g mol^{-1}; *Đ*: 1.21. **^{1}H-NMR** (400 MHz, $CDCl_3$): δ 8.72 (s, 1H), 8.44-8.35 (m, 2H), 7.86 (s, 1H), 7.35 (s, 1H), 2.56 (bm, 27H), 2.02 (bs, 50H).

A.5.3.4 Typical grafting procedure

The precursor polymer (1 eq.) was dissolved in THF under argon. Histamine (10 eq.) was dissolved in DMF under argon separately. The Histamine solution was added to the polymer solution by syringe and the mixture was heated to 100 oC to fully dissolve both components. Triethylamine (10 eq.) was was added to the reaction mixture and the reaction was refluxed for 48 hr. THF and DMF were removed by distillation. The polymer was dissolved in a small amount of dichloromethane and precipitated in water, followed by washing with a methanol/water (1:1) solution.

PS_{25}-b-P(PFS-g-His)$_{75}$: GPC (THF) Mn: 22000 g mol^{-1}; *Đ*: 1.28.

PS_{50}-b-P(PFS-g-His)$_{50}$: GPC (THF) Mn: 11000 g mol^{-1}; *Đ*: 1.22.

P(PFS-g-His): GPC (THF) Mn: 8500 g mol^{-1}; *Đ*: 1.21.

A.6 References

1. Carrette, L.; Friedrich, K. A.; Stimming, U., Fuel Cells - Fundamentals and Applications. *Fuel Cells* **2001**, 1, 5-39.

2. Carter, D.; Wing, J. *The Fuel Cell Industry Review*; Fuel Cell Today: 2013.

3. Steele, B. C.; Heinzel, A., Materials for fuel-cell technologies. *Nature* **2001**, 414, 345-352.

4. Wang, Y.; Chen, K. S.; Mishler, J.; Cho, S. C.; Adroher, X. C., A review of polymer electrolyte membrane fuel cells: Technology, applications, and needs on fundamental research. *Appl Energ* **2011**, 88, 981-1007.

5. Gong, M.; Zhou, W.; Tsai, M. C.; Zhou, J.; Guan, M.; Lin, M. C.; Zhang, B.; Hu, Y.; Wang, D. Y.; Yang, J.; Pennycook, S. J.; Hwang, B. J.; Dai, H., Nanoscale nickel oxide/nickel heterostructures for active hydrogen evolution electrocatalysis. *Nat. Commun.* **2014**, 5, 4695.

6. Mauritz, K. A.; Moore, R. B., State of understanding of nafion. *Chem. Rev.* **2004**, 104, 4535-85.

7. Sahu, A. K.; Pitchumani, S.; Sridhar, P.; Shukla, A. K., Nafion and modified-Nafion membranes for polymer electrolyte fuel cells: An overview. *B Mater Sci* **2009**, 32, 285-294.

8. Hsu, W. Y.; Gierke, T. D., Ion-Transport and Clustering in Nafion Perfluorinated Membranes. *J. Member. Sci.* **1983**, 13, 307-326.

9. Sone, Y.; Ekdung, P.; Simonsson, D., Proton Conductivily of Nafion 117 as Measured by a Four-Electrode AC Impedance Method. *J. Electrochem. Soc.* **1996**, 143, 1254-1259.

10. Mehta, V.; Cooper, J. S., Review and analysis of PEM fuel cell design and manufacturing. *J Power Sources* **2003**, 114, 32-53.

11. Schuster, M. E.; Meyer, W. H., Anhydrous proton-conducting polymers. *Annu Rev Mater Res* **2003**, 33, 233-261.

12. Bermudez, V. D.; Armand, M.; Poinsignon, C.; Abello, L.; Sanchez, J. Y., Proton-Vacancy Conducting Polymers Based on Polyethylene Oxide and Sulfamide-Type Salts. *Electrochim Acta* **1992**, 37, 1603-1609.

13. Sun, J. Z.; Jordan, L. R.; Forsyth, M.; MacFarlane, D. R., Acid-organic base swollen polymer membranes. *Electrochim Acta* **2001**, 46, 1703-1708.

14. Narayanan, S. R.; Yen, S. P.; Liu, L.; Greenbaum, S. G., Anhydrous proton-conducting polymeric electrolytes for fuel cells. *J. Phys. Chem. B* **2006**, 110, 3942-8.

15. Kreuer, K. D., Proton conductivity: Materials and applications. *Chem. Mater.* **1996**, 8, 610-641.

16. Agmon, N., The Grotthuss mechanism. *Chem. Phys. Lett.* **1995**, 244, 456-462.

17. Chen, Y.; Thorn, M.; Christensen, S.; Versek, C.; Poe, A.; Hayward, R. C.; Tuominen, M. T.; Thayumanavan, S., Enhancement of anhydrous proton transport by supramolecular nanochannels in comb polymers. *Nature chemistry* **2010**, 2, 503-8.

18. Nagamani, C.; Versek, C.; Thorn, M.; Tuominen, M. T.; Thayumanavan, S., Proton Conduction in 1H-1,2,3-triazole Polymers: Imidazole-Like or Pyrazole-Like? *J. Poly. Sci. A: Poly. Chem* **2010**, 48, 1851-1858.

19. Nagamani, C.; Viswanathan, U.; Versek, C.; Tuominen, M. T.; Auerbach, S. M.; Thayumanavan, S., Importance of dynamic hydrogen bonds and reorientation barriers in proton transport. *Chem. Commun.* **2011**, 47, 6638-40.

20. Hadjichristidis, N.; Pitsikalis, M.; Iatrou, H., Synthesis of block copolymers. In *Block Copolymers I*, 2005; Vol. 189, pp 1-124.

21. Keddie, D. J., A guide to the synthesis of block copolymers using reversible-addition fragmentation chain transfer (RAFT) polymerization. *Chem. Soc. Rev.* **2014**, 43, 496-505.

22. Mai, Y.; Eisenberg, A., Self-assembly of block copolymers. *Chem. Soc. Rev.* **2012**, 41, 5969-85.

23. Hu, H.; Gopinadhan, M.; Osuji, C. O., Directed self-assembly of block copolymers: a tutorial review of strategies for enabling nanotechnology with soft matter. *Soft Matter* **2014**, 10, 3867-89.

24. Rosler, A.; Vandermeulen, G. W. M.; Klok, H. A., Advanced drug delivery devices via self-assembly of amphiphilic block copolymers. *Adv Drug Deliver Rev* **2012**, 64, 270-279.

25. Schacher, F. H.; Rupar, P. A.; Manners, I., Functional block copolymers: nanostructured materials with emerging applications. *Angewandte Chemie* **2012**, 51, 7898-921.

26. Krafft, M. P.; Riess, J. G., Chemistry, physical chemistry, and uses of molecular fluorocarbon--hydrocarbon diblocks, triblocks, and related compounds--unique "apolar" components for self-assembled colloid and interface engineering. *Chem. Rev.* **2009**, 109, 1714-92.

27. Becer, C. R.; Babiuch, K.; Pilz, D.; Hornig, S.; Heinze, T.; Gottschaldt, M.; Schubert, U. S., Clicking Pentafluorostyrene Copolymers: Synthesis, Nanoprecipitation, and Glycosylation. *Macromolecules* **2009**, 42, 2387-2394.

28. Xue, Y.; Lu, H. C.; Zhao, Q. L.; Huang, J.; Xu, S. G.; Cao, S. K.; Ma, Z., Polymethylene-b-poly(styrene-co-2,3,4,5,6-pentafluoro styrene) copolymers: synthesis and fabrication of their porous films. *Polym. Chem.* **2013**, 4, 307-312.

29. Ott, C.; Hoogenboom, R.; Schubert, U. S., Post-modification of poly(pentafluorostyrene): a versatile "click" method to create well-defined multifunctional graft copolymers. *Chem. Commun.* **2008**, 3516-8.

30. Gan, D.; Mueller, A.; Wooley, K. L., Amphiphilic and hydrophobic surface patterns generated from hyperbranched fluoropolymer/linear polymer networks: Minimally adhesive coatings via the crosslinking of hyperbranched fluoropolymers. *J. Poly. Sci. A: Poly. Chem* **2003**, 41, 3531-3540.

BIBLIOGRAPHY

Annual Energy Review (2012); U.S. Energy Information Administration.

Best Research-Cell Efficiencies
http://www.nrel.gov/ncpv/images/efficiency_chart.jpg.

Agmon, N., The Grotthuss mechanism. *Chem. Phys. Lett.* **1995**, 244, 456-462.

Anthony, J. E., Small-Molecule, Nonfullerene Acceptors for Polymer Bulk Heterojunction Organic Photovoltaics. *Chem. Mater.* **2011**, 23, 583-590.

Anthony, J. E.; Facchetti, A.; Heeney, M.; Marder, S. R.; Zhan, X., n-Type organic semiconductors in organic electronics. *Adv. Mater.* **2010**, 22, 3876-3892.

Ashraf, R. S.; Shahid, M.; Klemm, E.; Al-Ibrahim, M.; Sensfuss, S., Thienopyrazine-Based Low-Bandgap Poly(heteroaryleneethynylene)s for Photovoltaic Devices. *Macromol. Rapid. Commun.* **2006**, 27, 1454-1459.

Beaujuge, P. M.; Frechet, J. M., Molecular design and ordering effects in pi-functional materials for transistor and solar cell applications. *J. Am. Chem. Soc.* **2011**, 133, 20009-20029.

Becer, C. R.; Babiuch, K.; Pilz, D.; Hornig, S.; Heinze, T.; Gottschaldt, M.; Schubert, U. S., Clicking Pentafluorostyrene Copolymers: Synthesis, Nanoprecipitation, and Glycosylation. *Macromolecules* **2009**, 42, 2387-2394.

Benanti, T. L.; Venkataraman, D., Organic solar cells: an overview focusing on active layer morphology. *Photosyn. Res.* **2006**, 87, 73-81.

Benniston, A. C.; Copley, G., Lighting the way ahead with boron dipyrromethene (Bodipy) dyes. *Phys. Chem. Chem. Phys.* **2009**, 11, 4124-4131.

Benniston, A. C.; Copley, G.; Harriman, A.; Rewinska, D. B.; Harrington, R. W.; Clegg, W., A donor-acceptor molecular dyad showing multiple electronic energy-transfer processes in crystalline and amorphous states. *J. Am. Chem. Soc.* **2008**, 130, 7174-7175.

Bermudez, V. D.; Armand, M.; Poinsignon, C.; Abello, L.; Sanchez, J. Y., Proton-Vacancy Conducting Polymers Based on Polyethylene Oxide and Sulfamide-Type Salts. *Electrochim Acta* **1992**, 37, 1603-1609.

Bloking, J. T.; Han, X.; Higgs, A. T.; Kastrop, J. P.; Pandey, L.; Norton, J. E.; Risko, C.; Chen, C. E.; Brédas, J.-L.; McGehee, M. D.; Sellinger, A., Solution-Processed Organic Solar Cells with Power Conversion Efficiencies of 2.5% using Benzothiadiazole/Imide-Based Acceptors. *Chem. Mater.* **2011**, 23, 5484-5490.

Bura, T.; Leclerc, N.; Fall, S.; Leveque, P.; Heiser, T.; Retailleau, P.; Rihn, S.; Mirloup, A.; Ziessel, R., High-performance solution-processed solar cells and ambipolar behavior in organic field-effect transistors with thienyl-BODIPY scaffoldings. *J. Am. Chem. Soc.* **2012**, 134, 17404-17407.

Carrette, L.; Friedrich, K. A.; Stimming, U., Fuel Cells - Fundamentals and Applications. *Fuel Cells* **2001**, 1, 5-39.

Carsten, B.; Szarko, J. M.; Son, H. J.; Wang, W.; Lu, L.; He, F.; Rolczynski, B. S.; Lou, S. J.; Chen, L. X.; Yu, L., Examining the effect of the dipole moment on charge separation in donor-acceptor polymers for organic photovoltaic applications. *J. Am. Chem. Soc.* **2011**, 133, 20468-20475.

Carter, D.; Wing, J. *The Fuel Cell Industry Review*; Fuel Cell Today: 2013.

Chen, C.-P.; Chan, S.-H.; Chao, T.-C.; Ting, C.; Ko, B.-T., Low-Bandgap Poly(Thiophene-Phenylene-Thiophene) Derivatives with Broaden Absorption Spectra for Use in High-Performance Bulk-Heterojunction Polymer Solar Cells. *J. Am. Chem. Soc.* **2008**, 130, 12828-12833.

Chen, Y.; Thorn, M.; Christensen, S.; Versek, C.; Poe, A.; Hayward, R. C.; Tuominen, M. T.; Thayumanavan, S., Enhancement of anhydrous proton transport by supramolecular nanochannels in comb polymers. *Nature chemistry* **2010**, 2, 503-8.

Chi, C.-C.; Huang, Y.-J.; Chen, C.-T., Synthesis and Spectroscopic Characterization of Dual Absorption BODIPY Type Dyes and their Light Harvesting Application in Polymer-Based Bulk Hetrojunction Organic Photovoltaics. *J. Chin. Chem. Soc.* **2012**, 59, 305-316.

Chochos, C. L.; Choulis, S. A., How the structural deviations on the backbone of conjugated polymers influence their optoelectronic properties and photovoltaic performance. *Prog. Polym. Sci.* **2011**, 36, 1326-1414.

Chochos, C. L.; Tagmatarchis, N.; Gregoriou, V. G., Rational design on n-type organic materials for high performance organic photovoltaics. *Rsc Adv* **2013**, 3, 7160-7181.

Chu, S.; Majumdar, A., Opportunities and challenges for a sustainable energy future. *Nature* **2012**, 488, 294-303.

Collado, D.; Casado, J.; Rodriguez Gonzalez, S.; Lopez Navarrete, J. T.; Suau, R.; Perez-Inestrosa, E.; Pappenfus, T. M.; Raposo, M. M., Enhanced functionality for donor-acceptor oligothiophenes by means of inclusion of BODIPY: synthesis, electrochemistry, photophysics, and model chemistry. *Chem. Eur. J.* **2011**, 17, 498-507.

Dang, M. T.; Hirsch, L.; Wantz, G., P3HT:PCBM, Best Seller in Polymer Photovoltaic Research. *Adv. Mater.* **2011**, 23, 3597-3602.

del Alamo, J. A., Nanometre-scale electronics with III-V compound semiconductors. *Nature* **2011**, 479, 317-323.

Della Pelle, A. M.; Homnick, P. J.; Bae, Y.; Lahti, P. M.; Thayumanavan, S., Effect of Substituents on Optical Properties and Charge-Carrier Polarity of Squaraine Dyes. *J. Phys. Chem. C* **2014**, 118, 1793-1799.

Deng, P.; Zhang, Q., Recent developments on isoindigo-based conjugated polymers. *Polym. Chem.* **2014**, 5, 3298-3305.

Dickinson, R. E.; Cicerone, R. J., Future Global Warming from Atmospheric Trace Gases. *Nature* **1986**, 319, 109-115.

Dong, H.; Fu, X.; Liu, J.; Wang, Z.; Hu, W., 25th anniversary article: key points for high-mobility organic field-effect transistors. *Adv. Mater.* **2013**, 25, 6158-6183.

Dresselhaus, M. S.; Thomas, I. L., Alternative energy technologies. *Nature* **2001**, 414, 332-337.

Dumur, F.; Gautier, N.; Gallego-Planas, N.; Sahin, Y.; Levillain, E.; Mercier, N.; Hudhomme, P.; Masino, M.; Girlando, A.; Lloveras, V.; Vidal-Gancedo, J.; Veciana, J.; Rovira, C., Novel fused D-A dyad and A-D-A triad incorporating tetrathiafulvalene and p-benzoquinone. *J. Org. Chem.* **2004**, 69, 2164-2177.

Durban, M. M.; Kazarinoff, P. D.; Luscombe, C. K., Synthesis and Characterization of Thiophene-Containing Naphthalene Diimide n-Type Copolymers for OFET Applications. *Macromolecules* **2010**, 43, 6348-6352.

Eftaiha, A. F.; Sun, J.-P.; Hill, I. G.; Welch, G. C., Recent advances of non-fullerene, small molecular acceptors for solution processed bulk heterojunction solar cells. *J. Mater. Chem. A* **2014**, 2, 1201-1213.

Erb, T.; Zhokhavets, U.; Gobsch, G.; Raleva, S.; Stühn, B.; Schilinsky, P.; Waldauf, C.; Brabec, C. J., Correlation Between Structural and Optical Properties of Composite Polymer/Fullerene Films for Organic Solar Cells. *Adv. Funct. Mater.* **2005**, 15, 1193-1196.

Facchetti, A., π-Conjugated Polymers for Organic Electronics and Photovoltaic Cell Applications. *Chem. Mater.* **2011**, 23, 733-758.

Frisch, M. J.; Trucks, G. W.; Schlegel, H. B.; Scuseria, G. E.; Robb, M. A.; Cheeseman, J. R.; Scalmani, G.; Barone, V.; Mennucci, B.; Petersson, G. A.; Nakatsuji, H.; Caricato, M.; Li, X.; Hratchian, H. P.; Izmaylov, A. F.; Bloino, J.; Zheng, G.; Sonnenberg, J. L.; Hada, M.; Ehara, M.; Toyota, K.; Fukuda, R.; Hasegawa, J.; Ishida, M.; Nakajima, T.; Honda, Y.; Kitao, O.; Nakai, H.; Vreven, T.; Montgomery, J., J. A.; Peralta, J. E.; Ogliaro, F.; Bearpark, M.; Heyd, J. J.; Brothers, E.; Kudin, K. N.; Staroverov, V. N.; Kobayashi, R.; Normand, J.; Raghavachari, K.; Rendell, A.; Burant, J. C.; Iyengar, S. S.; Tomasi, J.; Cossi, M.; Rega, N.; Millam, J. M.; Klene, M.; Knox, J. E.; Cross, J. B.; Bakken, V.; Adamo, C.; Jaramillo, J.; Gomperts, R.; Stratmann, R. E.; Yazyev, O.; Austin, A. J.; Cammi, R.; Pomelli, C.; Ochterski, J. W.; Martin, R. L.; Morokuma, K.; Zakrzewski, V. G.; Voth, G. A.; Salvador, P.; Dannenberg, J. J.; Dapprich, S.; Daniels, A. D.; Farkas, O.; Foresman, J. B.; Ortiz, J. V.; Cioslowski, J.; Fox, D. J., Gaussian 09. Gaussian, Inc.: Wallingford CT, 2009; Vol. Revision A.1.

Fthenakis, V.; Alsema, E., Photovoltaics Energy Payback Times, Greenhouse Gas Emissions and External Costs: 2004–early 2005 Status. *Prog. Photovolt. Res. Appl.* **2006**, 14, 275-280.

Gan, D.; Mueller, A.; Wooley, K. L., Amphiphilic and hydrophobic surface patterns generated from hyperbranched fluoropolymer/linear polymer networks: Minimally adhesive coatings via the crosslinking of hyperbranched fluoropolymers. *J. Poly. Sci. A: Poly. Chem* **2003**, 41, 3531-3540.

Glowatzki, H.; Sonar, P.; Singh, S. P.; Mak, A. M.; Sullivan, M. B.; Chen, W.; Wee, A. T. S.; Dodabalapur, A., Band Gap Tunable N-Type Molecules for Organic Field Effect Transistors. *J. Phys. Chem. C* **2013**, 117, 11530-11539.

Gong, M.; Zhou, W.; Tsai, M. C.; Zhou, J.; Guan, M.; Lin, M. C.; Zhang, B.; Hu, Y.; Wang, D. Y.; Yang, J.; Pennycook, S. J.; Hwang, B. J.; Dai, H., Nanoscale nickel oxide/nickel heterostructures for active hydrogen evolution electrocatalysis. *Nat. Commun.* **2014**, 5, 4695.

Goud, T. V.; Tutar, A.; Biellmann, J.-F., Synthesis of 8-heteroatom-substituted 4,4-difluoro-4-bora-3a,4a-diaza-s-indacene dyes (BODIPY). *Tetrahedron* **2006**, 62, 5084-5091.

Gregg, B. A.; Hanna, M. C., Comparing Organic to Inorganic Photovoltaic Cells: Theory, Experiment, and Simulation. *J. Appl. Phys.* **2003**, 93, 3605-3614.

Günes, S.; Neugebauer, H.; Sariciftci, N. S., Conjugated polymer-based organic solar cells. *Chem. Rev.* **2007**, 107, 1324-1338.

Guo, H.; Jing, Y.; Yuan, X.; Ji, S.; Zhao, J.; Li, X.; Kan, Y., Highly selective fluorescent OFF-ON thiol probes based on dyads of BODIPY and potent intramolecular electron sink 2,4-dinitrobenzenesulfonyl subunits. *Organic & biomolecular chemistry* **2011**, 9, 3844-3853.

Hadjichristidis, N.; Pitsikalis, M.; Iatrou, H., Synthesis of block copolymers. In *Block Copolymers I*, 2005; Vol. 189, pp 1-124.

Hayashi, Y.; Obata, N.; Tamaru, M.; Yamaguchi, S.; Matsuo, Y.; Saeki, A.; Seki, S.; Kureishi, Y.; Saito, S.; Yamaguchi, S.; Shinokubo, H., Facile synthesis of biphenyl-fused BODIPY and its property. *Org. Lett.* **2012**, 14, 866-869.

He, G.; Li, Z.; Wan, X.; Liu, Y.; Zhou, J.; Long, G.; Zhang, M.; Chen, Y., Impact of dye end groups on acceptor–donor–acceptor type molecules for solution-processed photovoltaic cells. *J. Mater. Chem.* **2012**, 22, 9173-9180.

He, Z.; Zhong, C.; Su, S.; Xu, M.; Wu, H.; Cao, Y., Enhanced power-conversion efficiency in polymer solar cells using an inverted device structure. *Nat. Photon.* **2012**, 6, 593-597.

Homnick, P. J.; Tinkham, J. S.; Devaughn, R.; Lahti, P. M., Engineering frontier energy levels in donor-acceptor fluoren-9-ylidene malononitriles versus fluorenones. *J. Phys. Chem. A* **2014**, 118, 475-486.

Horowitz, G.; Kouki, F.; Spearman, P.; Fichou, D.; Nogues, C.; Pan, X.; Garnier, F., Evidence for n-type conduction in a perylene tetracarboxylic diimide derivative. *Adv. Mater.* **1996**, 8, 242-245.

Hou, J.; Park, M.-H.; Zhang, S.; Yao, Y.; Chen, L.-M.; Li, J.-H.; Yang, Y., Bandgap and Molecular Energy Level Control of Conjugated Polymer Photovoltaic Materials Based on Benzo[1,2-b:4,5-b′]dithiophene. *Macromolecules* **2008**, 41, 6012-6018.

Hsu, W. Y.; Gierke, T. D., Ion-Transport and Clustering in Nafion Perfluorinated Membranes. *J. Member. Sci.* **1983**, 13, 307-326.

Hu, H.; Gopinadhan, M.; Osuji, C. O., Directed self-assembly of block copolymers: a tutorial review of strategies for enabling nanotechnology with soft matter. *Soft Matter* **2014**, 10, 3867-89.

Huang, J. D.; Wen, S. H.; Han, K. L., First-principles investigation of the electronic and conducting properties of oligothienoacenes and their derivatives. *Chem. Asian J.* **2012**, 7, 1032-1040.

Huang, X.; Zhu, C.; Zhang, S.; Li, W.; Guo, Y.; Zhan, X.; Liu, Y.; Bo, Z., Porphyrin-Dithienothiophene π-Conjugated Copolymers: Synthesis and Their Applications in Field-Effect Transistors and Solar Cells. *Macromolecules* **2008**, 41, 6895-6902.

Huo, L.; Zhang, S.; Guo, X.; Xu, F.; Li, Y.; Hou, J., Replacing alkoxy groups with alkylthienyl groups: a feasible approach to improve the properties of photovoltaic polymers. *Angewandte Chemie* **2011**, 50, 9697-9702.

Ie, Y.; Nitani, M.; Uemura, T.; Tominari, Y.; Takeya, J.; Honsho, Y.; Saeki, A.; Seki, S.; Aso, Y., Comprehensive Evaluation of Electron Mobility for a Trifluoroacetyl-Terminated Electronegative Conjugated Oligomer. *J. Phys. Chem. C* **2009**, 113, 17189-17193.

Jo, J.; Pouliot, J. R.; Wynands, D.; Collins, S. D.; Kim, J. Y.; Nguyen, T. L.; Woo, H. Y.; Sun, Y.; Leclerc, M.; Heeger, A. J., Enhanced efficiency of single and tandem organic solar cells incorporating a diketopyrrolopyrrole-based low-bandgap polymer by utilizing combined ZnO/polyelectrolyte electron-transport layers. *Adv. Mater.* **2013**, 25, 4783-4788.

Kallmann, H.; Pope, M., Photovoltaic Effect in Organic Crystals. *J. Chem. Phys.* **1959**, 30, 585-586.

Kamat, P. V., Meeting the Clean Energy Demand: Nanostructure Architectures for Solar Energy Conversion. *J. Phys. Chem. C* **2007**, 111, 2834-2860.

Keddie, D. J., A guide to the synthesis of block copolymers using reversible-addition fragmentation chain transfer (RAFT) polymerization. *Chem. Soc. Rev.* **2014**, 43, 496-505.

Kim, B.; Ma, B.; Donuru, V. R.; Liu, H.; Frechet, J. M., Bodipy-backboned polymers as electron donor in bulk heterojunction solar cells. *Chem. Commun.* **2010**, 46, 4148-4150.

Kim, J.; Cho, N.; Ko, H. M.; Kim, C.; Lee, J. K.; Ko, J., Push-pull organic semiconductors comprising of bis-dimethylfluorenyl amino benzo[b]thiophene donor and various acceptors for solution processed small molecule organic solar cells. *Sol. Energ. Mat. Sol. Cells* **2012**, 102, 159-166.

Krafft, M. P.; Riess, J. G., Chemistry, physical chemistry, and uses of molecular fluorocarbon--hydrocarbon diblocks, triblocks, and related compounds--unique "apolar" components for self-assembled colloid and interface engineering. *Chem. Rev.* **2009**, 109, 1714-92.

Kreuer, K. D., Proton conductivity: Materials and applications. *Chem. Mater.* **1996**, 8, 610-641.

Kumaresan, D.; Thummel, R. P.; Bura, T.; Ulrich, G.; Ziessel, R., Color tuning in new metal-free organic sensitizers (Bodipys) for dye-sensitized solar cells. *Chem. Eur. J.* **2009**, 15, 6335-6339.

Lager, E.; Liu, J.; Aguilar-Aguilar, A.; Tang, B. Z.; Pena-Cabrera, E., Novel meso-polyarylamine-BODIPY hybrids: synthesis and study of their optical properties. *J. Org. Chem.* **2009**, 74, 2053-2058.

Lee, J. K.; Ma, W. L.; Brabec, C. J.; Yuen, J.; Moon, J. S.; Kim, J. Y.; Lee, K.; Bazan, G. C.; Heeger, A. J., Processing additives for improved efficiency from bulk heterojunction solar cells. *J. Am. Chem. Soc.* **2008**, 130, 3619-3623.

Leen, V.; Yuan, P.; Wang, L.; Boens, N.; Dehaen, W., Synthesis of meso-halogenated BODIPYs and access to meso-substituted analogues. *Org. Lett.* **2012**, 14, 6150-6153.

Li, C.; Liu, M.; Pschirer, N. G.; Baumgarten, M.; Mullen, K., Polyphenylene-Based Materials for Organic Photovoltaics. *Chem. Rev.* **2010**, 110, 6817-6855.

Li, C.-Z.; Chueh, C.-C.; Yip, H.-L.; Zou, J.; Chen, W.-C.; Jen, A. K. Y., Evaluation of structure–property relationships of solution-processible fullerene acceptors and their n-channel field-effect transistor performance. *J. Mater. Chem.* **2012**, 22, 14976-14981.

Li, Y., Molecular design of photovoltaic materials for polymer solar cells: toward suitable electronic energy levels and broad absorption. *Acc. Chem. Res.* **2012**, 45, 723-733.

Lin, H. Y.; Huang, W. C.; Chen, Y. C.; Chou, H. H.; Hsu, C. Y.; Lin, J. T.; Lin, H. W., BODIPY dyes with beta-conjugation and their applications for high-efficiency inverted small molecule solar cells. *Chem. Commun.* **2012**, 48, 8913-5.

Lin, H. Y.; Huang, W. C.; Chen, Y. C.; Chou, H. H.; Hsu, C. Y.; Lin, J. T.; Lin, H. W., BODIPY dyes with beta-conjugation and their applications for high-efficiency inverted small molecule solar cells. *Chem. Commun.* **2012**, 48, 8913-8915.

Lin, Y.; Li, Y.; Zhan, X., Small molecule semiconductors for high-efficiency organic photovoltaics. *Chem. Soc. Rev.* **2012**, 41, 4245-4272.

Lin, Y.; Zhan, X., Non-fullerene acceptors for organic photovoltaics: an emerging horizon. *Mater. Horiz.* **2014**, 1, 470.

Lin, Y.; Zhang, Z. G.; Bai, H.; Li, Y.; Zhan, X., A star-shaped oligothiophene end-capped with alkyl cyanoacetate groups for solution-processed organic solar cells. *Chem. Commun.* **2012**, 48, 9655-9657.

Liu, J. H.; Walker, B.; Tamayo, A.; Zhang, Y.; Nguyen, T. Q., Effects of Heteroatom Substitutions on the Crystal Structure, Film Formation, and Optoelectronic Properties of Diketopyrrolopyrrole-Based Materials. *Adv. Funct. Mater.* **2013**, 23, 47-56.

Liu, T.; Troisi, A., What makes fullerene acceptors special as electron acceptors in organic solar cells and how to replace them. *Adv. Mater.* **2013**, 25, 1038-1041.

Maeda, T.; Tsukamoto, T.; Seto, A.; Yagi, S.; Nakazumi, H., Synthesis and Characterization of Squaraine-Based Conjugated Polymers With Phenylene Linkers for Bulk Heterojunction Solar Cells. *Macromol Chem Phys* **2012**, 213, 2590-2597.

Mai, Y.; Eisenberg, A., Self-assembly of block copolymers. *Chem. Soc. Rev.* **2012**, 41, 5969-85.

Mauritz, K. A.; Moore, R. B., State of understanding of nafion. *Chem. Rev.* **2004**, 104, 4535-85.

Mehta, V.; Cooper, J. S., Review and analysis of PEM fuel cell design and manufacturing. *J Power Sources* **2003**, 114, 32-53.

Mikhnenko, O. V.; Azimi, H.; Scharber, M.; Morana, M.; Blom, P. W. M.; Loi, M. A., Exciton diffusion length in narrow bandgap polymers. *Energy Environ. Sci.* **2012**, 5, 6960-6965.

Moon, J. S.; Takacs, C. J.; Sun, Y.; Heeger, A. J., Spontaneous formation of bulk heterojunction nanostructures: multiple routes to equivalent morphologies. *Nano letters* **2011**, 11, 1036-1039.

Nagamani, C.; Versek, C.; Thorn, M.; Tuominen, M. T.; Thayumanavan, S., Proton Conduction in 1H-1,2,3-triazole Polymers: Imidazole-Like or Pyrazole-Like? *J. Poly. Sci. A: Poly. Chem* **2010**, 48, 1851-1858.

Nagamani, C.; Viswanathan, U.; Versek, C.; Tuominen, M. T.; Auerbach, S. M.; Thayumanavan, S., Importance of dynamic hydrogen bonds and reorientation barriers in proton transport. *Chem. Commun.* **2011**, 47, 6638-40.

Narayanan, S. R.; Yen, S. P.; Liu, L.; Greenbaum, S. G., Anhydrous proton-conducting polymeric electrolytes for fuel cells. *J. Phys. Chem. B* **2006**, 110, 3942-8.

Newman, C. R.; Frisbie, C. D.; da Silva Filho, D. A.; Brédas, J.-L.; Ewbank, P. C.; Mann, K. R., Introduction to Organic Thin Film Transistors and Design of n-Channel Organic Semiconductors. *Chem. Mater.* **2004**, 16, 4436-4451.

Odom, S. A.; Lancaster, K.; Beverina, L.; Lefler, K. M.; Thompson, N. J.; Coropceanu, V.; Bredas, J. L.; Marder, S. R.; Barlow, S., Bis[bis-(4-alkoxyphenyl)amino] derivatives of dithienylethene, bithiophene, dithienothiophene and dithienopyrrole: palladium-catalysed synthesis and highly delocalised radical cations. *Chem. Eur. J.* **2007**, 13, 9637-46.

Ott, C.; Hoogenboom, R.; Schubert, U. S., Post-modification of poly(pentafluorostyrene): a versatile "click" method to create well-defined multifunctional graft copolymers. *Chem. Commun.* **2008**, 3516-8.

Park, O. Y.; Kim, H. U.; Kim, J.-H.; Park, J. B.; Kwak, J.; Shin, W. S.; Yoon, S. C.; Hwang, D.-H., Tetrafluorene-9,9′-bifluorenylidene as a non-fullerene type electron acceptor for P3HT-based bulk-heterojunction polymer solar cells. *Sol. Energ. Mat. Sol. Cells* **2013**, 116, 275-282.

Peet, J.; Heeger, A. J.; Bazan, G. C., "Plastic" solar cells: self-assembly of bulk heterojunction nanomaterials by spontaneous phase separation. *Acc. Chem. Res.* **2009**, 42, 1700-1708.

Pena-Cabrera, E.; Aguilar-Aguilar, A.; Gonzalez-Dominguez, M.; Lager, E.; Zamudio-Vazquez, R.; Godoy-Vargas, J.; Villanueva-Garcia, F., Simple, general, and efficient synthesis of meso-substituted borondipyrromethenes from a single platform. *Org. Lett.* **2007**, 9, 3985-3988.

Poe, A. M.; Della Pelle, A. M.; Subrahmanyam, A. V.; White, W.; Wantz, G.; Thayumanavan, S., Small molecule BODIPY dyes as non-fullerene acceptors in bulk heterojunction organic photovoltaics. *Chem. Commun.* **2014**, 50, 2913-2915.

Popere, B. C.; Della Pelle, A. M.; Poe, A.; Balaji, G.; Thayumanavan, S., Predictably tuning the frontier molecular orbital energy levels of panchromatic low band gap BODIPY-based conjugated polymers. *Chem. Sci.* **2012**, 3, 3093-3102.

Popere, B. C.; Della Pelle, A. M.; Poe, A.; Balaji, G.; Thayumanavan, S., Predictably tuning the frontier molecular orbital energy levels of panchromatic low band gap BODIPY-based conjugated polymers. *Chem. Sci.* **2012**, 3, 3093-3102.

Popere, B. C.; Della Pelle, A. M.; Thayumanavan, S., BODIPY-Based Donor–Acceptor π-Conjugated Alternating Copolymers. *Macromolecules* **2011**, 44, 4767-4776.

Potscavage, W. J.; Sharma, A.; Kippelen, B., Critical interfaces in organic solar cells and their influence on the open-circuit voltage. *Acc. Chem. Res.* **2009**, 42, 1758-1767.

Reddy, J. S.; Kale, T.; Balaji, G.; Chandrasekaran, A.; Thayumanavan, S., Cyclopentadithiophene-Based Organic Semiconductors: Effect of Fluorinated Substituents on Electrochemical and Charge Transport Properties. *J. Phys. Chem. Lett.* **2011**, 2, 648-654.

Reese, C.; Roberts, M.; Ling, M.-m.; Bao, Z., Organic thin film transistors. *Mater. Today* **2004**, 7, 20-27.

Rosler, A.; Vandermeulen, G. W. M.; Klok, H. A., Advanced drug delivery devices via self-assembly of amphiphilic block copolymers. *Adv Drug Deliver Rev* **2012**, 64, 270-279.

Rousseau, T.; Cravino, A.; Ripaud, E.; Leriche, P.; Rihn, S.; De Nicola, A.; Ziessel, R.; Roncali, J., A tailored hybrid BODIPY-oligothiophene donor for molecular bulk heterojunction solar cells with improved performances. *Chem. Commun.* **2010**, 46, 5082-5084.

Sahu, A. K.; Pitchumani, S.; Sridhar, P.; Shukla, A. K., Nafion and modified-Nafion membranes for polymer electrolyte fuel cells: An overview. *B Mater Sci* **2009**, 32, 285-294.

Schacher, F. H.; Rupar, P. A.; Manners, I., Functional block copolymers: nanostructured materials with emerging applications. *Angewandte Chemie* **2012**, 51, 7898-921.

Scharber, M. C.; Mühlbacher, D.; Koppe, M.; Denk, P.; Waldauf, C.; Heeger, a. J.; Brabec, C. J., Design Rules for Donors in Bulk-Heterojunction Solar Cells—Towards 10 % Energy-Conversion Efficiency. *Adv. Mater.* **2006**, 18, 789-794.

Schuster, M. E.; Meyer, W. H., Anhydrous proton-conducting polymers. *Annu Rev Mater Res* **2003**, 33, 233-261.

Shi, M.-M.; Deng, D.; Chen, L.; Ling, J.; Fu, L.; Hu, X.-L.; Chen, H.-Z., Design and synthesis of dithieno[3,2-b:2′3′-d]pyrrole-based conjugated polymers for photovoltaic applications: consensus between low bandgap and low HOMO energy level. *J. Poly. Sci. A: Poly. Chem.* **2011**, 49, 1453-1461.

Silvestri, F.; Marrocchi, A., Acetylene-based materials in organic photovoltaics. *International journal of molecular sciences* **2010**, 11, 1471-1508.

Singh, S.; Venugopalan, V.; Krishnamoorthy, K., Organic soluble and uniform film forming oligoethylene glycol substituted BODIPY small molecules with improved hole mobility. *Phys. Chem. Chem. Phys.* **2014**, 16, 13376-82.

Smith, J.; Hamilton, R.; McCulloch, I.; Stingelin-Stutzmann, N.; Heeney, M.; Bradley, D. D. C.; Anthopoulos, T. D., Solution-processed organic transistors based on semiconducting blends. *J. Mater. Chem.* **2010**, 20, 2562-2574.

Sokolov, A. N.; Roberts, M. E.; Bao, Z., Fabrication of low-cost electronic biosensors. *Mater. Today* **2009**, 12, 12-20.

Sonar, P.; Ng, G.-M.; Lin, T. T.; Dodabalapur, A.; Chen, Z.-K., Solution processable low bandgap diketopyrrolopyrrole (DPP) based derivatives: novel acceptors for organic solar cells. *J. Mater. Chem.* **2010**, 20, 3626-3636.

Sone, Y.; Ekdung, P.; Simonsson, D., Proton Conductivily of Nafion 117 as Measured by a Four-Electrode AC Impedance Method. *J. Electrochem. Soc.* **1996**, 143, 1254-1259.

Spanggaard, H.; Krebs, F. C., A brief history of the development of organic and polymeric photovoltaics. *Sol. Energ. Mat. Sol. Cells* **2004**, 83, 125-146.

Steele, B. C.; Heinzel, A., Materials for fuel-cell technologies. *Nature* **2001**, 414, 345-352.

Subramaniyan, S.; Xin, H.; Kim, F. S.; Jenekhe, S. A., New Thiazolothiazole Copolymer Semiconductors for Highly Efficient Solar Cells. *Macromolecules* **2011**, 44, 6245-6248.

Sun, J. Z.; Jordan, L. R.; Forsyth, M.; MacFarlane, D. R., Acid-organic base swollen polymer membranes. *Electrochim Acta* **2001**, 46, 1703-1708.

Swanson, R. M., Applied physics. Photovoltaics power up. *Science* **2009**, 324, 891-892.

Takacs, C. J.; Sun, Y.; Welch, G. C.; Perez, L. A.; Liu, X.; Wen, W.; Bazan, G. C.; Heeger, A. J., Solar cell efficiency, self-assembly, and dipole-dipole interactions of isomorphic narrow-band-gap molecules. *J. Am. Chem. Soc.* **2012**, 134, 16597-16606.

Tang, C. W., Two-layer organic photovoltaic cell. *Appl. Phys. Lett.* **1986**, 48, 183-185.

Thambidurai, M.; Kim, J. Y.; Ko, Y.; Song, H. J.; Shin, H.; Song, J.; Lee, Y.; Muthukumarasamy, N.; Velauthapillai, D.; Lee, C., High-efficiency inverted organic solar cells with polyethylene oxide-modified Zn-doped TiO2 as an interfacial electron transport layer. *Nanoscale* **2014**, 6, 8585-8589.

Thompson, A. L.; Ahn, T. S.; Thomas, K. R.; Thayumanavan, S.; Martinez, T. J.; Bardeen, C. J., Using meta conjugation to enhance charge separation versus charge recombination in phenylacetylene donor-bridge-acceptor complexes. *J. Am. Chem. Soc.* **2005**, 127, 16348-16349.

Thompson, B. C.; Frechet, J. M., Polymer-fullerene composite solar cells. *Angewandte Chemie* **2008**, 47, 58-77.

Usta, H.; Yilmaz, M. D.; Avestro, A. J.; Boudinet, D.; Denti, M.; Zhao, W.; Stoddart, J. F.; Facchetti, A., BODIPY-thiophene copolymers as p-channel semiconductors for organic thin-film transistors. *Adv. Mater.* **2013**, 25, 4327-4334.

Wang, Y.; Chen, K. S.; Mishler, J.; Cho, S. C.; Adroher, X. C., A review of polymer electrolyte membrane fuel cells: Technology, applications, and needs on fundamental research. *Appl Energ* **2011**, 88, 981-1007.

Wei, G.; Xiao, X.; Wang, S.; Sun, K.; Bergemann, K. J.; Thompson, M. E.; Forrest, S. R., Functionalized squaraine donors for nanocrystalline organic photovoltaics. *ACS Nano* **2012**, 6, 972-8.

Wu, P.-T.; Xin, H.; Kim, F. S.; Ren, G.; Jenekhe, S. A., Regioregular Poly(3-pentylthiophene): Synthesis, Self-Assembly of Nanowires, High-Mobility Field-Effect Transistors, and Efficient Photovoltaic Cells. *Macromolecules* **2009**, 42, 8817-8826.

Xue, Y.; Lu, H. C.; Zhao, Q. L.; Huang, J.; Xu, S. G.; Cao, S. K.; Ma, Z., Polymethylene-b-poly(styrene-co-2,3,4,5,6-pentafluoro styrene) copolymers: synthesis and fabrication of their porous films. *Polym. Chem.* **2013**, 4, 307-312.

Yan, H.; Chen, Z.; Zheng, Y.; Newman, C.; Quinn, J. R.; Dotz, F.; Kastler, M.; Facchetti, A., A high-mobility electron-transporting polymer for printed transistors. *Nature* **2009**, 457, 679-686.

Yan, X.; Poxson, D. J.; Cho, J.; Welser, R. E.; Sood, A. K.; Kim, J. K.; Schubert, E. F., Enhanced Omnidirectional Photovoltaic Performance of Solar Cells Using Multiple-Discrete-Layer Tailored- and Low-Refractive Index Anti-Reflection Coatings. *Adv. Funct. Mater.* **2013**, 23, 583-590.

Yao, K.; Intemann, J. J.; Yip, H. L.; Liang, P. W.; Chang, C. Y.; Zang, Y.; Li, Z. A.; Chen, Y. W.; Jen, A. K. Y., Efficient all polymer solar cells from layer-evolved processing of a bilayer inverted structure. *J. Mater. Chem. C* **2014**, 2, 416-420.

Yin, S.; Leen, V.; Jackers, C.; Beljonne, D.; Van Averbeke, B.; Van der Auweraer, M.; Boens, N.; Dehaen, W., Oligo(p-phenylene ethynylene)-BODIPY derivatives: synthesis, energy transfer, and quantum-chemical calculations. *Chem. Eur. J.* **2011**, 17, 13247-13257.

Yoshii, R.; Yamane, H.; Nagai, A.; Tanaka, K.; Taka, H.; Kita, H.; Chujo, Y., π-Conjugated Polymers Composed of BODIPY or Aza-BODIPY Derivatives Exhibiting High Electron Mobility and Low Threshold Voltage in Electron-Only Devices. *Macromolecules* **2014**, 47, 2316-2323.

You, J.; Dou, L.; Yoshimura, K.; Kato, T.; Ohya, K.; Moriarty, T.; Emery, K.; Chen, C. C.; Gao, J.; Li, G.; Yang, Y., A polymer tandem solar cell with 10.6% power conversion efficiency. *Nat. Commun.* **2013**, 4, 1446.

Yu, G.; Pakbaz, K.; Heeger, A. J., Semiconducting polymer diodes: Large size, low cost photodetectors with excellent visibleultraviolet sensitivity. *Appl. Phys. Lett.* **1994**, 64, 3422-3424.

Yuan, J.; Huang, X.; Zhang, F.; Lu, J.; Zhai, Z.; Di, C.; Jiang, Z.; Ma, W., Design of benzodithiophene-diketopyrrolopyrrole based donor–acceptor copolymers for efficient organic field effect transistors and polymer solar cells. *J. Mater. Chem.* **2012**, 22, 22734-22742.

Zhao, Y.; Di, C. A.; Gao, X.; Hu, Y.; Guo, Y.; Zhang, L.; Liu, Y.; Wang, J.; Hu, W.; Zhu, D., All-solution-processed, high-performance n-channel organic transistors and circuits: toward low-cost ambient electronics. *Adv. Mater.* **2011**, 23, 2448-2453.

Zhao, Y.; Guo, Y.; Liu, Y., 25th anniversary article: recent advances in n-type and ambipolar organic field-effect transistors. *Adv. Mater.* **2013**, 25, 5372-91.

Zhou, H.; Yang, L.; Liu, S.; You, W., A Tale of Current and Voltage: Interplay of Band Gap and Energy Levels of Conjugated Polymers in Bulk Heterojunction Solar Cells. *Macromolecules* **2010**, 43, 10390-10396.

Zhou, H.; Yang, L.; You, W., Rational Design of High Performance Conjugated Polymers for Organic Solar Cells. *Macromolecules* **2012**, 45, 607-632.

Zhou, Y.; Dai, Y. Z.; Zheng, Y. Q.; Wang, X. Y.; Wang, J. Y.; Pei, J., Non-fullerene acceptors containing fluoranthene-fused imides for solution-processed inverted organic solar cells. *Chem. Commun.* **2013**, 49, 5802-5804.

Zhou, Y.; Ding, L.; Shi, K.; Dai, Y. Z.; Ai, N.; Wang, J.; Pei, J., A non-fullerene small molecule as efficient electron acceptor in organic bulk heterojunction solar cells. *Adv. Mater.* **2012**, 24, 957-961.

Zhu, Z.; Waller, D.; Gaudiana, R.; Morana, M.; Mühlbacher, D.; Scharber, M.; Brabec, C., Panchromatic Conjugated Polymers Containing Alternating Donor/Acceptor Units for Photovoltaic Applications. *Macromolecules* **2007**, 40, 1981-1986.